

## **INFORMATION TO USERS**

**The most advanced technology has been used to photograph and reproduce this manuscript from the microfilm master. UMI films the original text directly from the copy submitted. Thus, some dissertation copies are in typewriter face, while others may be from a computer printer.**

**In the unlikely event that the author did not send UMI a complete manuscript and there are missing pages, these will be noted. Also, if unauthorized copyrighted material had to be removed, a note will indicate the deletion.**

**Oversize materials (e.g., maps, drawings, charts) are reproduced by sectioning the original, beginning at the upper left-hand corner and continuing from left to right in equal sections with small overlaps. Each oversize page is available as one exposure on a standard 35 mm slide or as a 17" x 23" black and white photographic print for an additional charge.**

**Photographs included in the original manuscript have been reproduced xerographically in this copy. 35 mm slides or 6" x 9" black and white photographic prints are available for any photographs or illustrations appearing in this copy for an additional charge. Contact UMI directly to order.**



300 North Zeeb Road, Ann Arbor, MI 48106-1346 USA



**Order Number 8825468**

**Study of mixed mode stress intensity factors using the  
experimental method of caustics**

**Younis, Nashwan Thanoon, Ph.D.**

**Iowa State University, 1988**

**U·M·I**  
300 N. Zeeb Rd.  
Ann Arbor, MI 48106



**PLEASE NOTE:**

In all cases this material has been filmed in the best possible way from the available copy. Problems encountered with this document have been identified here with a check mark .

1. Glossy photographs or pages \_\_\_\_\_
2. Colored illustrations, paper or print \_\_\_\_\_
3. Photographs with dark background
4. Illustrations are poor copy \_\_\_\_\_
5. Pages with black marks, not original copy \_\_\_\_\_
6. Print shows through as there is text on both sides of page \_\_\_\_\_
7. Indistinct, broken or small print on several pages
8. Print exceeds margin requirements \_\_\_\_\_
9. Tightly bound copy with print lost in spine \_\_\_\_\_
10. Computer printout pages with indistinct print
11. Page(s) \_\_\_\_\_ lacking when material received, and not available from school or author.
12. Page(s) \_\_\_\_\_ seem to be missing in numbering only as text follows.
13. Two pages numbered \_\_\_\_\_. Text follows.
14. Curling and wrinkled pages \_\_\_\_\_
15. Dissertation contains pages with print at a slant, filmed as received \_\_\_\_\_
16. Other \_\_\_\_\_  
\_\_\_\_\_  
\_\_\_\_\_

**U·M·I**



**Study of mixed mode stress intensity factors  
using the experimental method of caustics**

by

**Nashwan Thanoon Younis**

**A Dissertation Submitted to the  
Graduate Faculty in Partial Fulfillment of the  
Requirements for the Degree of  
DOCTOR OF PHILOSOPHY  
Department: Engineering Science and Mechanics  
Major: Engineering Mechanics**

**Approved:**

Signature was redacted for privacy.

**In Charge of Major Work**

Signature was redacted for privacy.

**For the Major Department**

Signature was redacted for privacy.

**For the Graduate College**

**Iowa State University  
Ames, Iowa**

**1988**

## TABLE OF CONTENTS

	PAGE
DEDICATION	vii
I. INTRODUCTION	1
II. LITERATURE REVIEW	4
III. PHYSICAL AND MATHEMATICAL PRINCIPLES OF THE METHOD	15
A. Physical Principle of the Method of Caustics	16
B. The Basic Formulas and Procedures for Determining Mixed Mode Stress Intensity Factors	20
1. The difference between the longitudinal diameters method	27
2. The epicycloid's angle of symmetry method	33
3. An iterative least-squares method	35
C. The Three Dimensional Effects and the Effects of the Presence of Higher Order Terms	42
D. Methods of Determining the Stress Optical Constants	43
1. The technique of using a cracked plate	43
2. The technique of using a circular hole in a plate	45
IV. MIXED MODE STRESS INTENSITY FACTORS EXPERIMENTS	51
A. Test Specimen	51
1. Material and model preparation	51
2. Model geometries	53
B. Experimental Setup	57
C. Calibration Procedure	58
1. Calibration of the stress optical constants	58
2. Optical calibration	58
D. Test Procedure	59
E. Data Analysis and Results	62
1. Mixed mode SIFs by epicycloid's angle of symmetry	62
2. Mixed mode SIFs using an iterative least square method	75
F. Conclusion and Discussion	82
V. STRESS OPTICAL CONSTANTS EXPERIMENTS	86
A. Model Geometry	88
B. Test Procedure	89
C. Conclusions and Recommendations	101

<b>VI. REFERENCES</b>	<b>103</b>
<b>VII. ACKNOWLEDGEMENTS</b>	<b>109</b>
<b>VIII. APPENDIX: PROGRAMS</b>	<b>110</b>
<b>A. CAUSTIC 1 PROGRAM</b>	<b>110</b>
<b>B. CAUSTIC 2 PROGRAM</b>	<b>122</b>

## LIST OF TABLES

	PAGE
Table 2-1. Comparison between four different cases for the epicycloids generated in Fig. 2-1	10
Table 3-1. Comparison between the generalized epicycloids and ILSM	40
Table 4-1. Material properties of plexiglas	52
Table 4-2. Geometrical parameters of equal length crack specimens	53
Table 4-3. Geometrical parameters of unequal length crack specimens	54
Table 4-4. Experimental and numerical results for model A	64
Table 4-5. Experimental and numerical results for model B tip S	64
Table 4-6. Experimental and numerical results for model B tip L	65
Table 4-7. SIFs of crack tip S using an iterative least square technique	78
Table 4-8. SIFs of crack tip L using an iterative least square technique	78
Table 4-9. Calculated $K_I/K_{I0}$ and $K_{II}/K_I$ for crack tip S using four techniques	79
Table 4-10. Calculated $K_I/K_{I0}$ and $K_{II}/K_I$ for crack tip L using four techniques	79
Table 5-1. Geometrical parameters of model C	88
Table 5-2. Geometrical parameters of model D	89
Table 5-3. Load test results for $c_t$	91
Table 5-4. Load test results for $c_r$	92

## LIST OF FIGURES

	PAGE
Figure 2-1. The shape and size of different generalized epicycloids	11
Figure 2-2. Reflected caustic from a nontransparent material	13
Figure 2-3. Transmitted caustic through a transparent material	13
Figure 2-4. Reflected caustic from a transparent material	14
Figure 3-1. The principle of the method of caustics for transmission and reflection	18
Figure 3-2. Comparison between the theoretical and experimental caustics	19
Figure 3-3. Schematic reflected caustic setup	24
Figure 3-4. Geometrical conditions of the caustic analysis	25
Figure 3-5. Theoretical form of the caustic formed at a crack tip for $K_{II}/K_I=0.5$	26
Figure 3-6. Variation of the theoretical form of the caustic with the ratio $K_{II}/K_I$	29
Figure 3-7. Variation of $d_1$ , $d_2$ and $d_3$ with $u$	31
Figure 3-8. Variation of the ratio $(D_{x \max} - D_{x \min})/D_{x \max}$ with $u$	32
Figure 3-9. The epicycloid's angle of symmetry	34
Figure 3-10a. Geometry of the principal epicycloid	36a
Figure 3-10b. The difference between LM and LE	36b
Figure 3-11. Regions of the generalized epicycloid for $\phi$ of 0 to $4\pi$	41
Figure 3-12. Coordinate system with respect to the hole center	49
Figure 3-13. Theoretical form of the principal envelope around a central hole	50
Figure 4-1. Model A geometries of equal length cracks	55
Figure 4-2. Model B geometries of unequal length cracks	56
Figure 4-3. Experimental reflected caustic setup	60

Figure 4-4.	Loading apparatus	61
Figure 4-5.	Experimental and numerical $K_I/K_{Io}$ versus $H/a$ for Model A	66
Figure 4-6.	Experimental and numerical $K_{II}/K_{Io}$ versus $H/a$ for Model A	67
Figure 4-7.	Experimental and numerical $K_I/K_{Io}$ versus $H/a$ for Model B tip S	68
Figure 4-8.	Experimental and numerical $K_{II}/K_{Io}$ versus $H/a$ for Model B tip S	69
Figure 4-9.	Experimental and numerical $K_I/K_{Io}$ versus $H/a$ for Model B tip L	70
Figure 4-10.	Experimental and numerical $K_{II}/K_{Io}$ versus $H/a$ for Model B tip L	71
Figure 4-11.	$K_{I\text{exp.}}/K_{I\text{num.}}$ versus $r_o/d$ for Model A	72
Figure 4-12.	$K_{I\text{exp.}}/K_{I\text{num.}}$ versus $r_o/d$ for Model B tip S	73
Figure 4-13.	$K_{I\text{exp.}}/K_{I\text{num.}}$ versus $r_o/d$ for Model B tip L	74
Figure 4-14.	The EyeCom system	80
Figure 4-15.	Schematic diagram of the EyeCom system	81
Figure 5-1.	Schematic transmitted caustic setup	87
Figure 5-2.	Models C and D geometries	95
Figure 5-3.	Pressure loading apparatus	96
Figure 5-4.	Experimental transmitted caustic setup	97
Figure 5-5.	Reflected from a central hole caustic pattern	98
Figure 5-6.	Transmitted through a central hole caustic pattern	98
Figure 5-7.	Stress-optical constant $c_t$ versus $a/W$	99
Figure 5-8.	Stress-optical constant $c_r$ versus $a/W$	100

**DEDICATION**

**In loving memory of my daughter,  
Dena Enola Latifa Younis**

## I. INTRODUCTION

The essence of fast fracture is that it is a failure mechanism involving the unstable propagation of a crack in a structure. In other words, once the crack has started to move, the loading system is such that it produces accelerated growth. In the history of failure by fast fracture in service structures, fracture has almost always been produced by applied stresses less than the design stress calculated using the appropriate code and safety factor. This has naturally enhanced the catastrophic nature of the fractures and has led to the general description of them as being brittle. A brittle fracture is the start of unstable crack propagation produced by applied stress less than the general yield stress of the uncracked ligament remaining when instability first occurs. Such brittle fractures are related to fracture parameters, called the stress intensity factors (SIF). The goal of engineers is to avoid fracture in structural and machine elements by calculating the SIF for a particular crack geometry and loading condition.

Photoelastic experiments have been used to extract the SIF or K factors by taking data points from the fringe loops surrounding a crack tip. The SIF should be measured very close to a crack tip. The main disadvantage of using the method of photoelasticity is that we do not know the plastic zone size or dimpled area (lens effect) resulting from the stress intensification in the region surrounding the crack tip. In order to avoid these areas data are collected far from the singularity area.

The method of caustics in various investigations has proven to be a powerful method to measure SIF at a crack tip in static and dynamic fracture mechanics problems. In the method of caustics all the information is obtained from the initial curve (the lens effect) of the caustics lying in the close vicinity of the crack tip which is a region of much interest in fracture mechanics.

There are some difficulties in the determination of mixed mode SIFs, the opening Mode  $K_I$  and the sliding Mode  $K_{II}$ , using the experimental method of caustics. These are:

1. By the nature of the caustics resulting either from the light transmitted through a cracked transparent material or the light reflected from the front face of a cracked nontransparent material, it is difficult to extract  $K_{II}$ .
2. The reflected caustics from a cracked transparent material contains information to extract mixed mode SIFs. Current methods utilizing the method of caustics use only a limited amount of data from the generalized epicycloid. The angle between the axis of symmetry and the crack axis along with the maximum transverse diameter of the external caustic are used to determine  $K_I$  and  $K_{II}$ . If there are errors in these measurements, then the accuracy of the  $K_I$  and  $K_{II}$  results suffer.
3. The location of the crack tip is obscured by the caustic.
4. Due to the reduction of the thickness of the specimen, the area surrounding the crack tip acts similar to a divergent lens. As a consequence the light transmitted through or reflected from

the specimen is deflected outwards. As a result of a divergent factor, the initial curve size can not be seen on the caustic image.

The main goal in this dissertation has been to solve some of these difficulties. The experimental accuracy was improved by using the digital image analysis system (EYECOM III) to determine the crack orientation and the individual points of the caustics.

An interaction between two edge cracks for different cases has been studied. The validity of the experimental results is compared with the numerical results.

An iterative least-squares technique has been developed to extract  $K_I$ ,  $K_{II}$  and the initial curve radius  $r_0$  values from an overdetermined set of data. The method presented treats the crack tip location as an unknown and is determined numerically during the iteration process.

The method of caustics was extended to the determination of the stress optical constants by applying the method of caustics in the region very close to a circular hole in a thin plate. A new technique has been developed to determine both the transmitted and the reflected from the rear face stress optical constants.

## II. LITERATURE REVIEW

The theory of fracture strength in brittle materials in terms of their surface was introduced by Griffith [1]. This theory infers the existence or initiation of cracks in a solid during loading. A rapid extension of a crack occurs as soon as an increase of the external load creates a rate of strain energy release during extension of the crack which is larger than the rate of the gain of energy resulting from the formation of a new surface area. Irwin [2] suggested that Griffith's theory can be extended to any type of fracture by taking into consideration the energy spent in the localized plastic strain at the vicinity of a crack tip in estimating the resistance to crack extension. The existence of the plastic zone around a crack tip is related to the effective stress concentration at the crack tip. Considering the influence of plastic yielding at the root of a sharp notch, Neuber [3] suggested that the average stress ( $\sigma'$ ) from the root across the distance of the plastic zone for a single edge crack can be expressed by

$$\sigma' = K \sqrt{\frac{2}{\pi r}} \quad (2-1)$$

where  $K$  is the SIF and  $r$  is the radius of the plastic zone in the direction of the crack. Irwin [4] suggested that it is convenient and satisfactory to accept that the plastic zone has a circular shape and the crack tip is at the center of the circle. He introduced the plasticity correction to the crack size and estimated the radius of the plastic zone. The stress and displacement fields associated with each loading mode at the vicinity of the crack tip has been related to

the corresponding SIF by regarding the plastic zone to be negligibly small [5]. It has been observed in tests with cracked steel plates, that the plastic zone has a wedge shape [6,7,8]. Ault and Spretnak [9] with sharp notches, and Gerberich [10] with cracks in several aluminum alloys have detected that the plastic area has a circular shape. Theocaris [11] studied the constrained zone in plexiglas elastically loaded under mode one deformation and proved theoretically and experimentally that the shape of the constrained zone is a circle. He concluded that the stress field around the crack tip may be regarded as homogeneous, so that the elastic singularities at the crack tip dominate and control the enclosed plasticity around the tips. He also suggested that the dimensions of a thin cracked plate should be sufficiently large compared with the crack length for the constrained zone to be regarded as negligibly small and the elastic stress distribution dominating at the crack borders [12].

For the elastic infinite plate under conditions of generalized plane stress and the crack under the opening mode of deformation, a direct evaluation of the stress components around the crack can be derived from Westergaard's solution [13]. Westergaard made use of the properties of complex variable functions to show that the normal and shearing stresses in the x and y directions, with the origin at the crack tip and the x axis coinciding with the direction of the crack, can be stated in the form:

$$\begin{aligned}
 \sigma_x &= \operatorname{Re}Z(z) - y\operatorname{Im}Z'(z) \\
 \sigma_y &= \operatorname{Re}z(z) + y\operatorname{Im}Z'(z) \\
 \tau_{xy} &= -y\operatorname{Re}Z'(z)
 \end{aligned}
 \tag{2-2}$$

where  $z = x + iy$ ,  $Z(z)$  is the stress function in complex form

$Z' = \partial Z / \partial z$  and Re and Im indicate the real and imaginary components.

Westergaard proposed the following complex form for the stress function

$$Z(z) = \frac{\sigma z}{(z^2 - a^2)^{1/2}} \quad (2-3)$$

by substituting equation (2-2) and its derivative into equation (2-1),

the stress components in the vicinity of the crack are given by

$$\begin{aligned} \sigma_x &= \frac{K_I}{\sqrt{2\pi r}} \cos \frac{\theta}{2} \left( 1 - \sin \frac{\theta}{2} \sin \frac{3\theta}{2} \right) + \text{HOST} \\ \sigma_y &= \frac{K_I}{\sqrt{2\pi r}} \cos \frac{\theta}{2} \left( 1 + \sin \frac{\theta}{2} \sin \frac{3\theta}{2} \right) + \text{HOST} \\ \tau_{xy} &= \frac{K_I}{\sqrt{2\pi r}} \sin \frac{\theta}{2} \cos \frac{\theta}{2} \cos \frac{3\theta}{2} + \text{HOST} \end{aligned} \quad (2-4)$$

where HOST denotes a higher order stress terms and  $r$  and  $\theta$  are the polar coordinates with the origin at the crack tip. It was demonstrated that the shape of the caustic is virtually unaffected by the presence of higher order terms except when the crack tip reaches the boundary [14]. Through the use of the experimental method of photoelasticity, the Westergaard equations have proven not to be accurate. Therefore, Irwin suggested adding a nonsingular term  $\sigma_m$  to the  $\sigma_x$  expression in equation (2-3) [15]. Sneddon concluded that for an edge crack only  $\sigma_m/2$  should be added to the stress distribution at the vicinity of the crack tip [16].

For mixed mode loading, the stress distribution equations often called the modified Westergaard equations are:

$$\begin{aligned}\sigma_x &= \frac{K_I}{\sqrt{2\pi r}} \cos \frac{\theta}{2} \left(1 - \sin \frac{\theta}{2} \sin \frac{3\theta}{2}\right) - \frac{K_{II}}{\sqrt{2\pi r}} \sin \frac{\theta}{2} \left(2 + \cos \frac{\theta}{2} \cos \frac{3\theta}{2}\right) - \sigma_m \\ \sigma_y &= \frac{K_I}{\sqrt{2\pi r}} \cos \frac{\theta}{2} \left(1 + \sin \frac{\theta}{2} \sin \frac{3\theta}{2}\right) + \frac{K_{II}}{\sqrt{2\pi r}} \sin \frac{\theta}{2} \left(2 + \sin \frac{\theta}{2} \cos \frac{3\theta}{2}\right) \quad (2-5) \\ \tau_{xy} &= \frac{K_I}{\sqrt{2\pi r}} \sin \frac{\theta}{2} \cos \frac{\theta}{2} \cos \frac{3\theta}{2} + \frac{K_{II}}{\sqrt{2\pi r}} \cos \frac{\theta}{2} \left(1 - \sin \frac{\theta}{2} \sin \frac{3\theta}{2}\right)\end{aligned}$$

The addition of  $\sigma_m$  or  $\sigma_m/2$  to the stress equations has no effect on the shape of the generalized epicycloid using the experimental method of caustics as will be demonstrated in Chapter III. Since relations (2-5) were obtained by neglecting higher order terms in  $r$ , they may be regarded as approximations valid only in the region where  $r$  is small compared to the other dimensions of the specimen. These relations become exact in the limit as  $r \rightarrow 0$ . It is important to note that the method of caustics inherently provides information close to the crack tip where the theory of elasticity near field solution is valid. Thus the method of caustics can have an advantage over other optical techniques which require the use of data some distance from the crack tip.

The method of caustics, also known as "Shadow Spot Method", has proven to be a powerful optical method to measure stress intensity factors at a crack tip for static and dynamic fracture mechanics problems. In the method of caustics, all of  $K_I$  and  $K_{II}$  information is

obtained from the initial curve (the lens effect) of the caustic due to deformation in the close vicinity of the crack tip.

The word caustic is Greek for focal line. The method of caustics is a relatively new experimental technique for determining SIF. The first attempt to use the caustics and their properties for studying singular fields in elasticity was made by Manogg in 1966 [17]. He developed the theory for the transmitted Mode I caustics only. Theocaris in 1970 developed the technique where he used the reflected light from both the front and rear face [11]. The technique was extended later by Theocaris and Ioakimides [18], Theocaris [19,20], Rosakis and Freund [21], Rosakis et al. [22], Kalthoff et al. [23], Beinert and Kalthoff [24]. As shown in Fig. 2-1a, they determined Mode I SIFs by measuring the maximum transverse diameters ( $D_{t \max}$ ) of the caustics obtained from optically isotropic materials. Rosakis used the reflected caustics from nontransparent materials and Kalthoff used the transmitted caustics through transparent materials. The method of caustics was extended to study Mode I SIF by using optically anisotropic transparent materials [25-27].

The shape of the caustic is a generalized epicycloid as shown in Fig. 2-1a to Fig. 2-1d. Mode I effects the size of the caustic while mode II effects the shape of the caustics. A comparison between different  $K_I$  as normalized to  $K_I$  of Fig. 2-1a ( $K_{Ia}$ ) and  $u$  ( $u=K_{II}/K_I$ ) are listed in Table 2-1.

The first attempt to study mixed mode SIF using the experimental method of caustics was made by Theocaris and Gdoutos in 1972 [12]. The reflected light from both the front and rear face of an optically

isotropic material was used. Mixed mode SIF was determined by measuring the maximum ( $D_{x \max}$ ) and the minimum ( $D_{x \min}$ ) longitudinal diameters shown in Fig. 2-1d. This technique was used at Iowa State University as a part of this dissertation. It was used for the study of the interaction between two edge cracks and proved not to be a very accurate technique for that specific case. Theocaris [28], Theocaris and Razem [29], improved the technique by introducing the generalized epicycloid axis of symmetry. This axis can be determined experimentally from the inner caustic that results from the reflection of the light from the front face of a transparent material. The angle between the axis of symmetry and the crack axis along with the maximum transverse diameter of the external caustic Fig. 2-1d were used to determine  $K_I$  and  $K_{II}$ . It was established that the axis of symmetry of the reflected caustic represents the crack growth direction for a crack under combined environmental conditions and applied loads [30].

The experimental reflected caustics from nontransparent material and the transmitted caustics are shown in Figs. 2-2 and 2-3 respectively. The transmitted caustic is of better quality than the reflected caustic, but the transmitted caustic does not provide enough information for determining mixed mode SIF. This is due to the lack of information required to establish the axis of symmetry. This is also the case for the reflected caustic from nontransparent materials. From Fig. 2-4 the axis of symmetry can be determined by drawing a perpendicular line to the flanks' tangent and passing through the cusp point. The transmitted caustic is widely used for the determination of  $K_I$  for stationary and propagating cracks under dynamic loading [31,32].

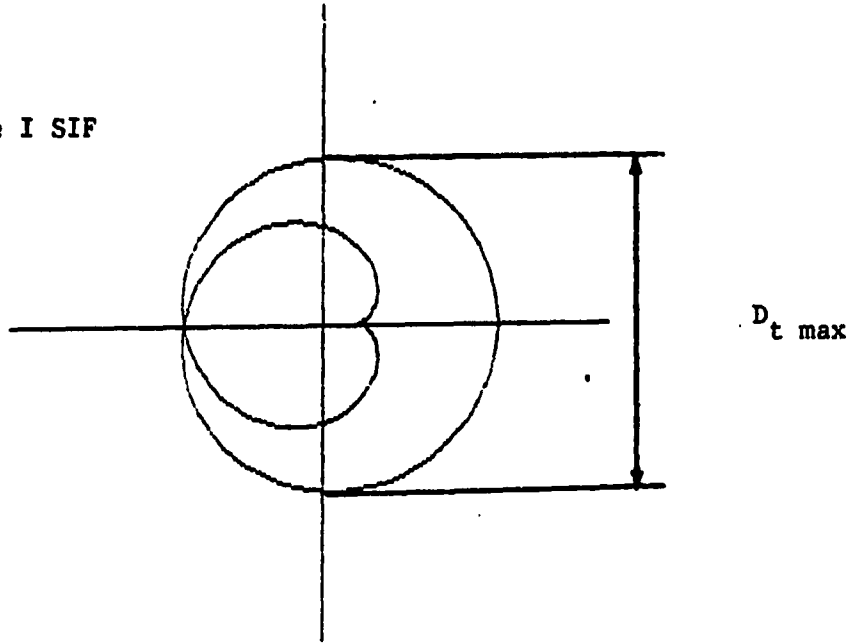
Mixed mode SIF of a crack propagating with constant velocity can be also determined by using the reflected caustics from both the front and rear faces [33].

The reflected caustics from optically isotropic material have been used to study the influence of the boundary or other singularities on the crack tip and then compared to the available analytical solutions. The method was used to study the interaction between two collinear and symmetric edge-cracks in addition to a single edge crack and a straight boundary [34]. It was also used to study the interaction between asymmetric collinear internal cracks of different lengths by varying the distance between the two cracks [35]. Theocaris also extended the method of reflected caustic to study mixed mode SIFs at bifurcated cracks where the side branch subtended different angles to the main branch [36].

Table 2-1. Comparison between four different cases for the epicycloids generated in Fig. 2-1

Fig. No.	$K_I/K_{Ia}$	u
2-1a	1.0	0
2-1b	1.5	0
2-1c	1.0	0.5
2-1d	1.5	0.5

a. Mode I SIF



b. The effect of mode I

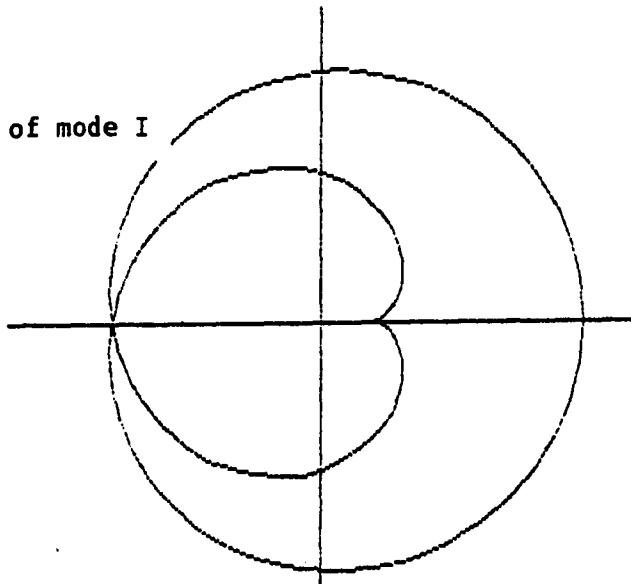
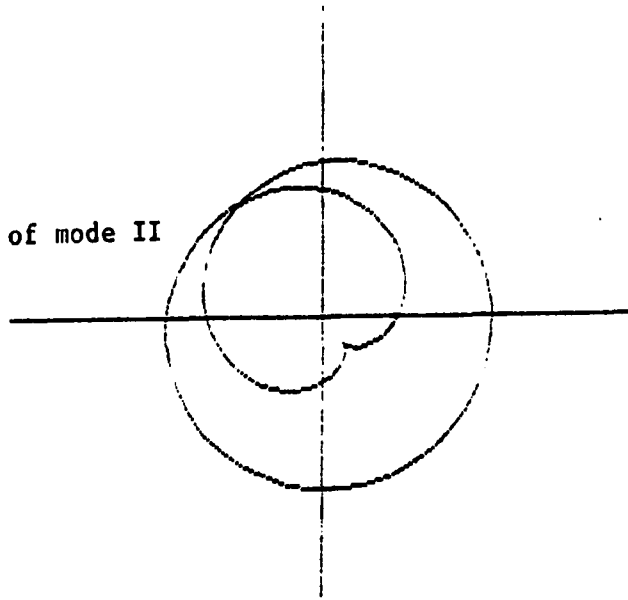


Fig. 2-1. The shape and size of different generalized epicycloids

c. The effect of mode II



d. Mode II techniques

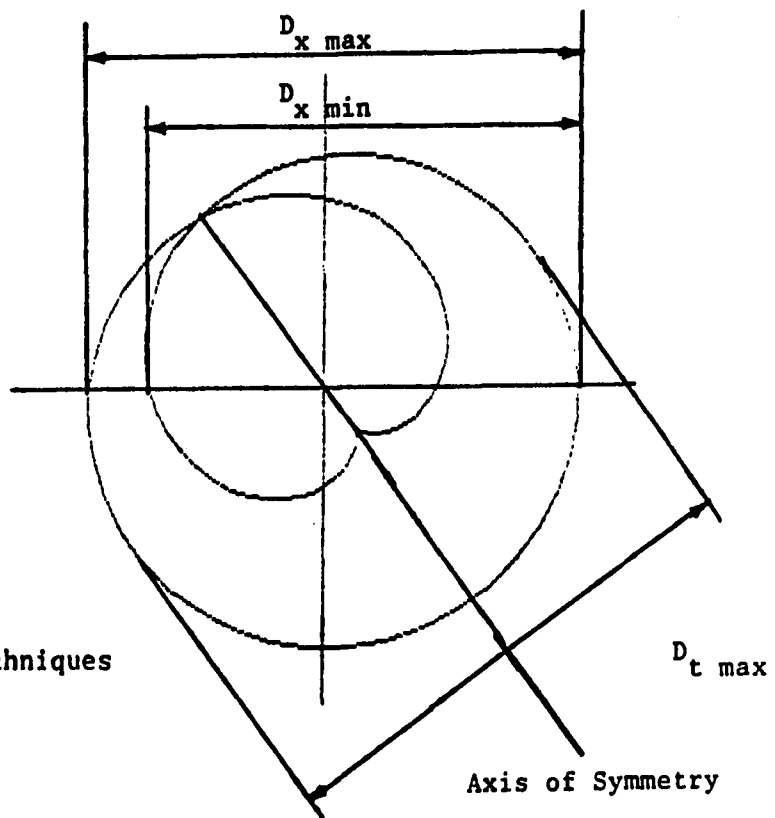


Fig. 2-1. (continued)

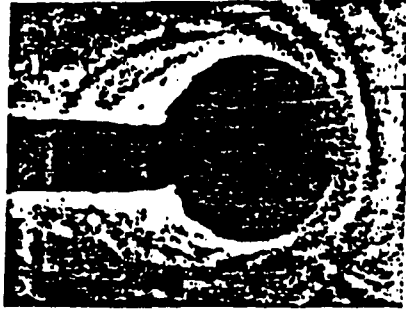


Fig. 2-2. Reflected caustic from a nontransparent material

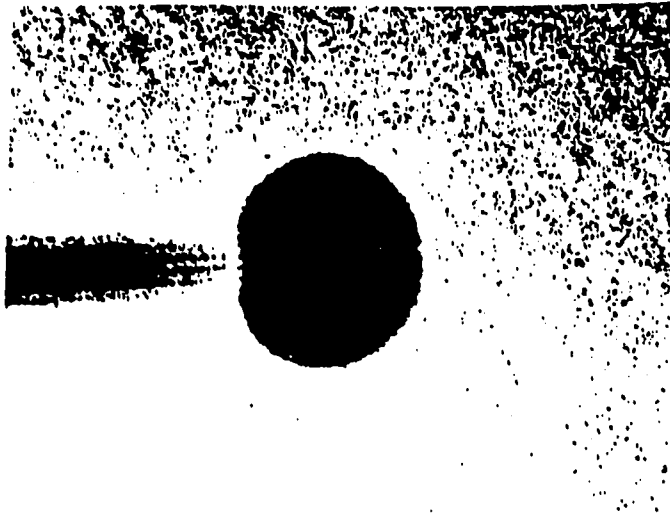


Fig. 2-3. Transmitted caustic through a transparent material



Fig. 2-4. Reflected caustic from a transparent material

### III. PHYSICAL AND MATHEMATICAL PRINCIPLES OF THE METHOD

As discussed in Chapter II, two caustic techniques for the determination of mixed mode stress intensity factors (SIF) have been developed. The two techniques use only a limited amount of data points from a well defined generalized epicycloid and can be applied only on a reflected caustic from a transparent material. The study presented in this dissertation takes advantage of the whole caustic image by taking a number of points from the epicycloid. One of the goals was to establish a new method which eventually will use only the inner caustic to determine SIFs. This would allow the use of the new method for determining mixed mode SIFs on nontransparent materials.

In this chapter, the basic formulas and the procedure for the interpretation of K-factors are presented for the current methods that utilize the method of caustics and the new method. The three available methods are tabulated as, 1) the difference between the longitudinal diameters, 2) the epicycloid's angle of symmetry, and 3) an iterative least squares method. The physical principle and comparison between the theoretical and experimental caustics are discussed. The extent of the three dimensional region of the crack tip stress field and the effects of higher order stress terms are presented.

### A. Physical Principle of the Method of Caustics

The basic physical principle describing the method of caustics is shown in Fig. 3-1 [24]. Due to the high stress concentration in the region surrounding the crack tip, both the thickness and the refractive index of the material change. As a consequence, the area surrounding the crack tip acts similar to a divergent lens and is also called the initial curve. A monochromatic light beam emitted from a He-Ne laser impinges on the stressed cracked specimen. The reason for using laser light beam is that such a beam has a greater intensity than an ordinary light source beam and can be concentrated in the vicinity of the crack tip to produce a clear caustic. Due to the presence of the lens effect very close to the crack tip, the reflected or transmitted light rays are deviated outwards. These deviated rays are concentrated along a strongly illuminated surface in space, which forms the caustic surface. Screens in front and behind the specimen are placed parallel to the specimen and at distances  $Z_0$ . When the caustic surface is projected on these screens a singular curve, called the caustic, is formed on them. Thus, the stress singularity of the elastic field is transformed to an optical singularity represented by the caustic. The shape and dimensions of the caustic, which is always a generalized epicycloid curve, depend on the stress field singularity, material properties and experimental set up.

The caustic is the resulting image of the light beam transmitted or reflected from the divergent lens. The transmitted or reflected light rays are deviated outwards as shown in Fig. 3-1 [24]. Thus, both the

crack tip and the initial curve can not be seen on the caustic image. Therefore, any iteration technique used to locate the individual points on the caustic image should treat the crack tip location as an unknown. Furthermore, the reflected caustic from the front face is related only to the mechanical properties ( $E, \nu$ ) of the material, whereas the transmitted caustic and the reflected caustic from the rear face are related to both the mechanical and optical properties of the material ( $E, \nu, n$ ).

The theoretical and experimental caustics are shown in Fig. 3-2. Both the crack tip and the initial curve can not be seen on the experimental caustics as mentioned earlier. Furthermore, the experimental inner caustic, resulting from the reflection from the front face, is not closed. This is due to the crack opening displacement [37,38].

As mentioned before,  $K_I$  can be determined by measuring the maximum transverse diameter. Theoretically the relevant caustic line should be defined by the transition from the dark inner region to the bright rim of the caustic pattern. Due to the light diffraction effects, the caustic rim will have a band shape rather than a fine line. It was confirmed that correct results would be obtained if the line of maximum light intensity within the bright rim is considered [32,39]. More recently, the wave-optics aspects of caustic analysis has been used [40]. It was suggested that if the mean distance between the shadow edge and the first intensity peak was used, optimum accuracy in evaluating  $K_I$  would be achieved [41].

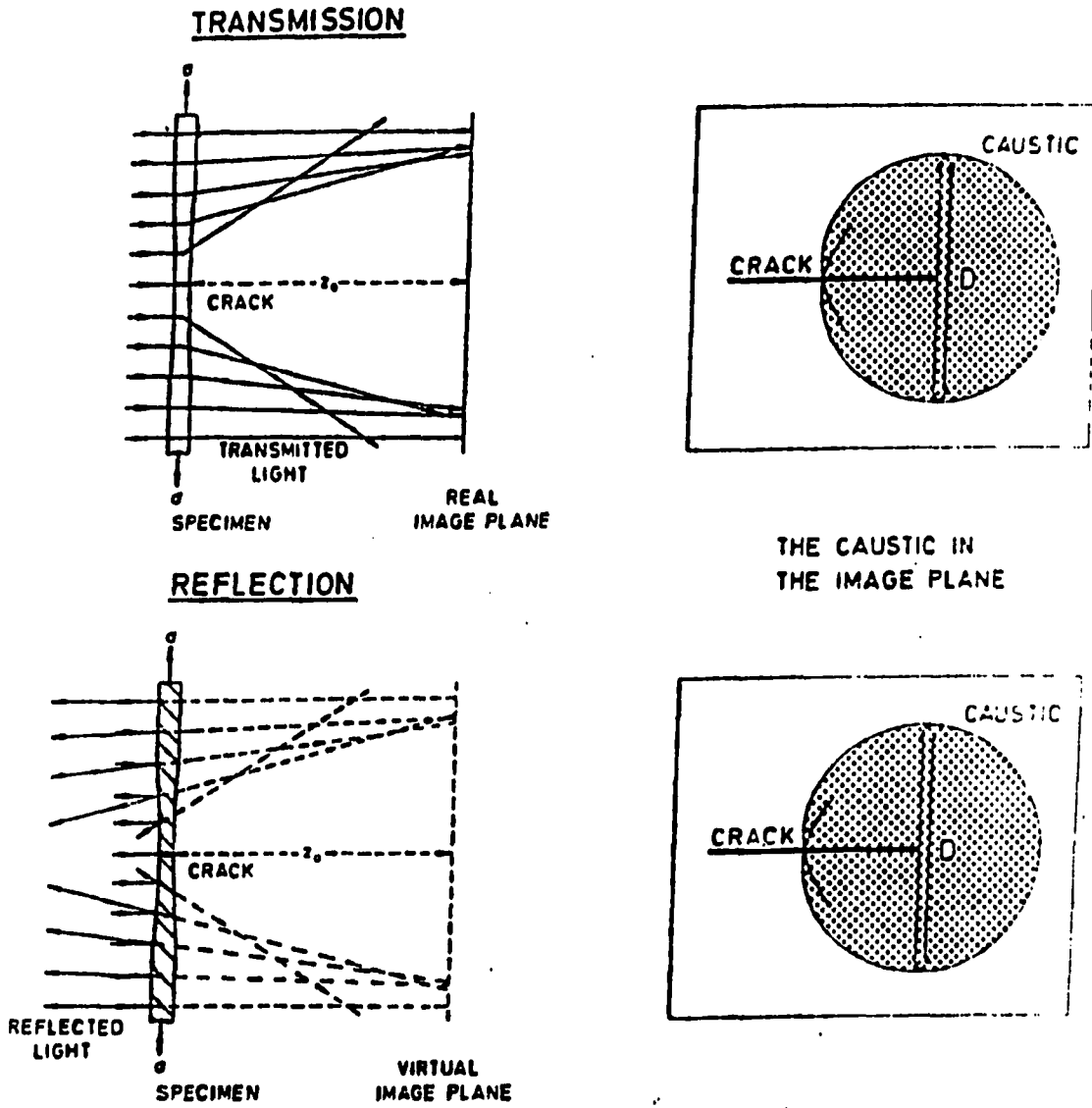


Fig. 3-1. The principle of the method of caustics for transmission and reflection

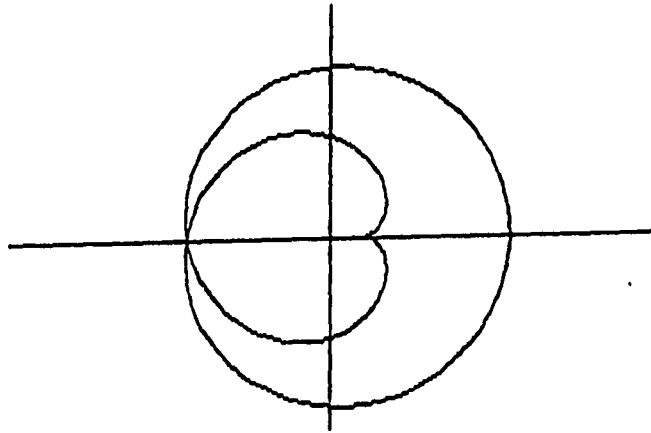


Fig. 3-2. Comparison between the theoretical and experimental caustics

## B. The Basic Formulas and Procedures For Determining Mixed Mode Stress Intensity Factors

The reflected caustics from both the front and rear face of mechanically and optically isotropic materials are considered. The formulas for caustics transmitted or reflected from a nontransparent material are the same except for the optical path changes. The experimental setup is shown in Fig. 3-3. A light beam traverses the specimen at point  $P(r, \nu)$  in the object plane as shown in Fig. 3-4. The nondeflected beam would pass the shadow image plane, also called the reference plane, at point  $P_m$  defining the vector  $\vec{r}_m$ . Due to the presence of the lens, the reflected light beam is displaced to point  $P'(x', y')$  by a vector  $\vec{W}$ .  $\vec{W}$  is a function of the coordinates  $r, \nu$  of point  $P$ . The vector  $\vec{r}'$  of the image point  $P'$  is given as

$$\vec{r}' = \vec{r}_m + \vec{W} \quad (3-1a)$$

When the light is slightly converging or diverging, the image size at the screen is not the same as that at the model. If the image magnification factor is  $\lambda$ , then the vector  $r'$  of the image point  $p'$  becomes

$$\vec{r}' = \lambda \vec{r}_m + \vec{W} \quad (3-1b)$$

The shadow optical image is completely described by Equation (3-1). For each point  $P(r, \nu)$  in the vicinity of the crack tip, the corresponding image point  $P'$  of the shadow image is obtained. After passing the object, the reflected light beams form a caustic on the reference plane. As an envelope, the caustic is a singular curve of the image Equation (3-1) and the necessary condition for the existence of

such a singularity is that the Jacobian determinant is zero

$$\frac{\partial x'}{\partial r} \frac{\partial y'}{\partial v} - \frac{\partial x'}{\partial v} \frac{\partial y'}{\partial r} = 0 \quad (3-2)$$

The vector  $r_m$  is the projection of  $r$  onto the image plane and can easily be determined. The light beam impinges under a small angle of incidence on the specimen. It is partly refracted through the thickness, then partly reflected on the back surface, and again partly refracted through the thickness when emerging from the specimen. This twice refracted and once reflected part of the light ray is absolutely retarded when passing through the specimen according to Maxwell and Neumann's law. The absolute retardation of the light rays depends on the change of the refractive index and the thickness variation of the plate. The emerging wave front satisfies the Eikonal relation [42] according to which the gradient of the geometric wave front  $S$  is constant. The vector  $\vec{W}$  is given as

$$\vec{W}(r, v) = Z_0 \text{ grad } \Delta s(r, v) \quad (3-3)$$

where  $\Delta s$  is the change of the optical path length caused by the specimen and  $Z_0$  is the distance from the model to the screen. The path length change  $\Delta s$  is correlated to the stresses  $\sigma(r, v)$  by the basic elasto-optical equations. The change in the optical path is given by [20]

$$\Delta s = c_r d (\sigma_1 + \sigma_2) \quad (3-4a)$$

$$\Delta s = c_f d (\sigma_1 + \sigma_2) \quad (3-4b)$$

$$\Delta s = c_t d (\sigma_1 + \sigma_2) \quad (3-4c)$$

where  $c_f$  and  $c_r$  are the reflected from the front face and rear face stress optical constants respectively.  $c_t$  is the transmitted caustic

stress optical constant.  $d$  is the optical path thickness,  $\sigma_1$  and  $\sigma_2$  are the principal stresses.

The stresses at each point near the crack tip are given by fracture mechanics equations (2-5). For mixed mode SIF, the sum of the principal stresses are

$$\sigma_1 + \sigma_2 = \sigma_x + \sigma_y = K_I \sqrt{\frac{2}{\pi r}} \cos \frac{\nu}{2} - K_{II} \sqrt{\frac{2}{\pi r}} \sin \frac{\nu}{2} - \sigma_m \quad (3-5)$$

Introducing Equation (3-4) into Equation (3-3) yields

$$\vec{W} = Z_0 d c \text{ grad } (\sigma_1 + \sigma_2) \quad (3-6)$$

where  $c$  is  $c_f$  for the caustic reflected from the front face and  $c_r$  for the reflected caustic from the rear face.

If the sum of principal stresses, Equation (3-5), is introduced in Equation (3-6), the deviation vector  $\vec{W}$  in the cartesian coordinates  $(u, v)$  shown in Fig. 3-3 is given by

$$\vec{W} = \delta r^{-3/2} \left[ \left( K_I \cos \frac{\nu}{2} - K_{II} \sin \frac{\nu}{2} \right) \hat{u} + \left( K_I \sin \frac{\nu}{2} + K_{II} \cos \frac{\nu}{2} \right) \hat{v} \right] \quad (3-7)$$

$$\text{Where } \delta = \frac{Z_0 dc}{(2\pi)^{1/2}} \quad (3-8)$$

From equations (3-1) and (3-7) the vector  $\vec{r}'$  in the cartesian coordinates  $(x, y)$  is

$$\begin{aligned} \vec{r}' = x\hat{i} + y\hat{j} = & \left[ r \cos \nu + \delta r^{-3/2} \left( K_I \cos \frac{3}{2} \nu - K_{II} \sin \frac{3}{2} \nu \right) \right] \hat{i} \\ & + \left[ r \sin \nu + \delta r^{-3/2} \left( K_I \sin \frac{3}{2} \nu + K_{II} \cos \frac{3}{2} \nu \right) \right] \hat{j} \end{aligned} \quad (3-9)$$

The evaluation of  $J=0$  gives

$$r = r_0 = (3\delta/2\lambda)^{2/5} (K_I^2 + K_{II}^2)^{1/5} \quad (3-10)$$

Equation (3-10) indicates that the constrained zone around the crack tip subjected to mixed mode deformation is a circle of radius  $r_0$  and is function of  $K_I$ ,  $K_{II}$ , the distance  $Z_0$  and the model thickness  $d$ . Using Equation (3-10) in Equation (3-9) then the image equations become (' means screen coordinates)

$$x' = r_0 \left[ \cos v + \frac{2}{3} (1+u^2)^{-1/2} \cos \frac{3}{2} v - \frac{2}{3} u(1+u^2)^{-1/2} \sin \frac{3}{2} v \right] \quad (3-11a)$$

$$y' = r_0 \left[ \sin v + \frac{2}{3} (1+u^2)^{-1/2} \sin \frac{3}{2} v + \frac{2}{3} u(1+u^2)^{-1/2} \cos \frac{3}{2} v \right] \quad (3-11b)$$

where  $u$  is the ratio of  $K_{II}/K_I$ . The angle  $v$  varies between 0 and  $4\pi$ , and the caustic image has the generalized epicycloid shape shown in Fig. 3-5. The points on the epicycloid are located by drawing a vector of magnitude  $2r_0(1+u^2)^{-1/2}/3$  from the initial curve of radius  $r_0$ . This vector forms an angle of  $3v/2$  with the  $x$  axis. From the end of this vector another vector of magnitude  $2r_0 u(1+u^2)^{-1/2}/3$  is drawn counterclockwise perpendicular to the first vector.

Solving relation (3-10) for  $K_I$  and  $K_{II}$  yields

$$K_I = \frac{1.671 r_0^{5/2}}{Z_0 d c (1+u^2)^{1/2}} \quad (3-12a)$$

$$u = K_{II}/K_I \quad (3-12b)$$

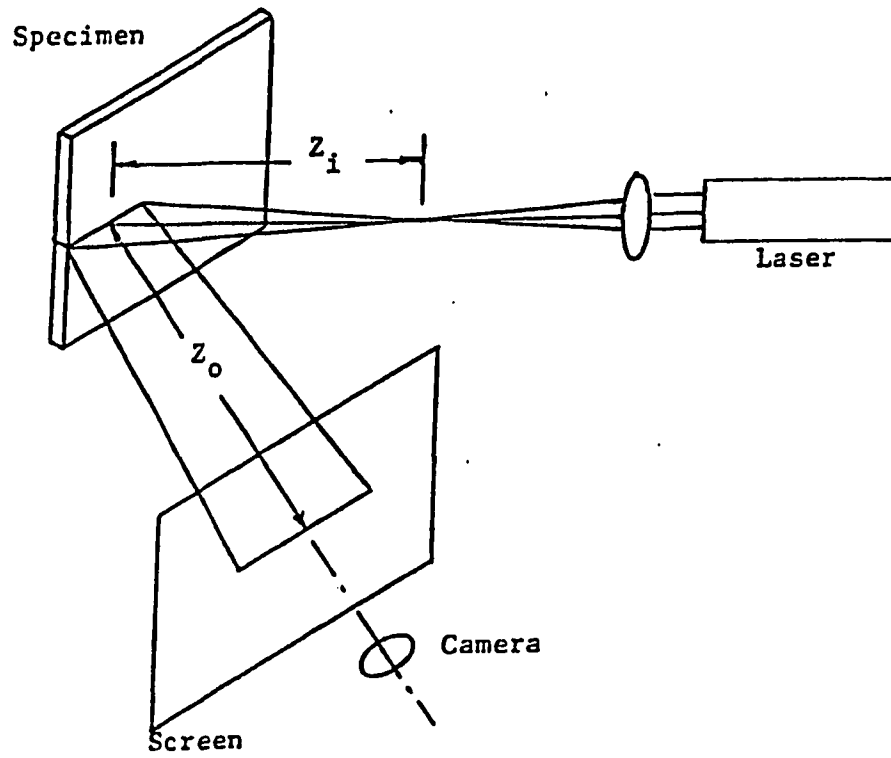


Fig. 3-3. Schematic reflected caustic setup

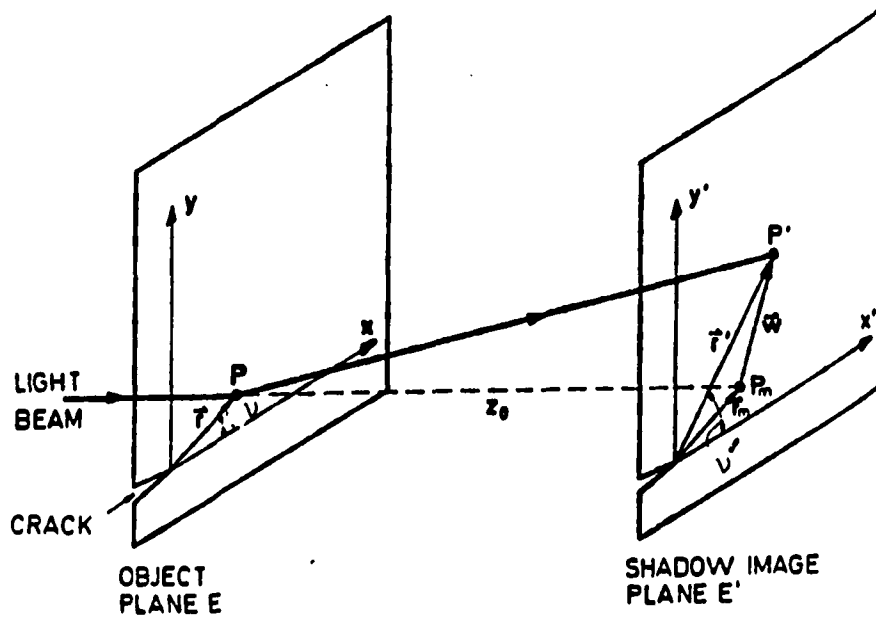


Fig. 3-4. Geometrical conditions of the caustic analysis

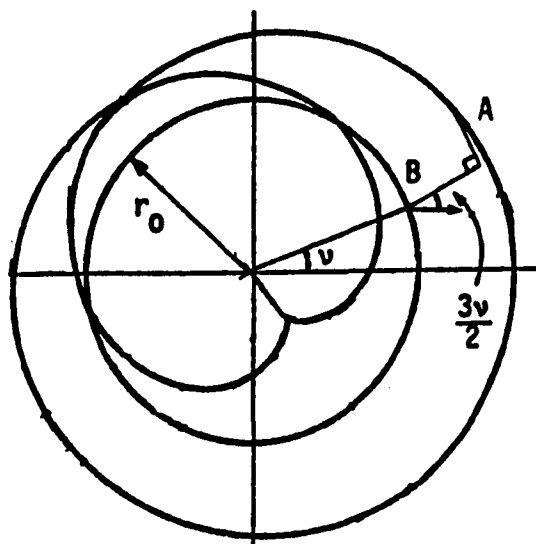


Fig. 3-5. Theoretical form of the caustic formed at a crack tip for  $K_{II}/K_I=0.5$

The current methods that utilize the method of caustics and the new method for the determination of mixed mode stress intensity factors are as follows.

1. The difference between the longitudinal diameters method [12,18,28]

This method was introduced by Theocaris and Gdoutos in 1972 [12] as a first attempt that utilizes the method of caustics to extract mixed mode stress intensity factors. This method was developed for the determination of mixed mode SIFs in internal symmetric cracks at different angles.

It can be concluded from equation 3-11 that the shape of the generalized epicycloid depends on the ratio  $u$  of the stress intensity factors. Four types of generalized epicycloids for different values of  $u$  are shown in Fig. 3-6. For  $u=0$ , the epicycloid is symmetric to the  $x$ -axis, which coincides with the crack direction. For  $u$  larger than 0 the epicycloids are asymmetric and their tails cut the negative  $x$ -axis at different points. As the values of  $u$  are increasing, the area contained by each principal generalized epicycloid is decreasing. Fig. 3-7 [12] shows the variation of the maximum longitudinal diameter  $D_{x \max}$ , the transverse diameter  $D_t$ , and the minimum longitudinal diameter  $D_{x \min}$  as normalized to the initial curve radius  $r_0$  versus the ratio  $u$ . The definitions of the symbols used in Fig. 3-7 are  $d_1=D_{x \max}/r_0$ ,  $d_2=D_t/r_0$ , and  $d_3=D_{x \min}/r_0$ . Each of the generalized epicycloids corresponding to each value of  $u$  has some particular properties, which are invariant. Thus, it is possible to make use of these invariant properties for interrelating the shape of the epicycloid to the corresponding value of  $u$ . Theocaris and Gdoutos concluded that

the most sensitive property is the distance along the negative x-axis. The ratio  $(D_{x \max} - D_{x \min})/D_{x \max}$  can be determined from the intersections of the curve with the x-axis. Fig. 3-8 [12] presents the variation of the ratio  $\phi = (D_{x \max} - D_{x \min})/D_{x \max}$  versus  $u$ . Introducing the terms  $\delta_{\max} = D_{x \max}/r_0$ ,  $\delta_t = D_t/r_0$ , and  $\delta_{\min} = D_{x \min}/r_0$  into Equation (3-12) gives

$$K_I = \frac{1.671}{Z_0 dc \lambda^{3/2} (1+u^2)^{1/2}} (D/\delta)^{5/2} \quad (3-13a)$$

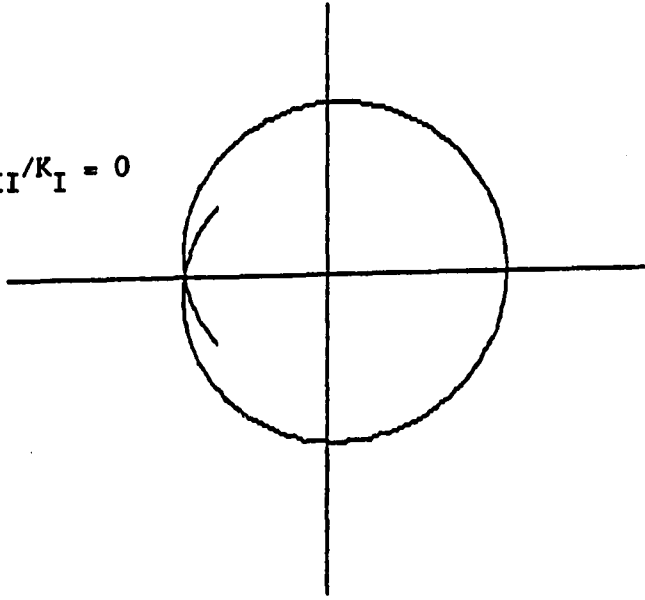
$$u = K_{II}/K_I \quad (3-13b)$$

where  $c$  is the reflected from the rear face stress optical constant. The ratio  $D/\delta$  takes any of the values  $D_{x \max}/\delta_{\max}$ ,  $D_t/\delta_t$ ,  $D_{x \min}/\delta_{\min}$ . Thus, mixed mode SIFs can be determined by determining the ratio  $\phi$  from the experimental caustic image. With the experimental value of  $\phi$ , Fig. 3-8 give the corresponding value of  $u$  which can be used in Fig. 3-7 and Equation (3-13) for the determination of  $K_I$  and  $K_{II}$ .

Some of the generalized epicycloid properties were studied by Theocaris [20]. The maximum distance from the crack tip to the caustic curve is  $OM$  shown in Fig. 3-9.  $OM = 5r_0/3$ . The minimum distance is from the crack tip to the cusp point  $ON$  and  $ON = r_0/3$ . Therefore, the crack tip can be located by measuring the distance  $b$  shown in Fig. 3-9 and  $OM/ON = 4$ . The disadvantages of this method are:

1. The difference between  $D_{x \max}$  and  $D_{x \min}$  can not be seen in many experimental situations. For example see Figs 2-2 and 2-4.
2. The crack tip location can not be determined accurately in actual caustic experiments.

a.  $K_{II}/K_I = 0$



b.  $K_{II}/K_I = 0.2$

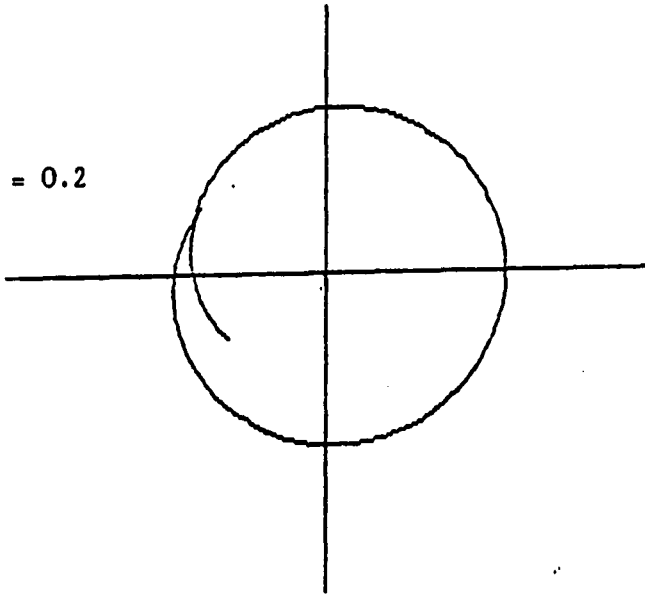
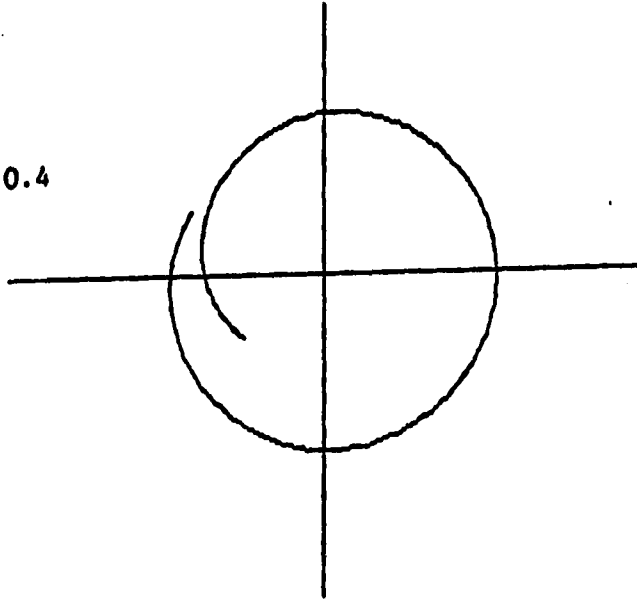


Fig. 3-6. Variation of the theoretical form of the caustic with the ratio  $K_{II}/K_I$

c.  $K_{II}/K_I = 0.4$



d.  $K_{II}/K_I = 0.6$

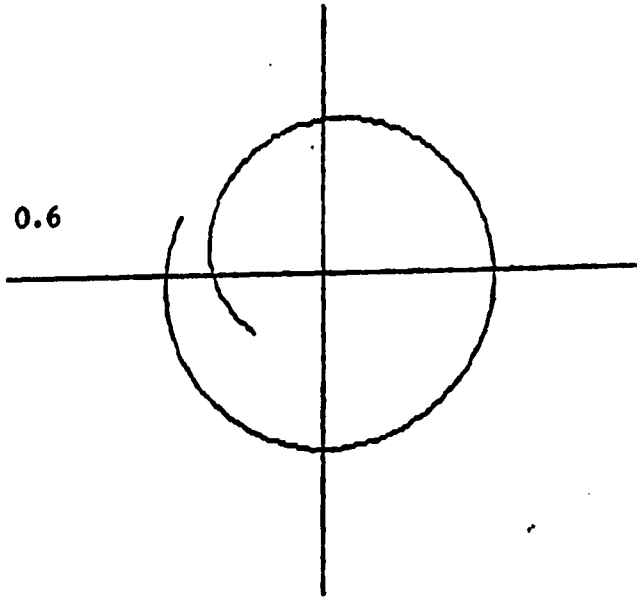


Fig. 3-6. (continued)

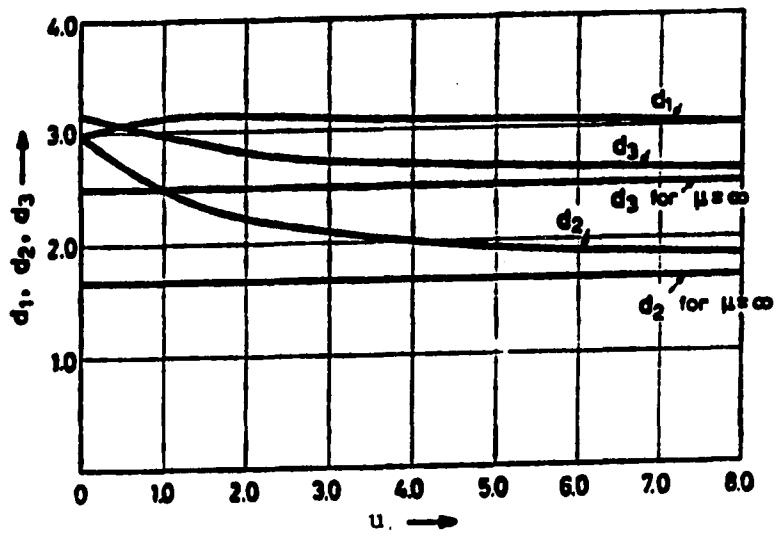


Fig. 3-7. Variation of  $d_1$ ,  $d_2$  and  $d_3$  with  $u$

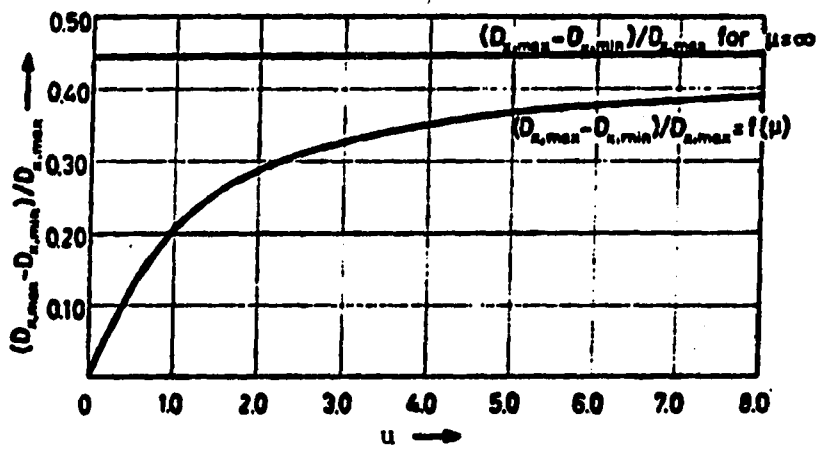


Fig. 3-8. Variation of the ratio  $(D_{x,max} - D_{x,min}) / D_{x,max}$  with  $u$

## 2. The epicycloid's angle of symmetry method [18,20,28,29]

Theocaris improved this technique by relating mixed mode SIFs to the maximum transverse diameter and the axis of symmetry of the generalized epicycloid. Introducing the complex stress intensity factor  $K^* = K_I - iK_{II}$ , that is  $|K^*|^2 = (K_I^2 + K_{II}^2)$ . Defining the argument of the complex SIF  $K^*$  as  $-\omega$ , Equation (3-11) can be written as

$$x' = r_0 \left[ \cos v + \frac{2}{3} \cos\left(\frac{3}{2}v + \omega\right) \right] \quad (3-14a)$$

$$y' = r_0 \left[ \sin v + \frac{2}{3} \sin\left(\frac{3}{2}v + \omega\right) \right] \quad (3-14b)$$

Taking into consideration that  $z' = x' + iy' = \rho \exp(i\phi)$ , it can be shown that the epicycloid is a symmetric curve to the x axis which subtends an angle to  $-2\omega$  with the x-axis. Furthermore, the maximum transverse diameter  $D_{t \max} = 3.17r_0$ . Then mixed mode SIFs can be determined from

$$K_I = 0.3735(D_t/\lambda)^{5/2}(1+u^2)^{-1/2}/|C| \quad (3-15a)$$

$$K_{II} = 6.6843(r_0/\lambda)^{5/2}(1+u^2)^{-1/2}/|C| \quad (3-15b)$$

where

$$u = \tan \omega = \tan(\theta_0/2) \quad (3-16)$$

$|C|$  is the overall constant =  $4cZ_0 t/\lambda$

Thus, mixed mode SIFs can be determined by using the angle between the axis of symmetry and the crack axis along with the maximum transverse diameter. The axis of symmetry can be determined by drawing a perpendicular line to the flanks' tangent and passing through the cusp point as shown in Fig. 3-9. It has been proven that the maximum transverse diameter is always parallel to the common tangent of the cusp internal caustic.

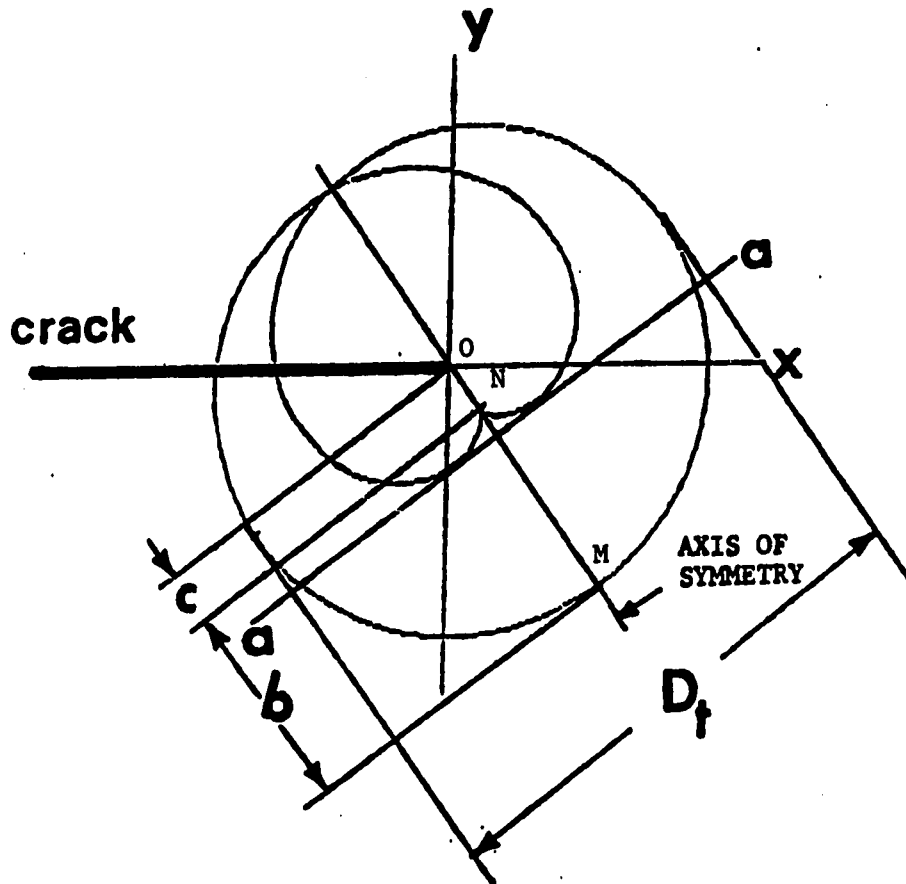


Fig. 3-9. The epicycloid's angle of symmetry

### 3. An iterative least-squares method

The two previous techniques use only a limited amount of data from the well defined generalized epicycloid to extract  $K_I$  and  $K_{II}$ . If there are errors in locating these data points, then the accuracy of the  $K_I$  and  $K_{II}$  results suffer. Furthermore, the two techniques can be applied to only the reflected caustics from a transparent material. In order to reduce the amount of possible error, more data points from the generalized epicycloid should be taken. Then by locating a number of data points on the inner and outer caustics  $r_0$ ,  $K_I$  and  $K_{II}$  can be determined. One of the goals of this dissertation was to eventually use the inner caustic to determine mixed mode stress intensity factors. This would allow the use of the method on nontransparent models which is of most interest. The least squares method has been applied to photoelastic problems by taking a number of data points from the whole field fringe pattern [43]. In order to use the whole caustic pattern an overdeterministic approach is used. A number of points from the generalized epicycloid are located. One problem that is immediately noted is that the location of the crack tip is obscured by the caustic as discussed earlier. Thus, the method presented treats the crack tip location as an unknown along with  $K_I$ ,  $K_{II}$  and  $r_0$ .

In Fig. 3-10a a line is drawn from the initial curve circumference to the point on the epicycloid. If  $\psi$  denotes the angle ABC it can be seen that the angle  $\psi$  is related to the mixed mode SIFs as follows

$$\tan \psi = AC/BC = u \quad (3-17)$$

Therefore, from Equations (3-16) and (3-17) it is found that  $\psi = \omega$ . From Fig. 3-10a it is seen that

$$\omega + \nu/2 = \theta \quad (3-18)$$

and

$$AB = 2r_0/3 \quad (3-19)$$

where  $\theta$  is the angle from the initial curve circumference to the axis of symmetry of the epicycloid. If  $(x_0, y_0)$  is the estimated location of the crack tip, then the measured length between the estimated crack tip and the point on the caustic (inner or outer) LM can be determined from Fig. 3-10b

$$LM = [(x-x_0)^2 + (y-y_0)^2]^{1/2} \quad (3-20)$$

From Fig 3-10a and by using the law of cosines

$$LE = [r_0(13+12 \cos \theta/2)]^{1/2}/3 \quad (3-21)$$

where LE is the distance from the expected crack tip location to the point on the epicycloid (inner or outer). By using the law of sines, the angle  $\alpha$  can be determined as

$$\sin \alpha = \frac{2 \sin \theta/2}{(13 + 12 \cos \theta/2)^{1/2}} \quad (3-22)$$

For a perfect fit the residuals  $\epsilon$  between LE and LM would be zero. However, the residuals are generally not zero and a best fit can be obtained by making them as small as possible. This is accomplished when the sum of the squares of the residuals is minimum [44]. That is

$$\sum_{i=1}^n (LE-LM)_i^2 = \sum_{i=1}^n [g_i(r_0, x_0, y_0, \theta_0)]^2 = \sum_{i=1}^n (\epsilon_i)^2 = \text{minimum} \quad (3-23a)$$

where  $n$  is the number of data points and must be larger than 4.

Minimizing the sum of squares of the residuals yields

$$\sum_{i=1}^n g_i \frac{\partial g_i}{\partial A_j} = 0 \quad (3-23b)$$

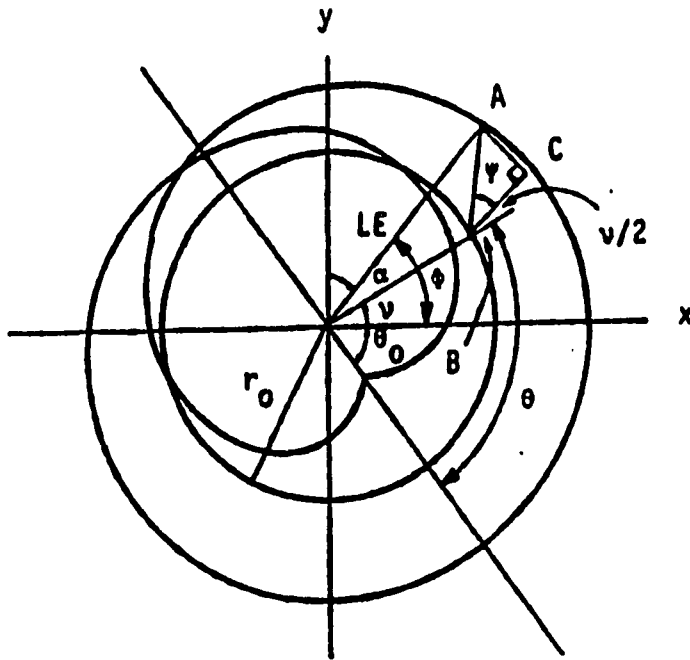


Fig. 3-10a. Geometry of the principal epicycloid

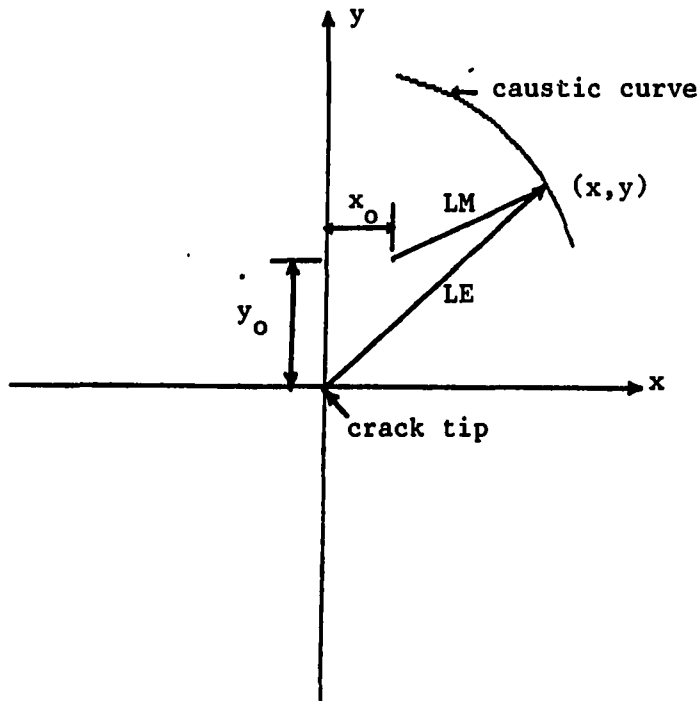


Fig. 3-10b. The difference between LM and LE

where  $A_j = (r_o, x_o, y_o, \theta_o)$ . If  $g_i$  is evaluated at initial values  $(r_{op}, x_{op}, y_{op}, \theta_{op})$ , the function  $g_i$  can be found using a Taylor series expansion [45].

$$g_i(A_j) = g_i(A_{jp}) + \sum_{k=1}^4 \left[ \frac{\partial g_i}{\partial A_k} \right]_{A_k=A_{kp}} (A_j - A_{jp}) \quad (3-24)$$

The initial values may be intelligent guesses or preliminary estimates based on available information. From equations (3-23) and (3-24)

$$[M] [B] = - [M] [M]^T [\Delta A] \quad (3-25)$$

where

$$[M] = \begin{bmatrix} \frac{\partial g_1}{\partial r_o} & \cdot & \cdot & \frac{\partial g_n}{\partial r_o} \\ \frac{\partial g_1}{\partial x_o} & \cdot & \cdot & \cdot \\ \frac{\partial g_1}{\partial y_o} & \cdot & \cdot & \cdot \\ \frac{\partial g_1}{\partial \theta_o} & \cdot & \cdot & \frac{\partial g_n}{\partial \theta_o} \end{bmatrix} \quad (3-26a)$$

$$[\Delta A] = \begin{bmatrix} \Delta r_o \\ \Delta x_o \\ \Delta y_o \\ \Delta \theta_o \end{bmatrix} \quad (3-26b)$$

$$[B] = \begin{bmatrix} g_1 \\ g_2 \\ \cdot \\ \cdot \\ g_n \end{bmatrix} \quad (3-26c)$$

$$g_i = \frac{r_0}{3} (13+12 \cos \frac{\theta_i}{2})^{1/2} - [(x_i-x_0)^2+(y_i-y_0)^2]^{1/2} \quad (3-27)$$

The angle of the points on the caustic with respect to the estimated crack tip is

$$\phi_i = \arctan \frac{y_i - y_0}{x_i - x_0} \quad (3-28)$$

The angles are positive counterclockwise. From Fig. 3-10 the angle  $\theta$  can be found from

$$\theta_i = \phi_i - \arcsin \left( \frac{2 \sin \theta_i/2}{(13+12 \cos \theta_i/2)^{1/2}} \right) - \theta_0 \quad (3-29)$$

All iterative procedures require initial values of the parameters to be determined. All available information should be used to make these starting values as reliable as possible. Good starting values will often allow an iterative technique to converge to a solution fast. The procedure for determining the best fit values of the four unknowns ( $r_0$ ,  $x_0$ ,  $y_0$ ,  $\theta_0$ ) is as follows:

1. Assume initial values of  $r_0$ ,  $x_0$ ,  $y_0$ ,  $\theta_0$ . A technique for estimating  $x_0$  and  $y_0$  utilizes the fact that  $b/c = 4$  in Fig. (3-9). The distance  $b$  can be measured from the caustic and is used in estimating the crack tip location [28]. The initial curve value can be estimated by measuring the maximum transverse diameter where  $D_{t \max} = 3.17 r_0$ . The angle between the axis of symmetry and the crack direction gives an estimate for  $\theta_0$ . A nonzero positive value for  $r_0$  is used. No difficulties were encountered even with  $r_0$  being 1/3 or 3 times the actual value.
2. Evaluate  $\phi_i$  from equation (3-28) for each data point.

3. Compute  $\theta_i$  from equation (3-29) for each data point by FNROOT program [46].
4. Evaluate the elements of matrices [M] and [B] for each data point from equations (3-26a) and (3-26c) respectively.
5. Compute [ΔA] by Gauss Elimination method from equation (3-25).
6. Repeat steps 2, 3, 4 and 5 with

$$(r_o)_{n+1} = (r_o)_n + \Delta r_o \quad (3-30a)$$

$$(x_o)_{n+1} = (x_o)_n + \Delta x_o \quad (3-30b)$$

$$(y_o)_{n+1} = (y_o)_n + \Delta y_o \quad (3-30c)$$

$$(\theta_o)_{n+1} = (\theta_o)_n + \Delta \theta_o \quad (3-30d)$$

until the absolute average error [ΔA] becomes small using CAUSTIC 1 program [47]. See the appendix for listing of the program.

7. Calculate  $K_I$  and  $K_{II}$  using Equations (3-15) and (3-16).

Several epicycloids with different sizes and shapes were generated similar to the one shown in Fig. 3-9. A digital image analysis system was used to determine the coordinates of selected points on the caustic. The crack tip was treated as unknown, the initial curve value was assumed to be 50% of its real value and the angle of symmetry was taken to be  $30^\circ$  the actual value. The angle  $\nu$  must range from 0 to  $4\pi$  in order for the complete caustic to be traced and obviously the angle  $\phi$  has the same range. Without additional information the computer program can not tell whether or not a point on the caustic is in the 0 to  $\pi$ ,  $\pi$  to  $2\pi$ ,  $2\pi$  to  $3\pi$  or  $3\pi$  to  $4\pi$  range for  $\phi$ . In actual experimental situations, the regions on the inner caustic from point a to b and point c to a are not visible because of the crack opening displacement. The

visible inner caustic regions bc and cd (the only parts of the inner caustic considered) are in the range of  $\phi$  between  $\pi$  to  $2\pi$ ,  $2\pi$  to  $3\pi$  respectively. The distinction of these two regions during the iteration was made from the fact that the distance LM is always less than the initial curve radius  $r_0$  as shown in Fig. 3-11 and  $\phi$  equals  $\phi+2\pi$ . The region oa of the outer caustic can be picked automatically since it is in the range 0 to  $\pi$ . Although the region ae (due to  $K_{II}$ ) of the outer caustic seems to be in the range 0 to  $\pi$ , it is actually part of the region in the range  $2\pi$  to  $3\pi$ . This part is predicted from the fact  $\phi-\theta_0$  is less than  $\pi$ , LM is greater than  $r_0$  and  $\phi$  is  $\phi+2\pi$ . The region eo of the outer caustic is in the range  $3\pi$  to  $4\pi$  as predicted from the negative  $\phi$  and then  $\phi=4\pi-\phi$ . The differences between the actual  $r_0$  and  $\theta_0$  values and the iterative least squares technique (ILSM) values were extremely small as shown in Table 3-1.

Table 3-1. Comparison between the generalized epicycloids and ILSM

Parameter	Generated values	Initial estimates	ILSM results
$r_0$	1.5	0.5	1.5132
$K_{II}/K_I$	0	0.4	$1.368 \times 10^{-4}$
$r_0$	1.0	2.5	1.0256
$K_{II}/K_I$	0.15	0	0.1526
$r_0$	1.5	3.0	1.4965
$K_{II}/K_I$	0.3	- 0.2	0.296

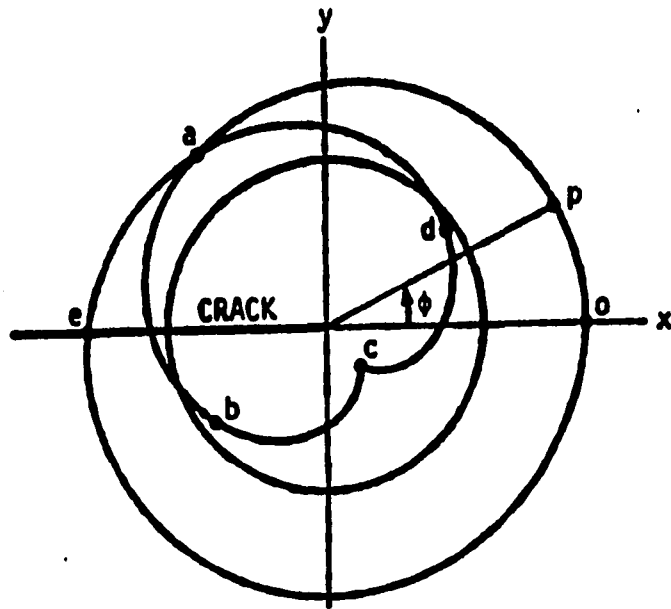


Fig. 3-11. Regions of the generalized epicycloid for  $\phi$  of 0 to  $4\pi$

### C. The Three Dimensional Effects and The Effects of the Presence of Higher Order Terms

It has been demonstrated experimentally that the radius  $r_0$  of the initial curve affects the results and it is necessary to use a value of  $r_0$  larger than a definite one [48]. The extent of the three dimensional region of the crack tip stress field has been investigated. It was concluded that plane stress conditions prevail at distances from the crack tip greater than 0.5 times the plate thickness [49]. It has been demonstrated that if  $r_0$  is not large enough in comparison to the thickness of the specimen the three dimensional effects produce significant errors and  $r_0$  should be at least 0.4 times the plate thickness [50].

The analysis of the caustic equations are based on neglecting the higher order terms in Equations (2-4) and (2-5). Neglecting higher order terms could produce significant errors in determining stress intensity factors. It was demonstrated theoretically that, except in extreme cases, the shape of the caustic is virtually unaffected by the presence of higher order terms. However, neglecting the higher order terms can result in significant errors when the crack in a birefringent material approaches the boundary [14,51,52,53]. It was proven experimentally that the near field solution (neglecting higher order terms) is accurate using optically isotropic materials. It was concluded that there is no necessity to resort to higher approximation solutions [54].

#### D. Methods of Determining the Stress Optical Constants

In addition to the experimental setup and the model thickness,  $K_I$  and  $K_{II}$  depend on the stress-optical constant for either the transmitted or reflected caustic (Equations 3-13a and 3-15). Studies that utilize the method of caustics usually use an optically isotropic material (PMMA, plexiglas) to extract  $K_I$  and  $K_{II}$  although a birefringent model material can also be used.

The experimental method of caustics has been used on cracked plates subjected to an uniaxial tensile load to determine the transmitted and reflected stress-optical constant. The maximum transverse diameters of the two caustics are used along with Poisson's ratio, Young's modulus, and the two magnification factors to determine the optical constants. A new technique has been developed to determine stress-optical constants for the transmitted caustic and the caustic reflected from the rear face of the model. The method does not require the use of Poisson's ratio or Young's modulus. The reflected caustic from the plate with a small circular hole will directly give the reflected stress optical constant. The transmitted caustic will directly give the transmitted stress-optical constant.

The current method and the new technique for the determination of the stress optical constants are as follows.

##### 1. The technique of using a cracked plate [55,56]

If a cracked plate is subjected to the opening mode only, then Equation (3-15) becomes

$$K_I = 0.3735 (D_t/\lambda)^{5/2} / |2c_r'| \quad (3-31)$$

For the transmitted caustic the opening mode can be determined from

$$K_I = 0.3735 (D_t/\lambda)^{5/2} / |c_t| \quad (3-32)$$

where  $c_t$  is the transmitted stress-optical constant. If the magnification factors for the transmitted and reflected caustics are not the same, then from Equations (3-31) and (3-32),  $c_r$  is related to  $c_t$  by

$$\frac{2c_r}{c_t} = \left(\frac{D_{tr}}{D_{tt}}\right)^{5/2} \left(\frac{\lambda_r}{\lambda_t}\right)^{3/2} \quad (3-33)$$

where  $D_{tr}$  and  $D_{tt}$  are the reflected and transmitted caustics transverse diameters, respectively.

The change of the optical path of the reflected light from the rear face (Mach-Zehnder interferometer) is given by Equation (3-4a). The change of the optical path of the transmitted light (Fizeau interferometer) is

$$\Delta s = c_t d(\sigma_1 + \sigma_2) \quad (3-34)$$

It has been proven that the relationship between  $c_t$  and  $c_r$  [53-54-57-58] is

$$c_r = c_t + \nu/E \quad (3-35)$$

where  $\nu$  is the Poisson's ratio and  $E$  is Young's modulus.

Thus the stress optical constants can be determined from Equations (3-34) and (3-35). This can be done by determining  $D_{tr}$ ,  $D_{tt}$ ,  $\nu$ ,  $E$ , and the magnification factors.

## 2. The technique of using a circular hole in a plate

There is no need to obtain both caustics if only one stress optical constant is needed. The first technique has been used to determine the transmitted and reflected stress-optical constants. The maximum transverse diameters of the two caustics are used along with Poisson's ratio, Young's modulus and the two magnification factors to determine the optical constants. Any measurement error in any of the six quantities will result in errors in both stress optical constants.

A new technique has been developed to determine both the transmitted constant and the reflected constant associated with the light reflected from the rear face of the plate. The physical principle of the method of caustics is extended to the determination of the stress-optical constant by applying the method of caustics in the region very close to a circular hole in a thin plate. Due to the high stress concentration in the region surrounding the hole, both the thickness and the refractive index of the material will change. As a consequence, the area surrounding the hole acts similar to a divergent lens. A thin plate of infinite length and width with a circular hole subjected to a uniform tensile stress in the y direction as shown in Figure 3-12 is considered. The two dimensional stress field about the hole can be determined by the following stress equations in polar coordinates given by [59].

$$\sigma_r = \frac{\sigma_0}{2} \left\{ \left( 1 - \frac{a^2}{r^2} \right) \left[ 1 + \left( \frac{3a^2}{r^2} - 1 \right) \cos 2\theta \right] \right\} \quad (3-36a)$$

$$\sigma_\theta = \frac{\sigma_0}{2} \left\{ \left( 1 + \frac{a^2}{r^2} \right) + \left( 1 + \frac{3a^4}{r^4} \right) \cos 2\theta \right\} \quad (3-36b)$$

$$\tau_{r\theta} = \frac{\sigma_0}{2} \left[ \left(1 + \frac{3a^2}{r^2}\right) \left(1 - \frac{a^2}{r^2}\right) \sin 2\theta \right] \quad (3-36c)$$

where  $\sigma_0$  is the uniform stress in the y direction and a is the circular hole radius. Following Equations (3-1) to (3-6), the only change is the stress Equation (3-5). Using Equations (3-36), the sum of the principal stresses  $\sigma_1$  and  $\sigma_2$  for a thin, infinite plate with a circular hole subjected to uniaxial tensile load is

$$\sigma_1 + \sigma_2 = \frac{\sigma_0}{2} \left( 2 + \frac{4a^2}{r^2} \cos 2\theta \right) \quad (3-37)$$

where  $\sigma_0$  is the uniform stress in the y direction and a is the circular hole radius. From equations (3-6) and (3-37)

$$W = Z_0 d c_{r,t} \frac{\sigma_0}{2} \left( 2 + \frac{4a^2}{r^2} \cos 2\theta \right) \quad (3-38)$$

$c_{r,t}$  is the reflected from the rear face and the transmitted stress-optical constant, respectively. d is the optical path thickness. The vector W in the cartesian coordinates (u, v) is

$$W = \delta r^{-3} (\cos 2\theta u + \sin 2\theta v) \quad (3-39)$$

where

$$\delta = 4Z_0 c d \sigma_0 a^2 \quad (3-40)$$

c is  $c_t$  for transmitted case and  $c_r$  for the light reflected from the rear face. From Equations (3-1) and (3-39), the vector  $r'$  is

$$r' = xi+yj = (r \cos \theta + \delta r^{-3} \sin 3\theta)i + (r \sin \theta + \delta r^{-3} \sin 3\theta)j \quad (3-41)$$

The caustic is a singular curve and should satisfy Equation (3-2). The evaluation of  $J=0$  gives

$$r = r_0 = (3\delta)^{1/4} = (12Z_0 c d a^2)^{1/4} \quad (3-42)$$

Equation (3-42) indicates that the constrained zone around the circular hole subjected to uniaxial tensile load  $\sigma_0$  is a circle of radius  $r_0$  and is a function of the hole size, the distance  $Z_0$  and the model thickness  $d$ . When the light is slightly converging or diverging, the image size at the screen is not the same as that at the model. If the image magnification factor is  $\lambda$  and substituting Equation (3-42) in Equation (3-41), then the image equations becomes (' means screen coordinates)

$$x' = \lambda r_0 \left( \cos \theta + \frac{1}{3} \cos 3\theta \right) \quad (3-43a)$$

$$y' = \lambda r_0 \left( \sin \theta + \frac{1}{3} \sin 3\theta \right) \quad (3-43b)$$

The angle  $\theta$  varies between 0 and  $2\pi$ , and the theoretical caustic image has the shape shown in Fig. 3-13. The points on the caustic are located by drawing a vector of magnitude  $r_0/3$  from the initial curve of radius  $r_0$ . The  $r_0/3$  term forms an angle of  $3\theta$  with the  $x$  axis. Taking into consideration that  $z' = x' + iy' = \rho \exp(i\phi)$ , then it can be shown that

$$\rho = r_0 \left[ \cos(\theta - \phi) + \frac{1}{3} \cos(3\theta - \phi) \right] \quad (3-44)$$

It is obvious that  $\rho$  has the maximum value when  $\theta = \phi = 0$  or  $\theta = \phi = \pi$ . Thus, from Equation (3-44), the maximum distance from the center is

$$\rho_{\max} = \frac{4}{3} r_0 \quad (3-45)$$

therefore, the maximum transverse diameter  $D_{\max}$  along the  $x'$  axis is

$$D_{\max} = \frac{8}{3} r_0 \quad (3-46)$$

From Equations (3-42) and (3-46) we obtain

$$c=0.001648 (D_{\max})^4 / (Z_o d \sigma_o^2 \lambda^3) \quad (3-47)$$

Thus, the stress-optical constants can be determined by measuring the maximum longitudinal diameter from the caustic image as shown in Fig. 3-13. The reflected caustic from the plate with a small circular hole will directly give the reflected stress optical constant. The transmitted caustic will directly give the transmitted stress optical constant. The method does not require the use of Poisson's ratio or Young's modulus.

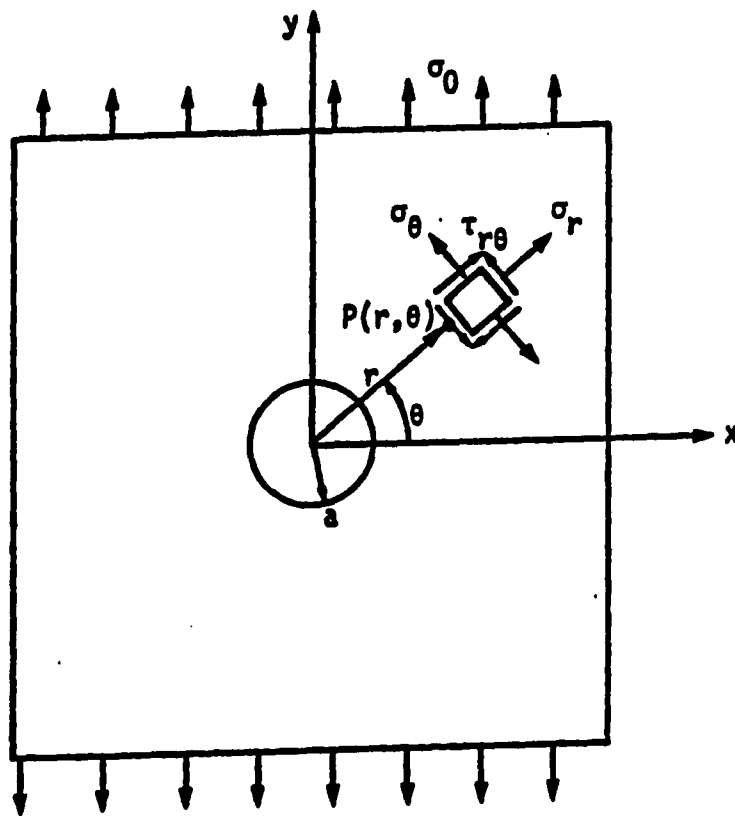


Fig. 3-12. Coordinate system with respect to the hole center

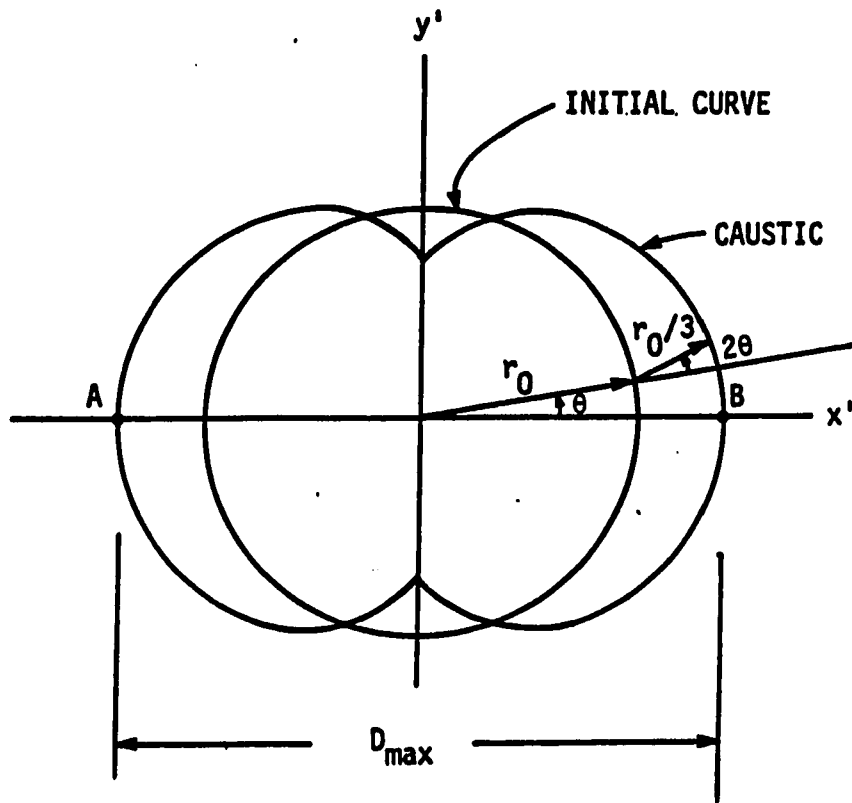


Fig. 3-13. Theoretical form of the principal envelope around a central hole

#### IV. MIXED MODE STRESS INTENSITY FACTORS EXPERIMENTS

The experimental method of caustics is a relatively new method. It has been widely used to estimate Mode I stress intensity factor for static and dynamic loading. Because the transmitted caustic has a sharper optical quality than the reflected caustic, it has been commonly used to determine Mode I. However, the transmitted caustic does not provide sufficient information to determine mixed mode stress intensity factors. Although the reflected caustics from the front and back face have a great potential to determine mixed modes SIFs, they are not widely used.

In this chapter, the methods from Chapter III-B are used to determine mixed mode SIFs. An interaction between two edge cracks was studied. A comparison between the experimental and the available numerical values are presented.

The detailed procedures from the preparation of the models to the final results are discussed and described.

##### A. Test specimen

###### 1. Material and model preparation

The material used for all models was polymethyl methacrylate (PMMA, plexiglas). In most experiments, plexiglas is proven to be a suitable material. It has the advantage of being a mechanically and optically isotropic material. Furthermore, it does not present an extensive plastic zone at room temperature even in the close vicinity of

the crack tip for sufficiently large loading. The material properties of plexiglas are given in Table 4-1.

While the exterior geometry was easily machined, achieving proper crack tip conditions was important. For the simple linear approach of the stress distribution around a stationary crack it is sufficient to replace an edge crack with an external slit which is perpendicular to the longitudinal boundary of the model and has a very small radius of curvature. The selected plates were first machined to their final sizes, the slit was then made by means of a metallic disc cutter with a thickness on the order of 0.006" to 0.008". Since, the root radius of the slit was sufficiently sharp, radius of curvature approaching zero, the slit simulates a real edge crack.

Table 4-1. Material properties of plexiglas

Property	Symbol	Value
Poisson's ratio	$\nu$	0.33
Young's modulus	E	3.34 Gpa 4.84 x 10 <sup>5</sup> psi
Reflected from the front face stress-optical constant	$c_f$	0.988 x 10 <sup>-10</sup> m <sup>2</sup> /N 0.681 x 10 <sup>-6</sup> in <sup>2</sup> /lb
Reflected from the rear face stress-optical constant	$c_r$	3.22 x 10 <sup>-10</sup> m <sup>2</sup> /N 2.22 x 10 <sup>-6</sup> in <sup>2</sup> /lb
Transmitted stress-optical constant	$c_t$	1.11 x 10 <sup>-10</sup> m <sup>2</sup> /N 0.77 x 10 <sup>-6</sup> in <sup>2</sup> /lb

## 2. Model geometries

For the determination of mixed mode stress intensity factors, an interaction between two edge cracks was studied. Two different cases were considered using plexiglas with a thickness of 1/8". In the first case an interaction between two equal length edge cracks was studied. The shape and size of the machined cracked specimen is shown in Fig. 4-1. The effect of the far boundary on the crack tip was kept small by holding the ratio of  $a/W$  to less than 0.137. To insure a uniform tensile type load, which produces a uniform far field tensile stress, models with the dimensions shown in Fig. 4-1 were used. Final dimensions of the six models used are shown in Table 4-2. All models were taken from the same plexiglas sheet.

Table 4-2. Geometrical parameters of equal length crack specimens<sup>a</sup>

Specimen No.	a (inch)	b (inch)	c (inch)	d (inch)	H (inch)	W (inch)
1A	0.25	0.25	4.195	4.180	0.125	1.827
2A	0.25	0.25	4.135	4.115	0.25	1.835
3A	0.25	0.25	4.052	4.073	0.375	1.833
4A	0.25	0.25	3.96	4.03	0.50	1.823
5A	0.25	0.25	3.82	3.93	0.75	1.825
6A	0.25	0.25	3.48	3.52	1.50	1.830

<sup>a</sup>See Figure 4-1 for the definition of the symbols.

In the second case an interaction between unequal length edge cracks was studied. The size and shape of the specimens are shown in Fig. 4-2. The effect of the far boundary on the crack tip was kept small by holding  $s/W$  less than 0.164 and  $l/W$  less than 0.21. All models are taken from the same plexiglas sheet and the final dimensions of the six models used are shown in Table 4-3.

Table 4-3. Geometrical parameters of unequal length crack specimens<sup>a</sup>

Specimen No.	s (inch)	l (inch)	c (inch)	d (inch)	H (inch)	W (inch)
1B	0.3	0.4	4.13	4.17	0.2	1.826
2B	0.3	0.4	4.035	4.065	0.4	1.829
3B	0.3	0.4	3.97	3.93	0.6	1.826
4B	0.3	0.4	3.85	3.85	0.8	1.835
5B	0.3	0.4	3.63	3.67	1.2	1.831
6B	0.3	0.4	3.1	3.06	2.4	1.831

<sup>a</sup>See Figure 4-2 for the definition of the symbols.

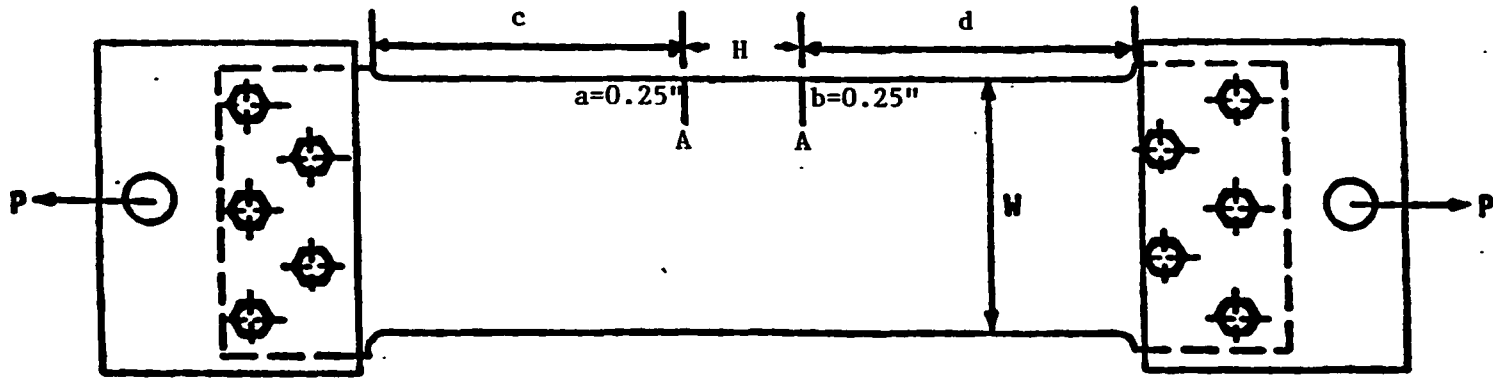


Fig. 4-1. Model A geometries of equal length cracks

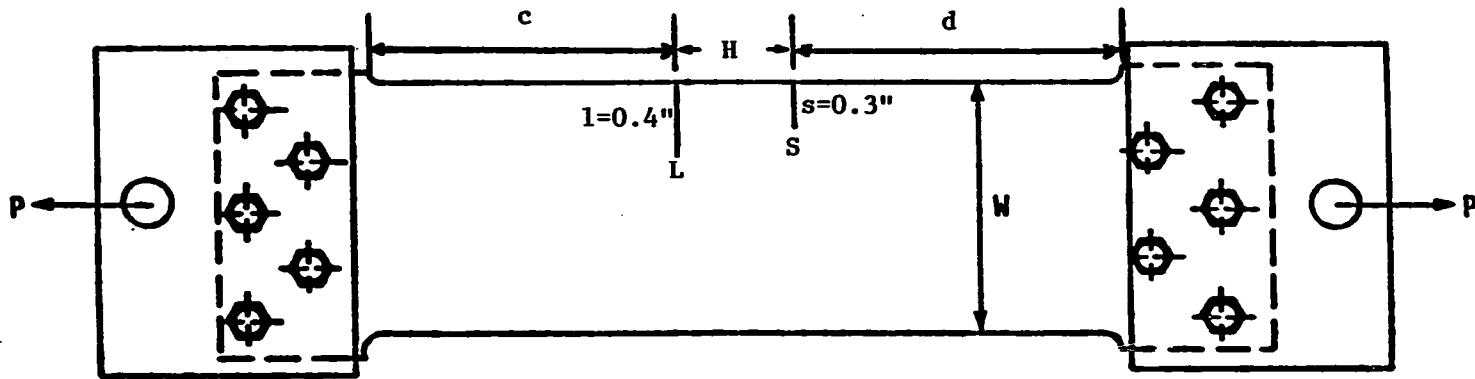


Fig. 4-2. Model B geometries of unequal length cracks

## B. Experimental Setup

The experimental set up for the reflected caustic is shown in Fig. 4-3. A monochromatic and coherent light beam emitted from a point source He-Ne laser, which is widened by spatial lens, impinges normally on the plexiglas cracked model. Divergent light is used primarily to enlarge the caustic image. The light is partially reflected from the front and eventually the rear face of the model. The deviated light rays from the area surrounding the crack tip are projected on the screen which is parallel to the model.

If the coordinates of the focus of the lens are not zero, then the optical axis of the lens is not coinciding with the center of the crack tip and a translation of the caustic takes place. A noncoincidence of the axis of the light beam and the crack tip produces only a displacement of the caustic without any modification in shape, size and relative position of the internal part or the external part of the caustic. The rotation of the the model about the x and y axes produces a light beam that is not perpendicular to the specimen. This rotation creates only a translation of the caustic without effecting the size, shape and relative position of the caustics. However, a rotation of the screen distorts the caustic image. Therefore, the screen should be always parallel to the model.

### C. Calibration Procedure

#### 1. Calibration of the stress optical constants

Although the reflected caustics were used for the determination of mixed mode stress intensity factors, the transmitted caustic was needed to determine the reflected from the back face stress optical constant. This is discussed in Chapter III Section D. An artificial edge crack, which is perpendicular to the longitudinal boundary, was seen in the middle of the calibration model. The crack is inserted the same way as the two edge cracks used for Models A and B. This will take care of the residual stress, if any exist. The residual stress can be predicted from the small pseudocaustic it produces. The residual caustic can be eliminated by applying a small compressive load and the zero load level is taken as the point when the pseudocaustic disappeared.

The transmitted and reflected caustics diameters along with the two magnification factors were measured. They are used in addition to the Poisson's ratio and Young's modulus to determine the stress-optical constant. The reflected from the back face stress optical constant was determined using Equations (3-33) and (3-35). The resulting values are shown in Table 4-1. The transmitted caustic, Poisson's ratio and Young's modulus would not be needed using the technique of a central hole in a plate discussed in Chapter III-D, but this technique had not yet been developed when the experiments were conducted.

#### 2. Optical calibration

The screen must always be parallel to the model. The rotation of the screen effects the shape and size of the caustic. The magnification

factor  $\lambda$  can be determined by using the following relation:

$$\lambda = \frac{\text{any length in the reference plane}}{\text{corresponding length in the image plane}} \quad (4-1)$$

However, if the screen is not parallel to the model, an error in the evaluation of magnification factor is obtained. This can be eliminated by using the well known divergent light magnification factor law:

$$\lambda = \frac{Z_0 + Z_1}{Z_1} \quad (4-2)$$

where  $Z_1$  is the distance between the divergent light source and the model and  $Z_0$  is the distance between the model and the screen.

The difference between the calculated magnification factor from Equations (4-1) and (4-2) indicates the extent of the errors. The main error is that the screen is not parallel to the model and can be easily eliminated.

#### D. Test Procedure

The tests for each model were conducted as follows. After the calibration stage, the test model was statically loaded in tension. The model was loaded by using the loading frame shown in Fig. 4-4. The static load was read on the load cell readout. The load range on the load cell readout is from 0 to 200 lb. The range of applied load was from 100 lb to 170 lb. To reduce the three dimensional effect, the load level was used that gave  $r_0/d$  greater than 0.4, where  $d$  is the model thickness and  $r_0$  is the initial curve size. The initial curve can be

determined from [24]

$$r_o = D_{t \max} / (3.17 \lambda_m) \quad (4-3)$$

Thus, the initial curve radius (the lens size) can be determined by measuring the maximum transverse diameter of the outer caustic. For the determination of mixed mode SIFs, the angle between the axis of symmetry and the crack axis along with the maximum transverse diameter of the external caustic were needed (Chapter III-B). The angle of symmetry was determined from the inner caustic resulting from the reflection from the front face. The axis of symmetry was traced by drawing the tangent to the two flanks and a normal to this tangent passing through the cusp point. The maximum transverse diameter  $D_{t \max}$  was determined from the outer caustic resulting from the reflection from the rear face.  $D_{t \max}$  is always parallel to the tangent to the two flanks and is a tangent to the external caustic.

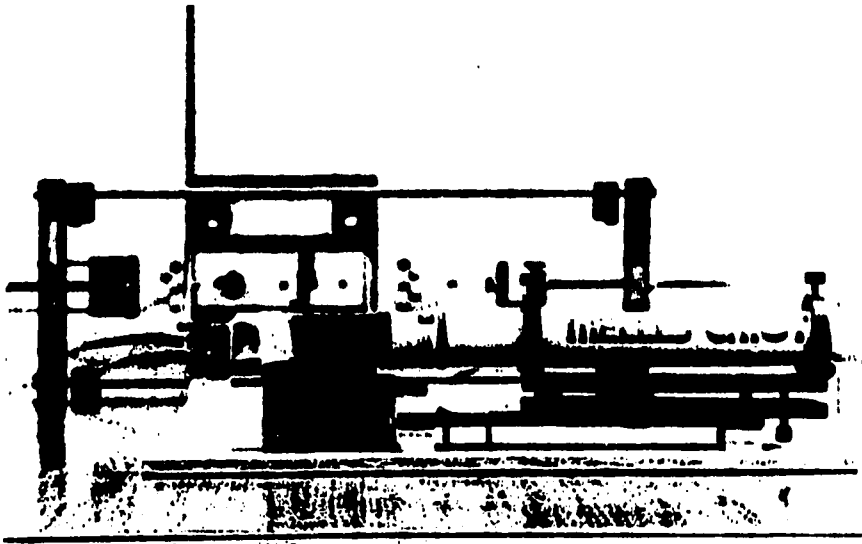
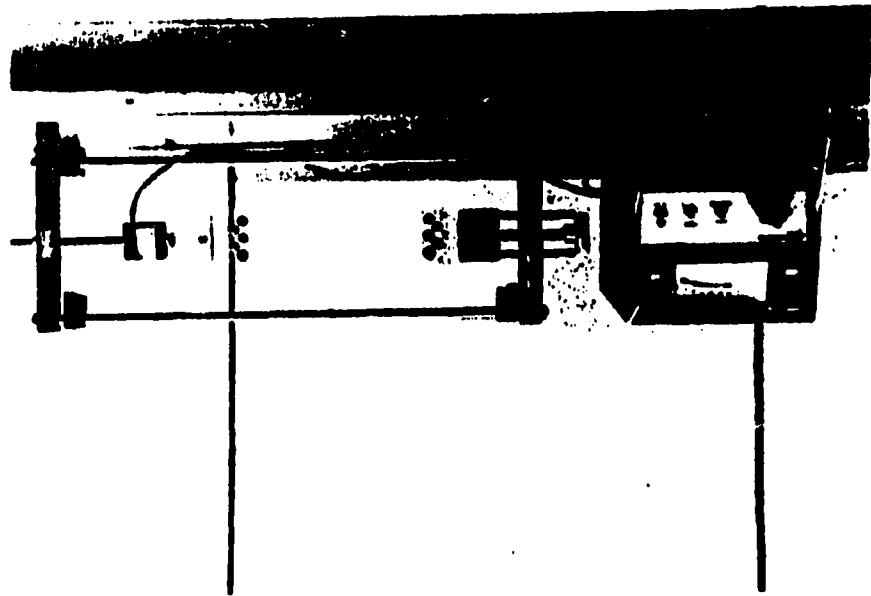


Fig. 4-3. Experimental reflected caustic setup

FIG. 4-6. Loading apparatus



## E. Data Analysis and Results

### 1. Mixed mode SIFs by epicycloid's angle of symmetry

Theocaris developed the the method of caustics using the reflected light from both the front face and the rear face for the determination of Mode I and mixed mode stress intensity factors. In his measurement of the maximum transverse diameter, the inside diameter of the caustic rim was considered. According to References 24 and 50, for experimental determination of dynamic stress intensity factor using the transmitted caustic, correct results are obtained when the line of maximum intensity within the caustic rim is considered [60] (in German). Most recently, after the auther had finished all the experiments, it was suggested that the average distance between the caustic edge and the maximum intensity point should be considered [41].

For the evaluation of mixed mode SIFs for Models A and B the inside diameter of the outer caustic was considered. The points of the maximum light intensity were not considered. The auther was unaware of Reference [60] at the time the interaction between two edge cracks was studied. However, the points with the maximum light intensity were considered (for Model 3B) for the measurement of the maximum transverse diameter in the comparison with the iterative least squares method. This will be discussed in the next section.

The estimated  $K_I/K_{I0}$  and  $K_{II}/K_{I0}$  values are compared to values obtained from using the numerical displacement discontinuity methods [61]. The SIFs results and the percentage difference between the

experimental and numerical results for Model A are shown in Table 4-4. The numerical and experimental results from Table 4-4 for  $K_I/K_{I0}$  and  $K_{II}/K_{I0}$  are plotted on Figs. 4-5 and 4-6 respectively. The definitions of the symbols used in these figures and tables are:

$K_I$  and  $K_{II}$  are Mode I and Mode II stress intensity factors, respectively.

$K_I/K_{I0}$  is the nondimensional Mode I stress intensity factor

$K_{II}/K_{I0}$  is the nondimensional Mode II stress intensity factor

$K_{I0} = \sigma \sqrt{\pi a}$ , normalized stress intensity factor

$\sigma$  is the applied stress as calculated from  $P/A$  ( $P$  is the applied load and  $A$  is the cross sectional area)

$a$  is the edge crack length

$H$  is the distance between the slits

% difference is the percentage difference between the experimental and the numerical values as calculated from:

$$\% \text{ difference} = \frac{\text{Experimental value} - \text{Numerical value}}{\text{Average of the experimental and numerical values}} \quad (4-4)$$

For Model B, the estimated  $K_I/K_{I0}$  and  $K_{II}/K_{I0}$  results and the numerical values for crack tip S and L (Fig. 4-2) are shown in Tables 4-5 and 4-6, respectively. A comparison between the numerical and the experimental  $K_I/K_{I0}$  and  $K_{II}/K_{I0}$  values for crack tip S is shown in Figs. 4-7 and 4-8 respectively. Fig. 4-9 shows the numerical and experimental  $K_I/K_{I0}$  values for crack tip L and Fig. 4-10 shows  $K_{II}/K_{I0}$  values.

Table 4-4. Experimental and numerical results for model A

Model No.	$K_I/K_{I_0}$	$K_I/K_{I_0}$	% Diff.	$K_{II}/K_{I_0}$	$K_{II}/K_{I_0}$	% Diff.
	Exp.	Num.		Exp.	Num.	
1A	0.74	0.797	7.41	0.16	0.152	5.1
2A	0.877	0.85	3.1	0.131	0.132	0.7
3A	0.904	0.885	2.1	0.117	0.109	7.1
4A	0.89	0.915	2.7	0.093	0.085	7.9
5A	0.94	0.96	2.1	0.057	0.054	5.4
6A	1.043	1.052	1.0	0.0109	0.012	9.1

Table 4-5. Experimental and numerical results for model B tip S

Model No.	$K_I/K_{I_0}$	$K_I/K_{I_0}$	% Diff.	$K_{II}/K_{I_0}$	$K_{II}/K_{I_0}$	% Diff.
	Exp.	Num.		Exp.	Num.	
1B	0.42	0.397	5.6	0.168	0.172	2.3
2B	0.65	0.635	2.3	0.144	0.158	9.1
3B	0.706	0.745	5.3	0.128	0.126	1.5
4B	0.836	0.819	0.9	0.0868	0.0939	7.5
5B	0.91	0.92	1.1	0.054	0.053	1.8
6B	1.054	1.048	0.5	0.0108	0.011	1.7

Table 4-6. Experimental and numerical results for model B tip L

Model No.	$K_I/K_{I0}$	$K_I/K_{I0}$	% Diff.	$K_{II}/K_{I0}$	$K_{II}/K_{I0}$	% Diff.
	Exp.	Num.		Exp.	Num.	
1B	1.09	1.062	2.6	0.045	0.049	8.4
2B	1.028	1.01	2.7	0.081	0.075	7.6
3B	0.950	0.995	4.6	0.069	0.0705	2.5
4B	1.01	0.998	1.2	0.061	0.0582	4.6
5B	1.03	1.04	0.9	0.036	0.037	2.7
6B	1.086	1.08	0.5	0.0	0.0072	0.0 <sup>a</sup>

<sup>a</sup>  $K_I \text{Exp.}/K_I \text{Num.}$

The size of the initial curve  $r_0$  affects Mode I stress intensity factor as discussed in Chapter III (Section C). The initial curve size  $r_0$  is calculated by measuring the maximum transverse diameter  $D_{t \text{ max}}$  and using Equation (4-3). The initial curve size is normalized to the model thickness to show the three dimensional effect for Model A, Fig. 4-11. The experimental SIF is normalized to the numerical value. The  $r_0/d$  versus the normalized SIF for tips S and L (model B) are shown in Figs. 4-12 and 4-13, respectively. The results of  $K_I/K_{I0}$  and  $K_{II}/K_{I0}$  are discussed in section F.

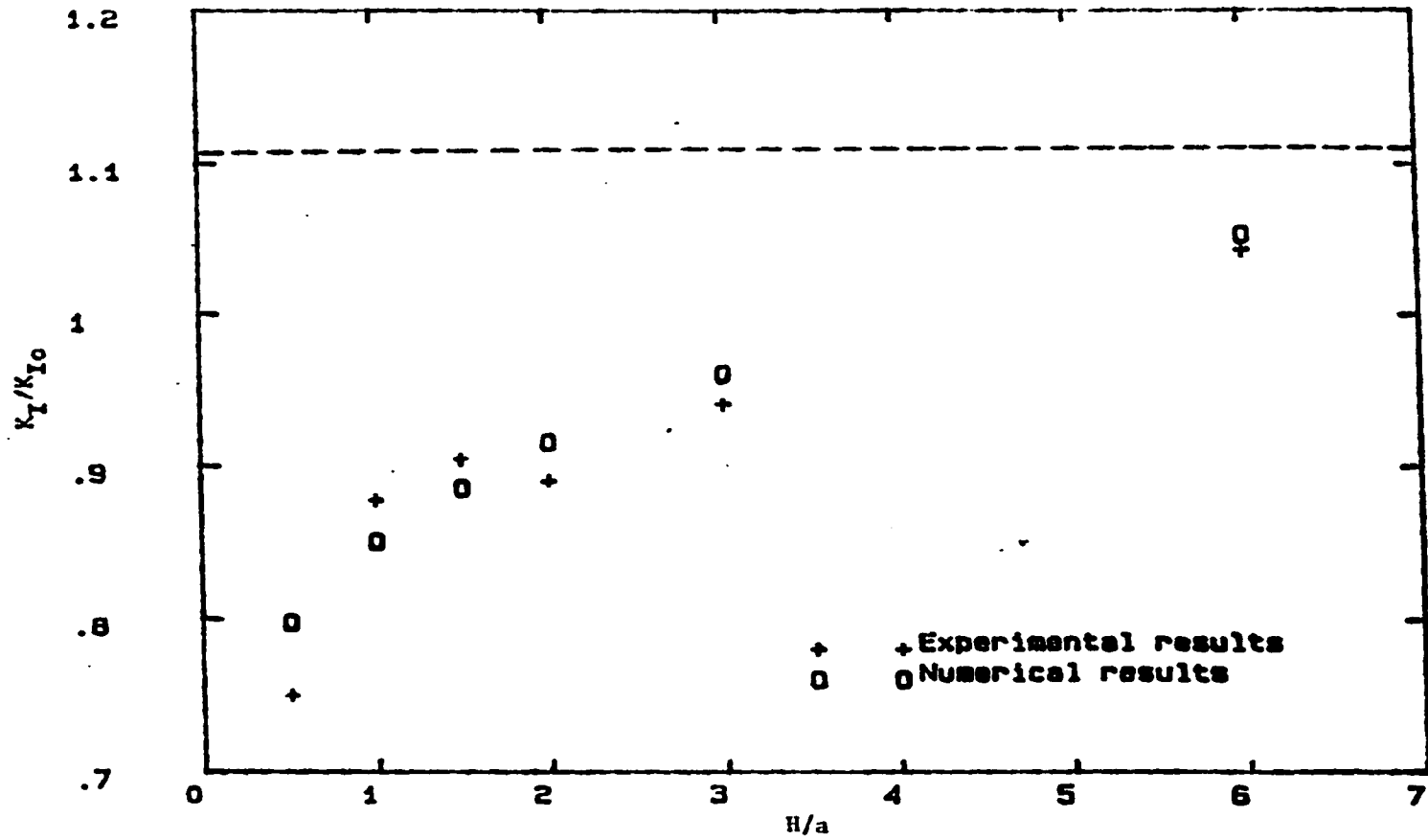


Fig. 4-5. Experimental and numerical  $K_I/K_{I0}$  versus  $H/a$  for Model A

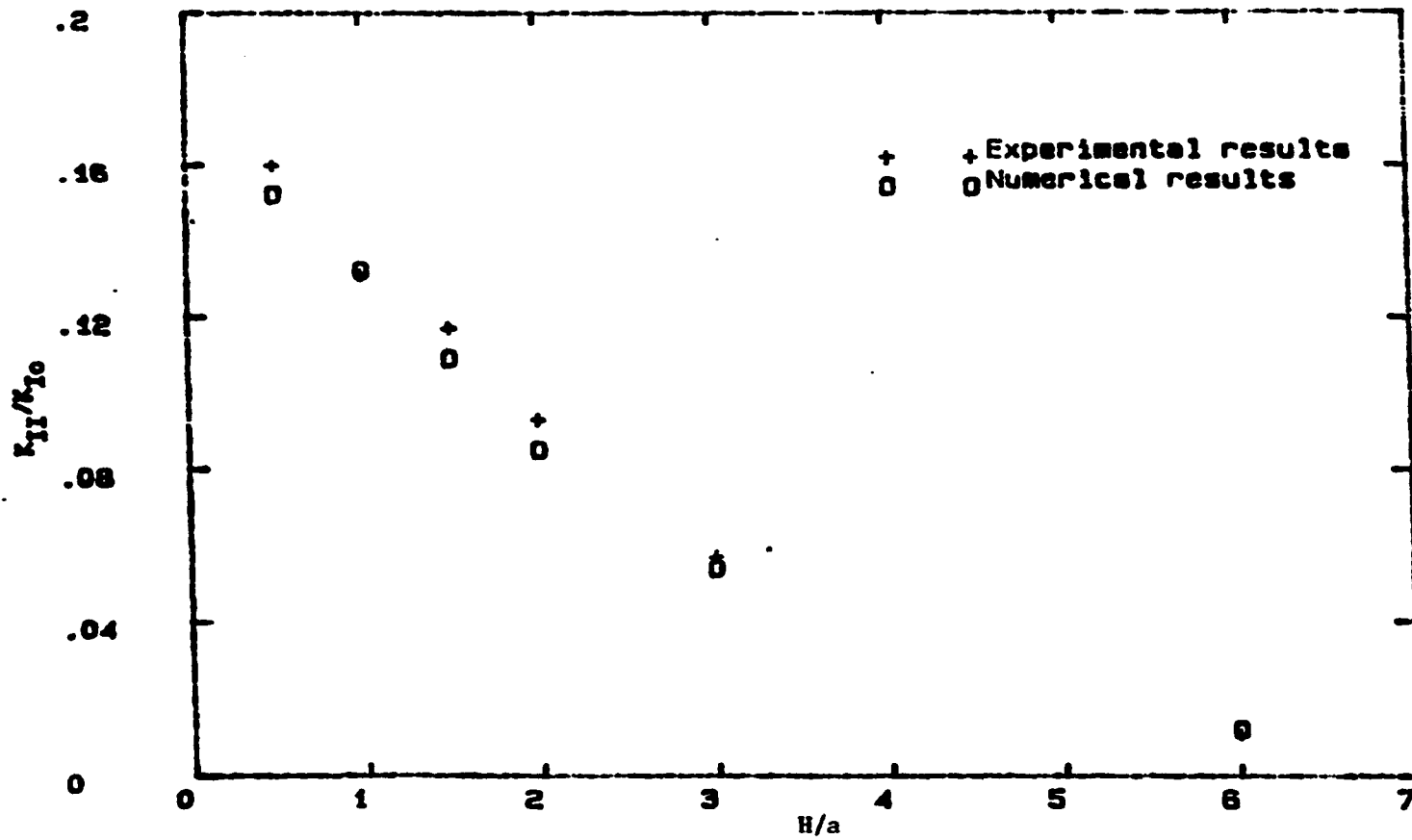


Fig. 4-6. Experimental and numerical  $K_{II}/K_{I0}$  versus  $H/a$  for Model A

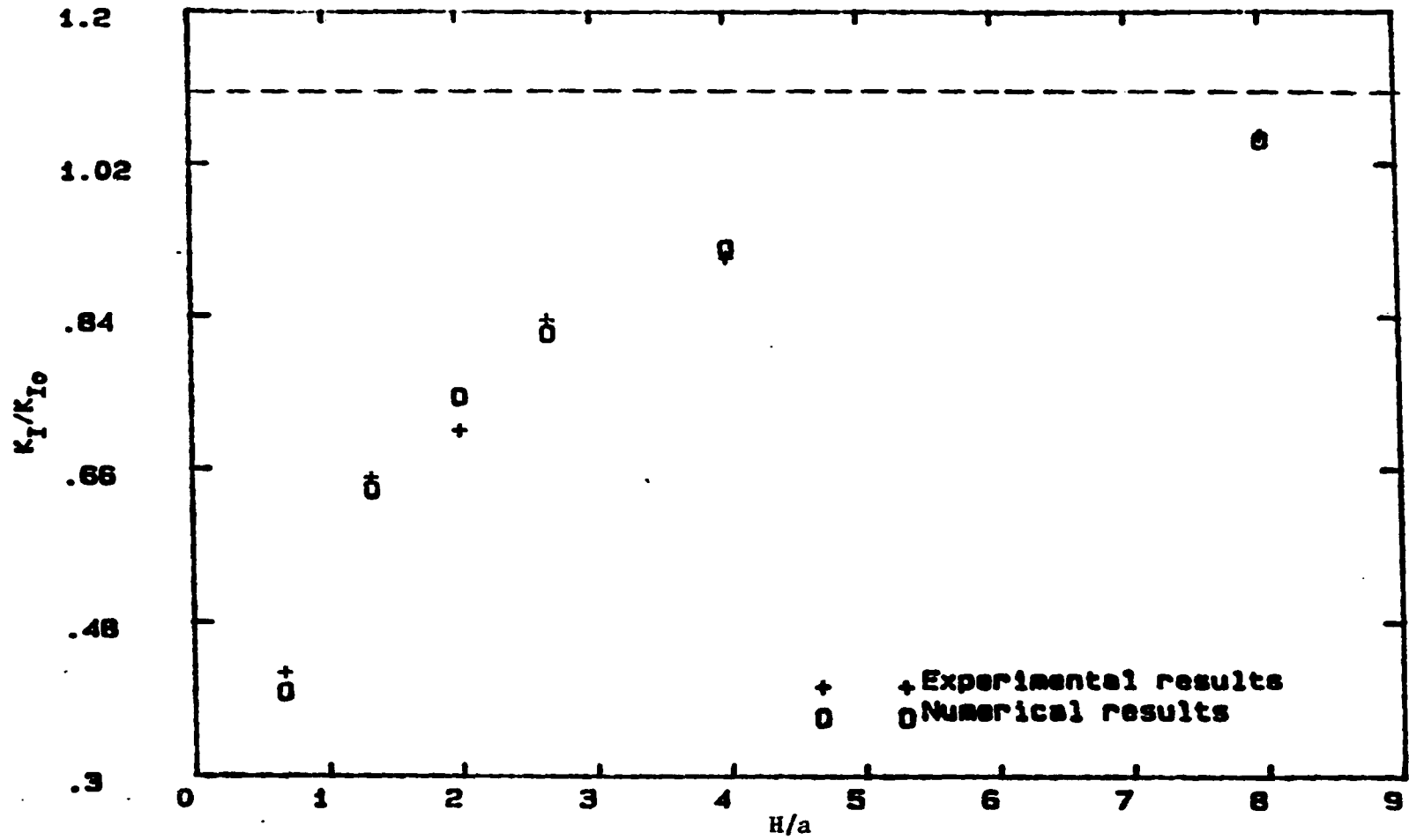


Fig. 4-7. Experimental and numerical  $K_I/K_{I0}$  versus  $H/a$  for Model B tip S

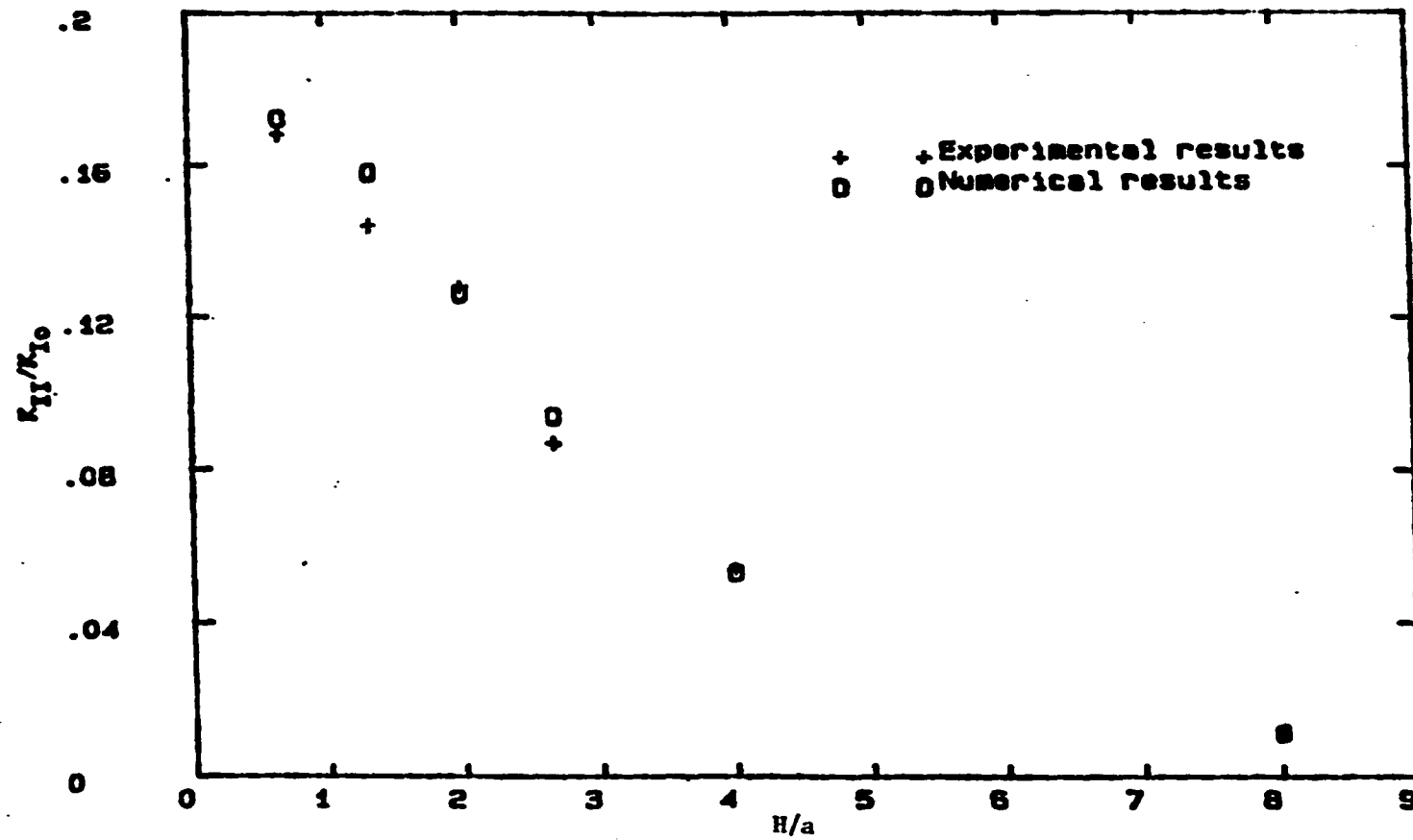


Fig. 4-8. Experimental and numerical  $K_{II}/K_{I0}$  versus  $H/a$  for Model B tip S

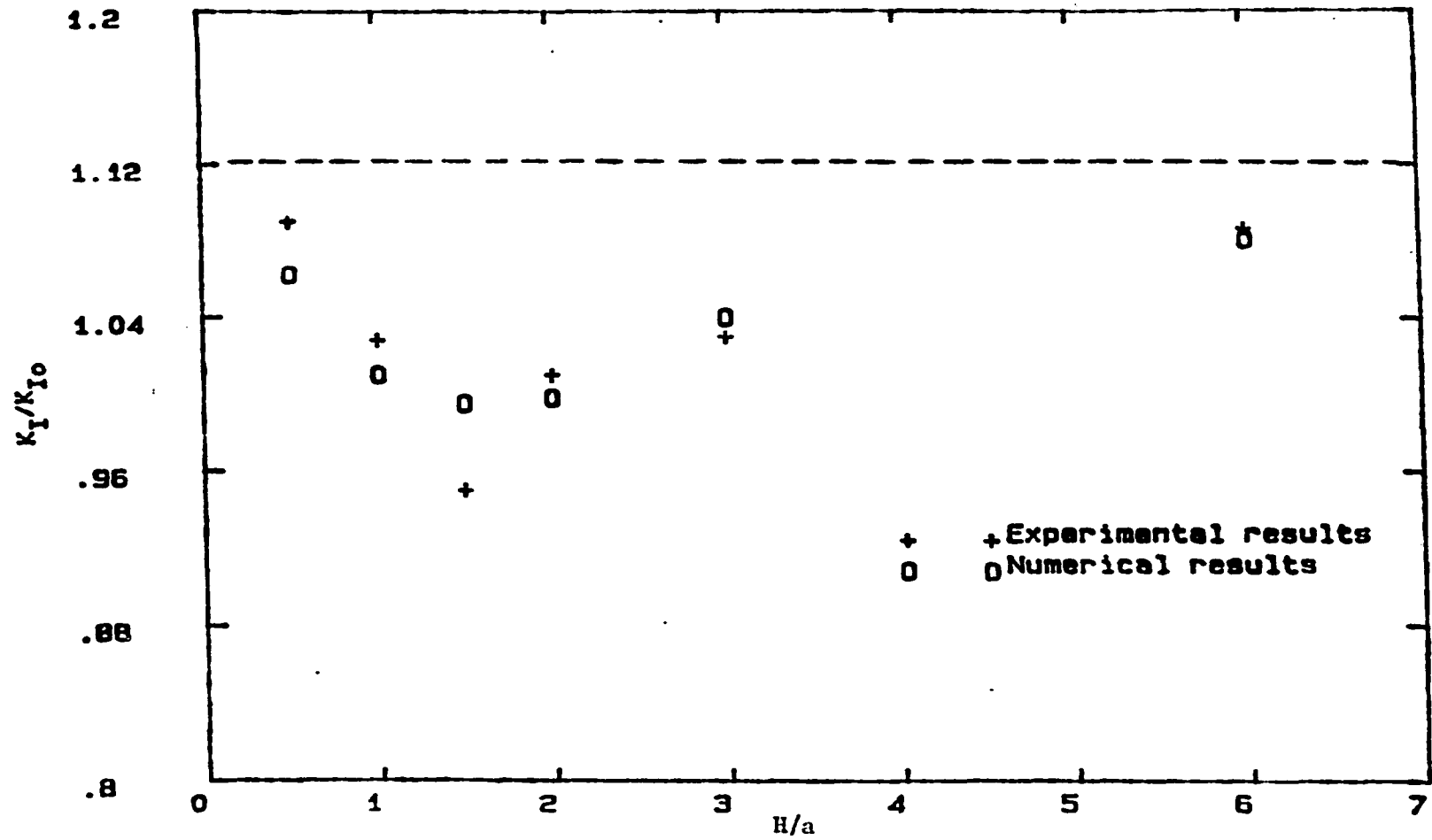


Fig. 4-9. Experimental and numerical  $K_I/K_{I0}$  versus  $H/a$  for Model B tip L.

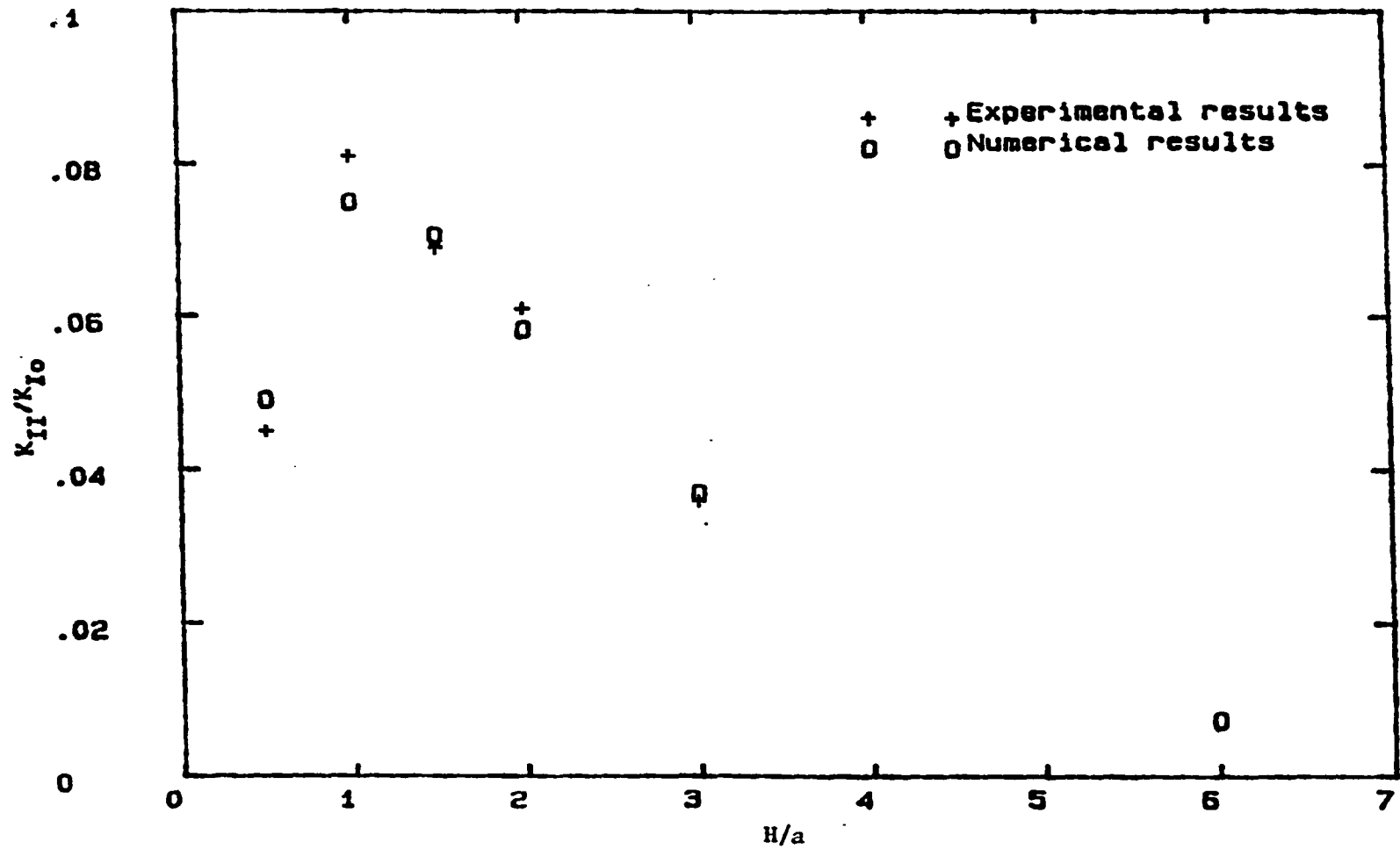


Fig. 4-10. Experimental and numerical  $K_{II}/K_{I0}$  versus  $H/a$  for Model B tip L

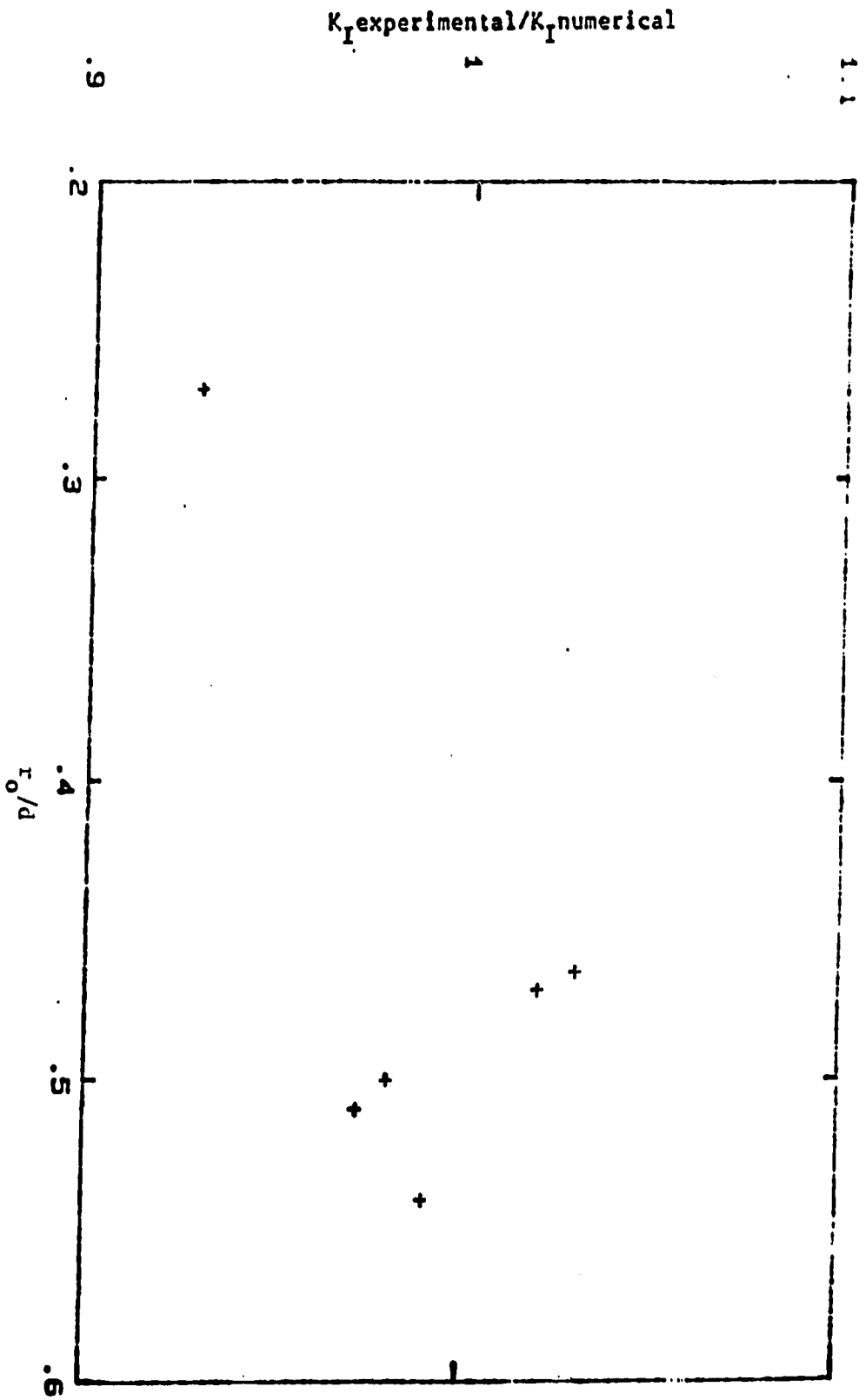


Fig. 4-11.  $K_I \text{ exp.} / K_I \text{ num.}$  versus  $r_0/d$  for Model A

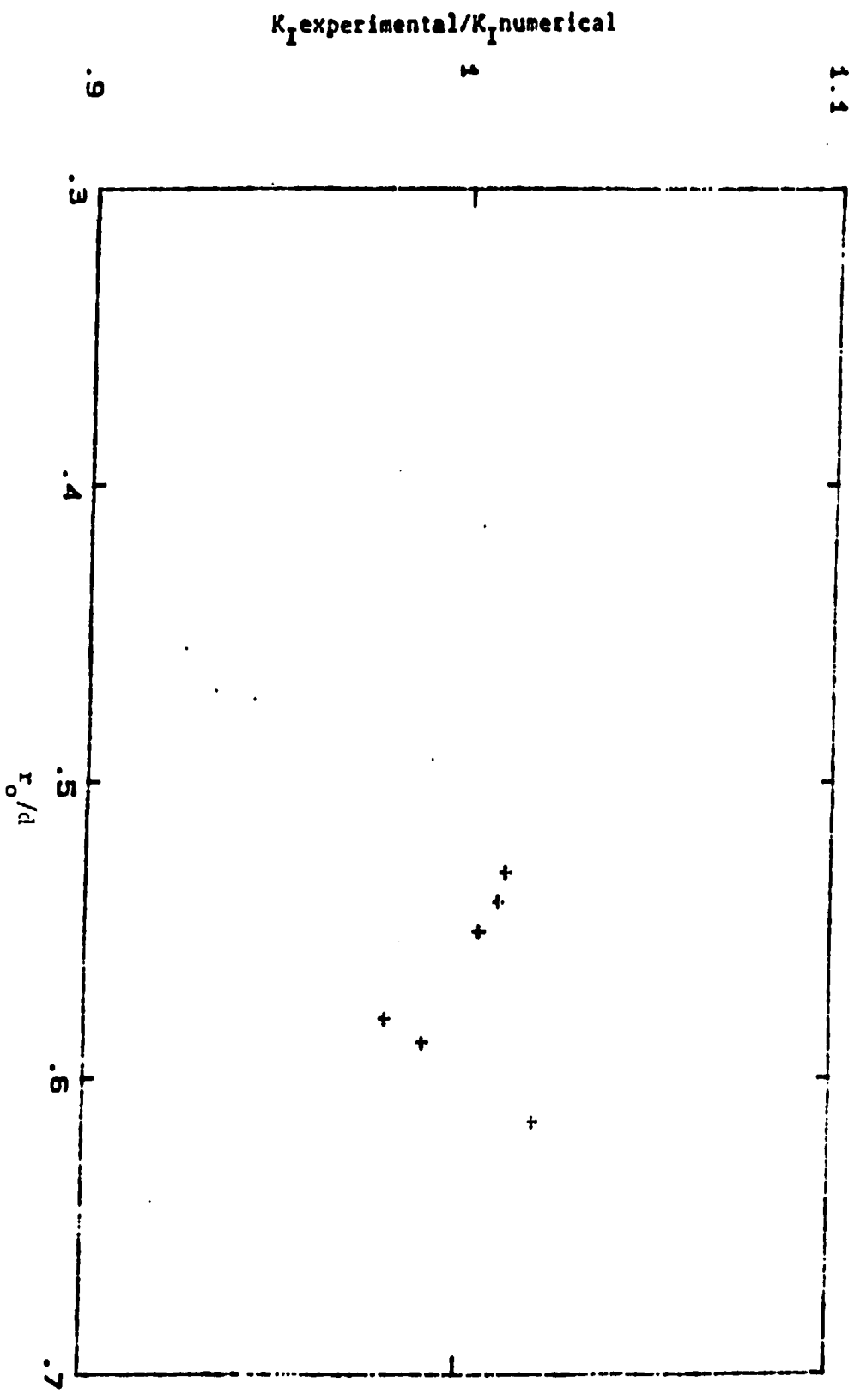


Fig. 4-12.  $K_{I \text{ exp.}}/K_{I \text{ num.}}$  versus  $r_0/d$  for Model II tip S

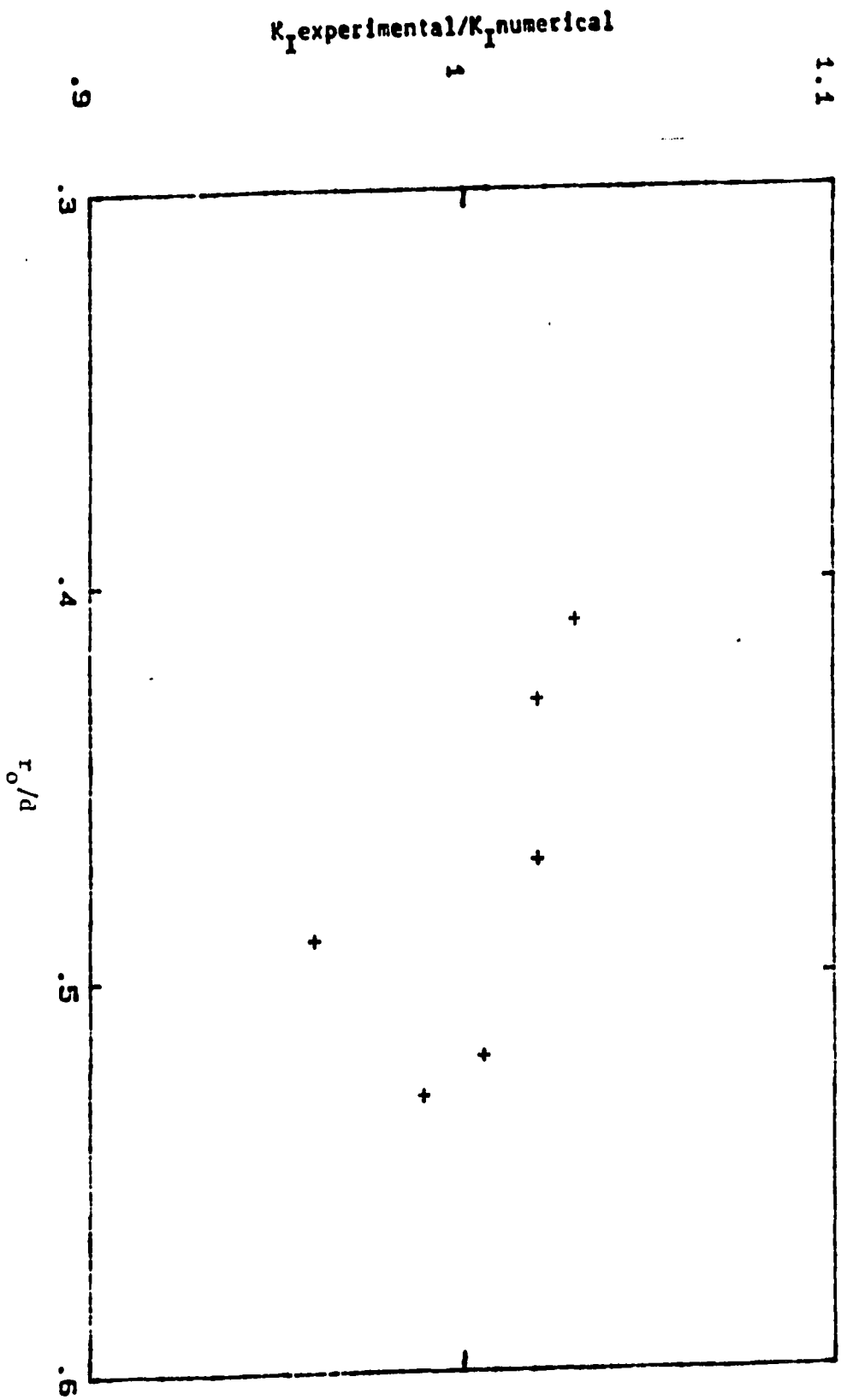


FIG. 4-13.  $K_{I \text{ exp.}}/K_{I \text{ num.}}$  versus  $r_0/d$  for Model B (lip L)

## 2. Mixed mode SIFs using an iterative least squares method

To determine pure mode one stress intensity factor the transmitted, the reflected from a nontransparent material, or the reflected from a transparent caustic can be used.  $K_I$  can be calculated by using only two data points which define the maximum transverse diameter. An error in locating these two points would cause error in calculating  $K_I$  using any of the three techniques previously discussed. Mixed mode SIFs can be determined using the reflected caustics from a transparent material by using only five points. The question posed is "Why do we use only two or five points from the well defined epicycloid and not any other points?". In order to use a large number of points the iterative least squares method (Chapter III) was used.

Two cases of different  $K_I$  and  $K_{II}$  values (Model 3B) were considered. The calibration technique and the material properties remained as before. The experimental set up is the same except that the camera was replaced with a video camera and the digital image analysis "EYECOM III" shown in Fig. 4-14.

The EyeCom unit consists of an image scanner, a real time digitizer, a display system, and a minicomputer [62]. The image scanner consists of a special vidicom television camera. The picture is divided into 480 lines and each line is divided into 640 picture elements, called pixels. The brightness or the light intensity of each pixel is converted into digital values (Z values). The real time digitizer digitize the image in 1/30 second and stores the resultant values in a fresh memory where it can be accessed later by the computer. The

display system or the monitor visualizes the information and acts as a graphics terminal for data processing and graphical data displays. Fig. 4-15 is a schematic diagram of the system.

A light intensity profile was generated and used to automatically pick the highly illuminated individual points on both the inner and outer caustics. The effects of the number of points on  $K_I$  and  $K_{II}$  values for tip S and L are shown on Tables 4-7 and 4-8, respectively.

In order to take points from the inner caustic and use the iterative least squares technique (Chapter III), a correction factor must be used. This is due to the fact that the stress optical constant in Eq. (3-15b) is associated with the outer caustic. The correction factor can be calculated from Eq. 3-10 and Table 4-1 as follows:

$$(r_o)_r / (r_o)_f = (c_r / c_f)^{2/5} = (3.22 \times 10^{-10} / 0.988 \times 10^{-10})^{2/5} = 1.604 \quad (4-5)$$

Therefore, every point location on the inner caustic must be multiplied by the correction factor (Eq. 3-11).

The graphical capability of the digital image analysis was used to visualize the generalized epicycloid characteristics. The initial values of the four unknown parameters ( $r_o$ ,  $x_o$ ,  $y_o$ ,  $\theta_o$ ) were estimated based on the the available information as follows:

1. The initial curve  $r_o$  value was estimated by measuring the longitudinal diameter ( $D_1 = 3r_o$ ). This was done by using CAUSTIC 1 program [46] by specifying the two flanks points and the cusp point of the inner caustic. A perpendicular line to the flank's tangent passing through the cusp point would be drawn, which was the axis of symmetry of the caustics, and intercepting the outer caustic on two points which defined the maximum longitudinal diameter. The

parallel line to the flank's tangent determined the maximum transverse diameter and  $r_0$  was estimated from the fact that

$$D_{tmax} = 3.17r_0.$$

2. It was essential to have a reasonable crack tip location estimate. The location of the crack tip  $(x_0, y_0)$  was estimated by utilizing the ratio of the distance between the flank's tangent and the cusp point to the distance between the cusp point and the crack tip is 4.0 (Chapter III-D). After specifying the two points of the longitudinal diameter in Step 1, a line was drawn from one of these points to the estimated crack tip. Hence, the estimated crack tip location was achieved by using both the inner and outer caustics.
3. The ratio of  $K_{II}/K_I$  was estimated by measuring the angle between the axis of symmetry (Step 1) and the crack axis. Therefore, the estimated value of the ratio  $K_{II}/K_I$  is determined from Equation (3-16).

The results of  $K_I/K_{I0}$  and  $K_{II}/K_I$  for crack tips S and L are shown in Tables 4-9 and 4-10, respectively. Since the points with the highest light intensity of the caustics were considered using the iterative least square technique, it was necessary to calculate  $K_I/K_{I0}$  based on the points of the highest light intensity of the maximum transverse diameter as shown in Tables 4-9 and 4-10. The ratio  $K_{II}/K_I$  is determined by measuring the angle between the crack axis and the caustic axis of symmetry.  $K_I$  and  $K_{II}/K_I$  are calculated from Equations (3-15a) and (3-15b), respectively.

**Table 4-7. SIFs of crack tip S using  
an iterative least square technique**

No. of points	$K_I/K_{Io}$	$K_{II}/K_I$
35	0.697	0.1583
40	0.708	0.161
45	0.724	0.1647
50	0.7216	0.1629

**Table 4-8. SIFs of crack tip L using  
an iterative least square technique**

No. of points	$K_I/K_{Io}$	$K_{II}/K_I$
35	0.975	0.0735
40	0.983	0.0721
45	0.985	0.0724
50	0.9846	0.0728

Table 4-9. Calculated  $K_I/K_{I0}$  and  $K_{II}/K_I$  for crack tip S using four techniques

Technique	$K_I/K_{I0}$	$K_{II}/K_I$
The outer caustic band, inner maximum transverse diameter <sup>a</sup>	0.706	0.172 <sup>b</sup>
The displacement discontinuity numerical method <sup>a</sup>	0.745	0.169
The outer caustic band, maximum light intensity, maximum transverse diameter	0.720	0.172 <sup>b</sup>
The iterative least square method	0.724	0.1647

<sup>a</sup>From Table 4-5.

<sup>b</sup>The same angle of symmetry.

Table 4-10. Calculated  $K_I/K_{I0}$  and  $K_{II}/K_I$  for crack tip L using four techniques

Technique	$K_I/K_{I0}$	$K_{II}/K_I$
The outer caustic band inner, maximum transverse diameter <sup>a</sup>	0.950	0.069 <sup>b</sup>
The displacement discontinuity numerical method <sup>a</sup>	0.995	0.0708
The outer caustic band, maximum light intensity, maximum transverse diameter	0.972	0.069 <sup>b</sup>
The iterative least square method	0.983	0.0721

<sup>a</sup>From Table 4-6.

<sup>b</sup>The same angle of symmetry.

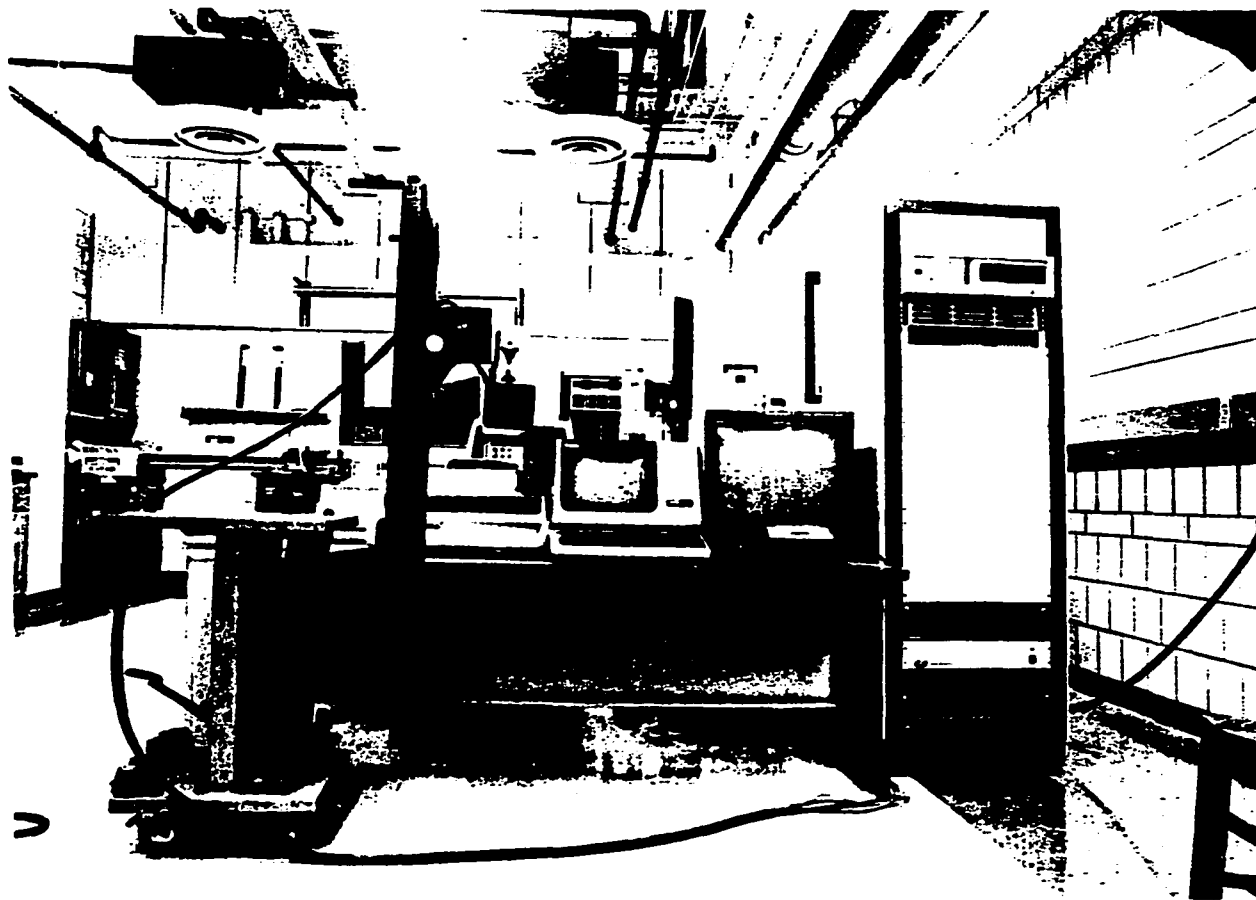
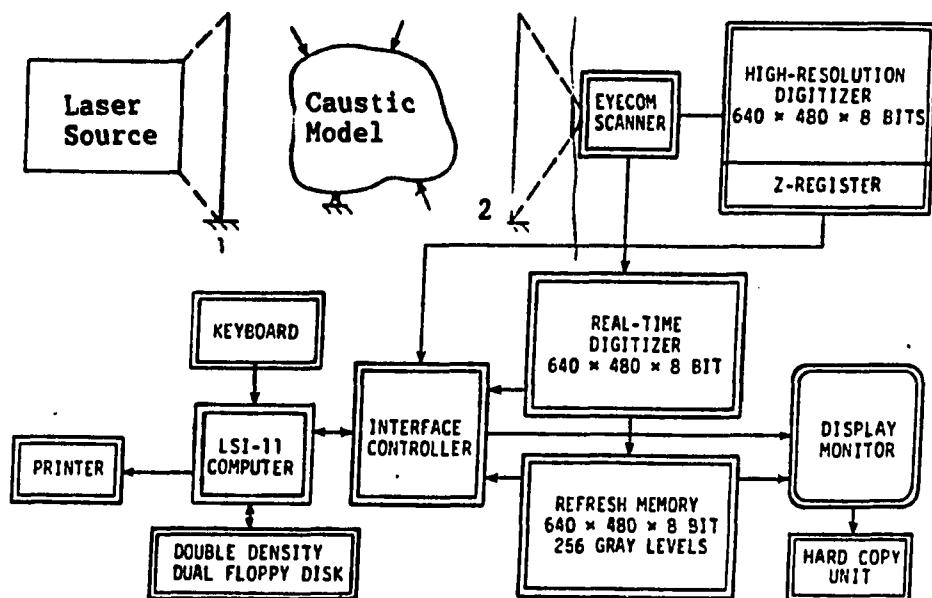


Figure 4-14. The EyeCom system



1-Special Filter      2-Screen

Fig. 4-15. Schematic diagram of the Eyecom system

## F. Conclusion and Discussion

In this study, experimental solutions for the interaction between two equal and different length parallel edge cracks is obtained. The slits are machined by a circular cutter which produces low pressure on the model and result in low heat generation. The experimental technique of caustics was used. Mixed mode stress intensity factors were determined by using the current technique and the developed iterative least squares method.

From the results obtained it is seen that the Mode I stress intensity factor is predominant as shown in Tables 4-4, 4-5 and 4-6. For the interaction between two equal length cracks (Model A),  $K_I$  increases as the distance between the two cracks increases, while  $K_{II}$  decreases. The numerical and experimental  $K_I$  results are in good agreement and the maximum percentage difference is 4.41% for Model 1A as indicated in Table 4-4. Although it is not necessary that the numerical results are the exact ones, there is an error in determining the experimental result for Model 1A. This is due to the three dimensional effect ( $r_o/d = 0.277$ ) as shown in Fig. 4-11. The ratio of  $r_o/d$  should be greater than 0.4. For Mode II, the numerical and experimental results are not as consistent as  $K_I$  and the percentage difference is up to 9.1 as shown in Table 4-4.

For Model B (crack tips S and L) there is no distinct difference between the numerical and experimental  $K_I$  values and the difference between the  $K_{II}$  results is less than that for Model A. It is seen that

for crack tip S,  $K_I$  increases and  $K_{II}$  decreases as the distance between the two cracks increases. Crack tip L results indicates that  $K_I$  decreases when the ratio of  $H/a$  increases from zero to two and then  $K_I$  increases for ratio  $H/a$  greater than two.  $K_{II}$  for tip L increases for the ratio of  $H/a$  increases from zero to one. For  $H/a$  ratio greater than one  $K_{II}$  decreases with increasing  $H/a$  ratio.

The dashed lines in Figs. 4-5, 4-7 and 4-9 represent the theoretical  $K_I/K_{I0}$  value of a single edge crack in semi-infinite plate ( $K_I/K_{I0}=1.12$ ). The zero lines in Figs. 4-6, 4-8 and 4-10 represent the theoretical  $K_{II}/K_{I0}$  results. The difference between the theoretical ( $K_I$  and  $K_{II}$ ) and the experimental (or the numerical) results is an indication of strong interaction between the two cracks, especially when  $H$  is small.

The opening mode for crack tips S and L for Model 3B is calculated by measuring the maximum transverse diameter based on the points of the maximum light intensity. The results are listed in Tables 4-9 and 4-10. The percentage difference between these results and the ones obtained by measuring the outer caustic band inner diameter is 1.97 for tip S and 2.28 for tip L. This shows a good correlation.

The iterative least square method results coincides with the  $K_I$  and  $K_{II}$  values calculated by measuring the maximum transverse diameter and the angle of symmetry of the generalized epicycloid. This indicates that  $K_I$  and  $K_{II}$  can be determined by taking a number of points from the caustic image and not by taking only five points defining the maximum transverse diameter and the axis of symmetry.

There are some areas that need to be explained. These areas

1. The difference between the longitudinal diameters method (Chapter III-B) was used in different studies for the determination of mixed mode stress intensity factors and the experimental results compared satisfactorily with the theoretical results [12,33-35]. For the particular case in this study, interaction between two edge cracks, the technique did not yield very accurate results. Errors in determining both Mode I and Mode II were noticed.
2. The ratio of the initial curve  $r_0$  to the model thickness  $d$  should be larger than 0.4 so that plane stress conditions prevail. The effect of the three dimensionality error of Model 1A ( $r_0/d = 0.277$ ) could not be eliminated, because when the load was increased the two caustics were distorted. This distortion was due to the interaction between the two epicycloids and the initial curves no longer had a circular shape. Thus, it could be concluded that there is a limitation as to where the experimental method of caustics can be used. It is concluded that the method of caustics can be used for the study of interaction of two edge cracks where the distance between the cracks is larger than the model thickness.
3. The initial estimation of the four unknown parameters, using the iterative least square technique, was based on the properties of the generalized epicycloid. A nonzero  $r_0$  estimate is necessary. This condition is mathematically due to Equation (3-25) and physically there will be no caustic without the initial curve. Estimation of the crack tip within  $r_0/3$

the initial curve. Estimation of the crack tip within  $r_0/3$  distance from the actual crack tip location is essential. This is mainly due to Equation (3-27) which is based on minimizing the residuals between LE and LM as shown in Equation (3-23).

The current method relies upon measuring the distance between two points that define the maximum transverse diameter. Since there could be a discrepancy in measuring the maximum transverse diameter, data from the whole caustic image should be used to help reduce the possible error. In this dissertation a first attempt to take a number of points from the caustic image was accomplished. The technique can be extended for the determination of mixed mode stress intensity factors from the transmitted or reflected from a nontransparent material caustics.

## V. STRESS OPTICAL CONSTANTS EXPERIMENTS

As demonstrated in Chapter III, in addition to the experimental setup and the model thickness,  $K_I$  and  $K_{II}$  depend on the model stress optical constant. The basic difference in calculating SIFs from the transmitted or the reflected caustics is the value of the stress-optical constants. Studies that utilize the method of caustics use an optically isotropic material (PMMA, Plexiglas) to extract  $K_I$  and  $K_{II}$  although a birefringent model material can be used.

A new technique has been developed to determine both the stress optical constants for the transmitted caustic and the caustic reflected from the rear face of the model. The maximum longitudinal diameters of the resulting transmitted and reflected caustics were used to determine the respective stress optical constant. The new caustic technique was applied to a thin plate with a circular hole where the caustic image is no longer a generalized epicycloid.

The schematic of the experimental setup for the reflected caustic is the same as the one shown in Fig. 3-3. The transmission caustic setup is shown in Fig. 5-1.

The transmitted and reflected stress-optical constants results are compared to the available reported values. The effect of the hole size is investigated.

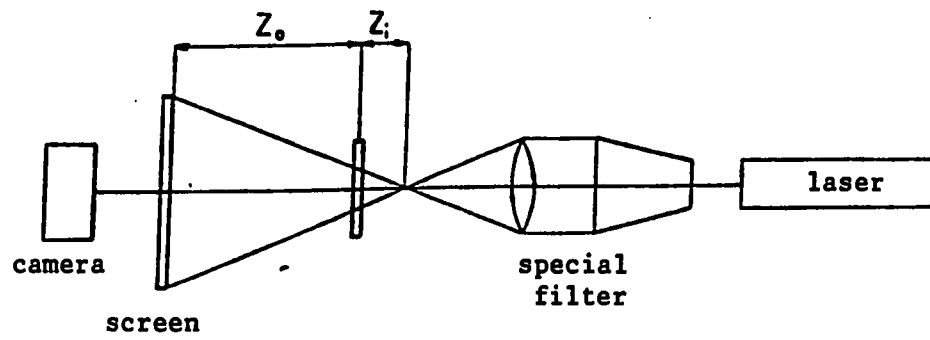


Fig. 5-1. Schematic transmitted caustic setup

### A. Model Geometry

An optically isotropic material, polymethyl methacrylate (PMMA, plexiglas) was used for the experiments. Thin plates with a thickness of 1/8" were used for all the models. To insure a uniform tensile type load, which produces a uniform stress  $\sigma_0$ , models with the dimensions shown in Fig. 5-2 were used. The loading apparatus used was the same as in Fig. 4-4. The effect of the hole size upon the determination of the stress optical constants was investigated by varying the ratio of the hole size  $a$  to the plate width  $W$ . A small drill was used to slowly bore the holes in the models. Final dimensions of the five models used (Model C) are shown in Table 5-1. All models were taken from the same plexiglas sheet.

Table 5-1. Geometrical parameters of model C

Specimen No.	2a (inch)	b (inch)	c (inch)	W (inch)	a/W
1C	0.0625	4.244	4.256	1.83	0.017
2C	0.0781	4.235	4.265	1.81	0.216
3C	0.125	4.262	4.237	1.81	0.034
4C	0.1875	4.213	4.286	1.80	0.052
5C	0.250	4.21	4.29	1.81	0.069

The maximum load of 200 lb can be applied using the loading apparatus in Fig. 4-4. More load was needed to complete the investigation of the hole size and the dimension of the model changed to model D shown in Fig. 5-2. The loading apparatus used for model D is shown in Fig. 5-3. The final dimensions of the four models used are shown on Table 5-2.

Table 5-2. Geometrical parameters of model D

Specimen No.	2a (inch)	b (inch)	c (inch)	W (inch)	a/W
1D	0.0625	4.54	4.46	3.4	0.009
2D	0.0781	4.544	4.456	3.394	0.0114
3D	0.125	4.5	4.5	3.41	0.0183
4D	0.1875	4.58	4.42	3.4	0.0275

#### B. Test Procedure

The calibration of the experimental setup remains the same. A monochromatic light beam emitted from a He-Ne laser impinges on the specimen. Screens in front and behind the specimen were placed parallel to the specimen at distance  $Z_0$ . On these screens the caustics resulting from the transmitted or reflected light rays were formed. The reflected experimental setup is shown in Fig. 4-3 and the transmitted setup is shown in Fig. 5-4. The experimental reflected caustic pattern is shown

in Fig. 5-5. The outer caustic is due to the light reflected from the rear face and the inner caustic is due to the light reflected from the front face. The outer caustic was considered for the determination of the reflected stress-optical constant. The experimental transmitted caustic is shown in Fig. 5-6. It was noticed during the experiment that the caustic band resulting from the light transmitted or reflected from the area surrounding a circular hole was wider than the epicycloid band that resulted from the area in the vicinity of a crack tip. Caution was taken in the determination of stress optical constant since not only is the caustic band wider, but the maximum transverse diameter is raised to the 4th power while the caustic diameter for a crack is raised to the  $5/2$  power.

All models were loaded in tension. Due to the diffraction effects, the points with the maximum light intensity within the bright rim were considered. The digital image analysis system was used to determine the light intensity profile at both ends of the maximum diameter. Each model was subjected to five different loads and the corresponding maximum diameter was measured. The maximum longitudinal diameter can be determined by moving the EyeCom cursor on the caustic rim at both ends of the maximum longitudinal diameter. To reduce the amount of possible error in moving from one side to the other of the maximum diameter, CAUSTIC 2 program was used [63] (see the appendix for listing of the program). A tangent line to points A and B shown in Fig. 3-12 is drawn. Different color parallel lines to line AB within 2 to 3 pixels are drawn and the cursor moved along the maximum longitudinal diameter indicating line:

The magnification factor for the transmitted setup was kept between 3.1 and 4.1. The applied stresses and the resulting transmitted stress-optical constants for each model are shown in Table 5-3. The average of the five  $c_t$  results for each model and also the percentage difference between the maximum and minimum values are presented in Table 5-3. The average  $c_t$ , the maximum  $c_t$  and minimum  $c_t$  versus  $a/w$  are shown in Fig. 5-7. The magnification factor for the reflected case was between 4.6 and 5.46 and the resulting  $c_r$ , corresponding to different load levels, for each model are shown in Table 5-4. The variation of the maximum and minimum values along with the average  $c_r$  are shown in Fig. 5-8.

Table 5-3. Load test results for  $c_t$

Model No.	$\sigma$ (psi)	$c_t$ ( $10^{-6}$ in <sup>2</sup> /lb)	avg. $c_t$ ( $10^{-6}$ in <sup>2</sup> /lb)	% difference
1C	515	0.752	0.750	0.73
	604	0.748		
	711	0.752		
	800	0.747		
	888	0.750		
2C	515	0.752	0.751	0.66
	604	0.753		
	711	0.748		
	800	0.749		
	888	0.754		
3C	400	0.764	0.759	0.78
	515	0.757		
	604	0.749		
	711	0.765		
	800	0.759		

Table 5-3. (Continued)

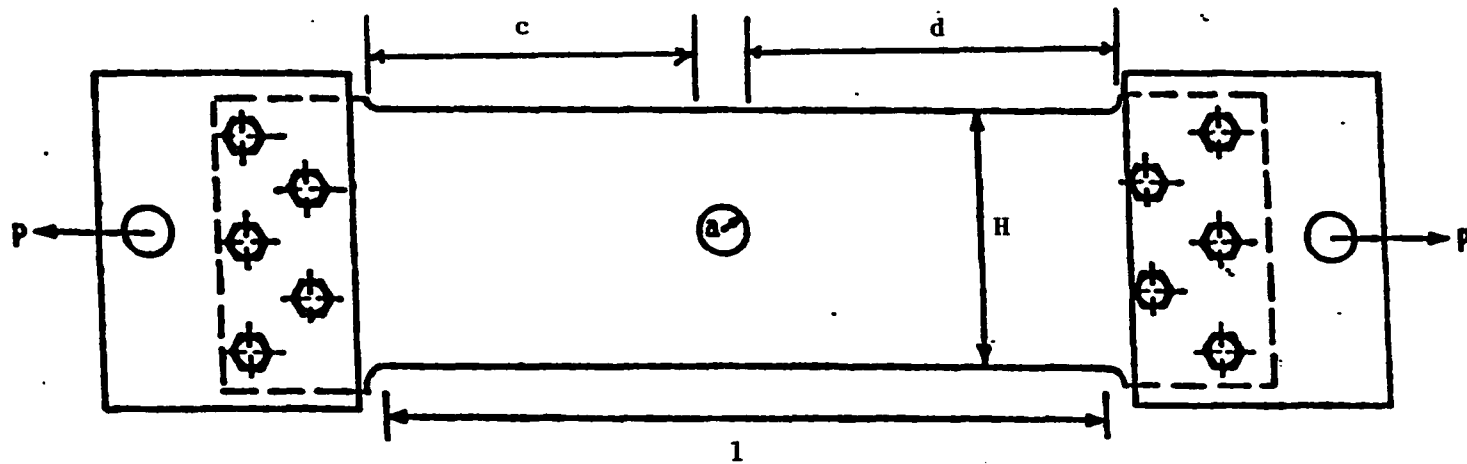
Model No.	$\sigma$ (psi)	$c_t$ ( $10^{-6}$ in <sup>2</sup> /lb)	avg. $c_t$ ( $10^{-6}$ in <sup>2</sup> /lb)	% difference
4C	400	0.805	0.807	1.05
	515	0.802		
	604	0.810		
	711	0.811		
	800	0.805		
5C	515	0.878	0.875	1.4
	604	0.881		
	711	0.866		
	800	0.871		
	888	0.878		
1D	660	0.757	0.752	1.2
	840	0.753		
	970	0.748		
	1067	0.754		
	1164	0.749		
2D	660	0.753	0.751	1.06
	840	0.752		
	970	0.750		
	1067	0.747		
	1164	0.755		
3D	660	0.757	0.753	1.08
	840	0.756		
	970	0.751		
	1067	0.753		
	1164	0.748		
4D	680	0.747	0.750	1.07
	873	0.748		
	1067	0.755		
	970	0.749		
	1164	0.753		

Table 5-4. Load test results for  $c_r$ 

Model No.	$\sigma$ (psi)	$c_r$ ( $10^{-6}$ in <sup>2</sup> /lb)	avg. $c_r$ ( $10^{-6}$ in <sup>2</sup> /lb)	% difference
1C	604	2.25	2.26	0.80
	711	2.26		
	755	2.26		
	800	2.27		
	888	2.25		
2C	515	2.26	2.27	0.88
	604	2.275		
	711	2.28		
	800	2.27		
	888	2.28		
3C	400	2.30	2.27	2.4
	515	2.29		
	604	2.247		
	711	2.29		
	800	2.28		
4C	400	2.30	2.31	0.86
	515	2.30		
	604	2.32		
	711	2.31		
	800	2.32		
5C	515	2.337	2.32	1.7
	604	2.330		
	711	2.330		
	800	2.300		
	888	2.32		

Table 5-4. (Continued)

Model No.	$\sigma$ (psi)	$c_r$ ( $10^{-6}$ in <sup>2</sup> /lb)	avg. $c_r$ ( $10^{-6}$ in <sup>2</sup> /lb)	% difference
1D	795	2.262	2.26	0.21
	873	2.267		
	970	2.263		
	1067	2.264		
	1164	2.263		
2D	660	2.268	2.26	0.35
	776	2.260		
	970	2.268		
	1067	2.264		
	1261	2.260		
3D	630	2.276	2.27	0.91
	776	2.273		
	970	2.225		
	1067	2.271		
	1164	2.264		
4D	660	2.275	2.276	1.0
	873	2.268		
	970	2.289		
	1116	2.266		
	1213	2.282		



	Model C	Model D
W	1.8"	3.4"
L	8.0"	8.2"

Fig. 5-2. Models C and D geometries

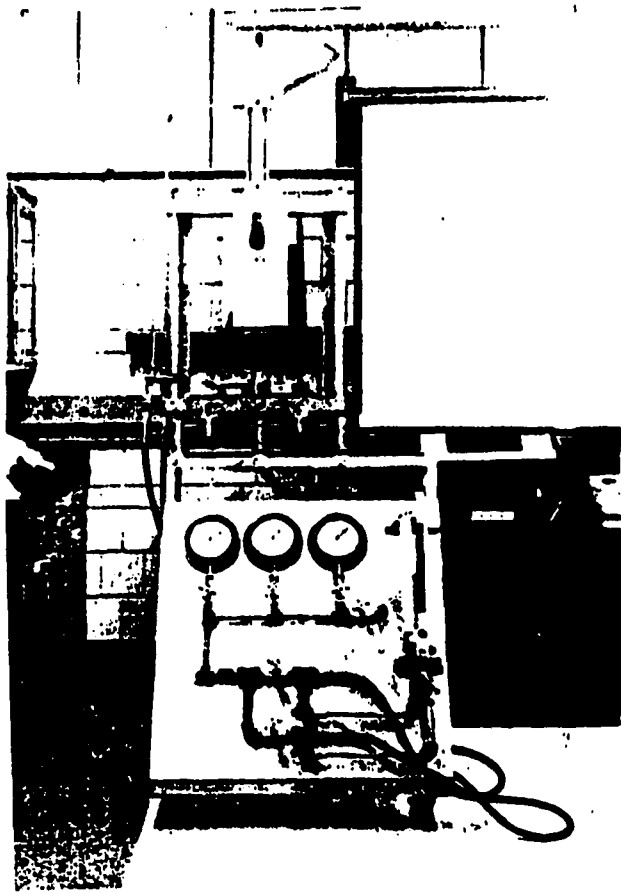


Fig. 5-3. Pressure loading apparatus

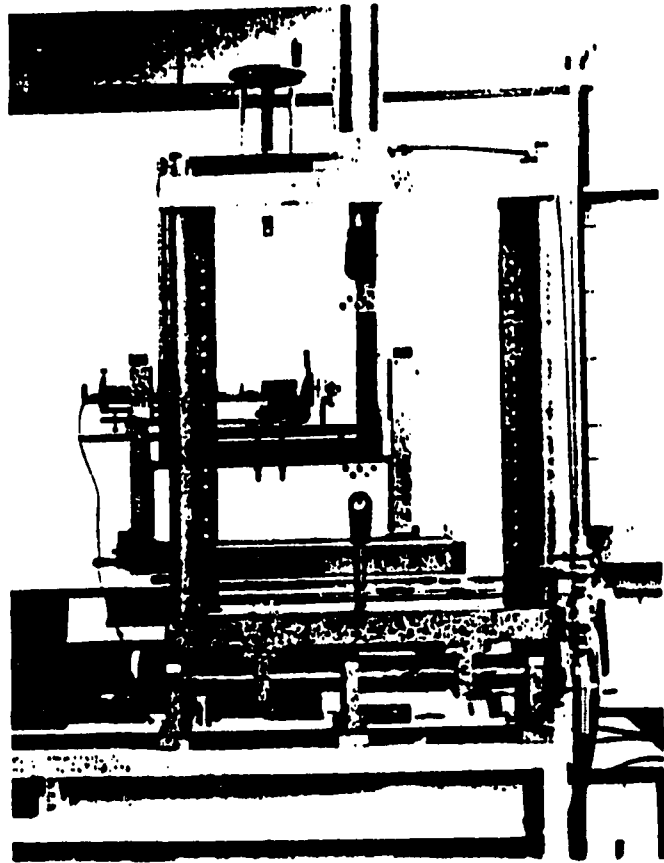


Fig. 5-4. Experimental transmitted caustic setup

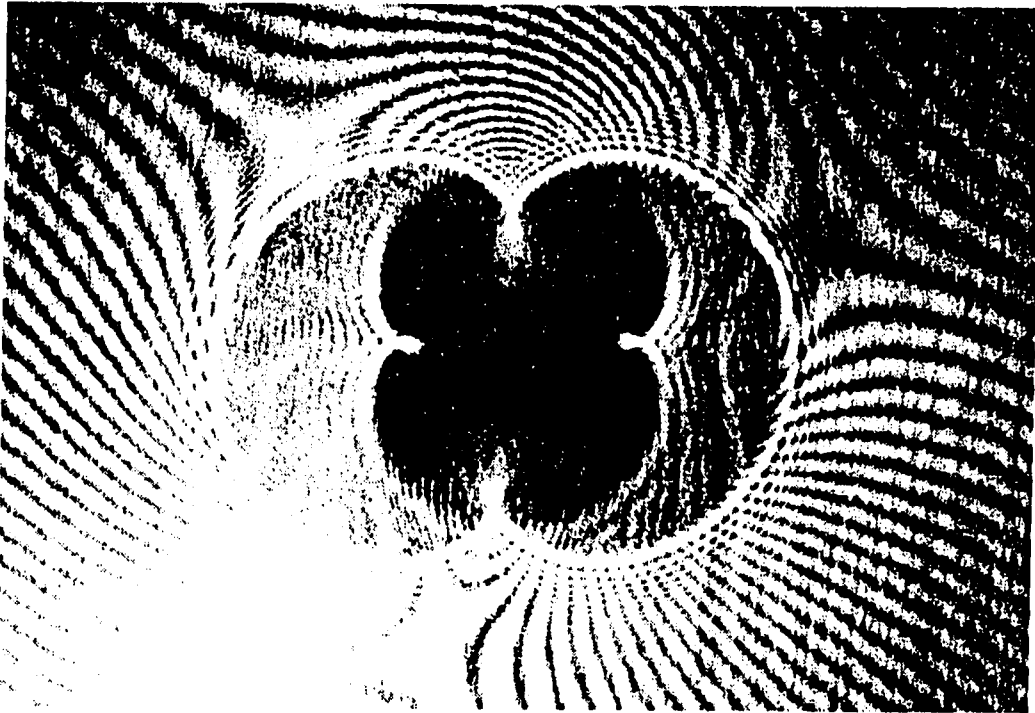


Fig. 5-5. Reflected from a central hole caustic pattern

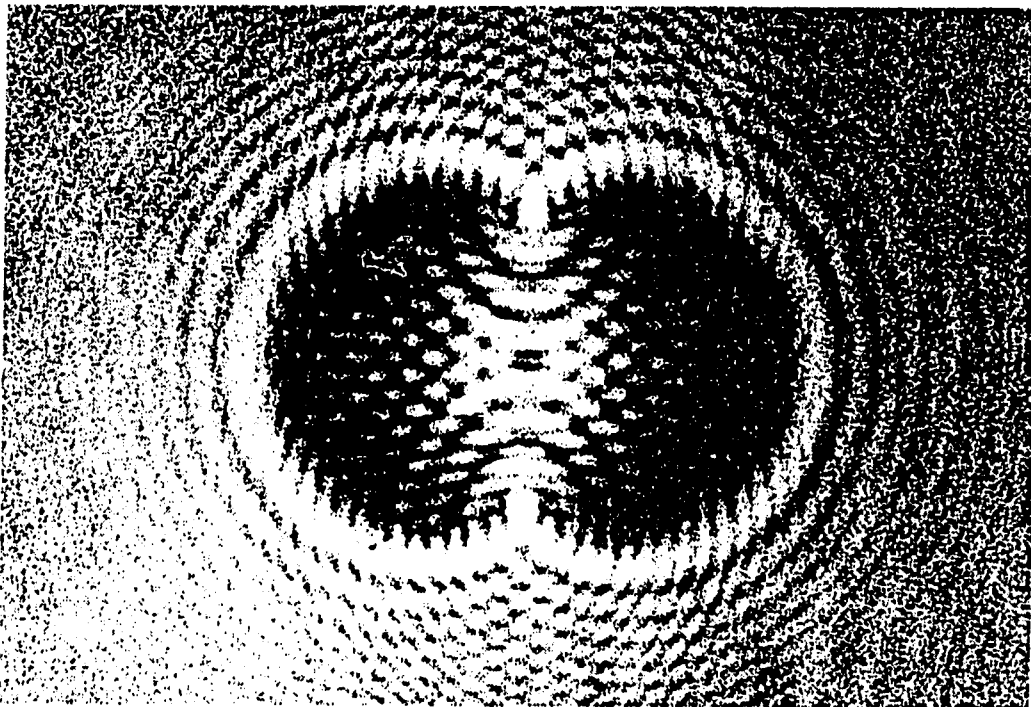


Fig. 5-6. Transmitted through a central hole caustic pattern

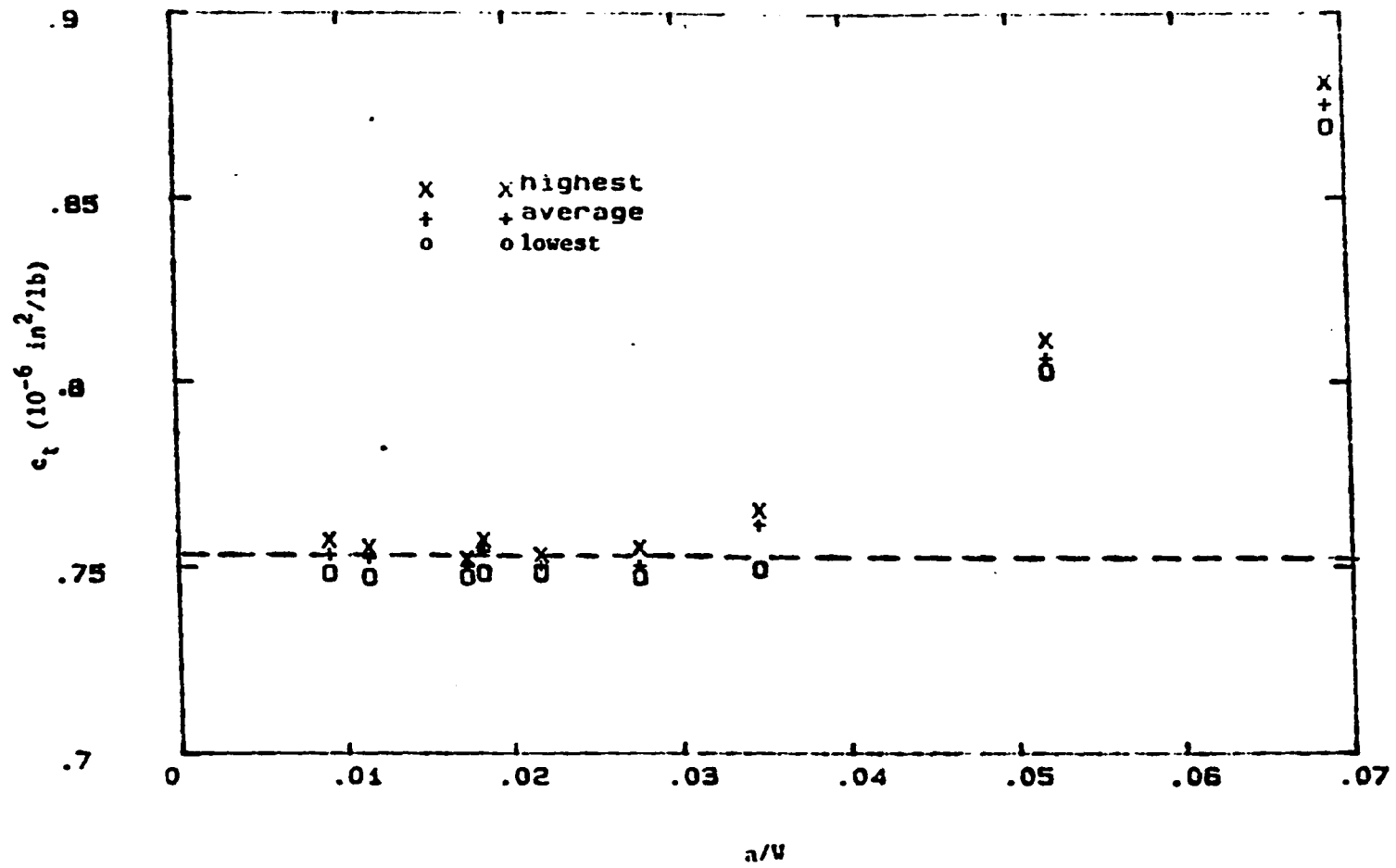


Fig. 5-7. Stress optical constant  $c_t$  versus  $a/W$

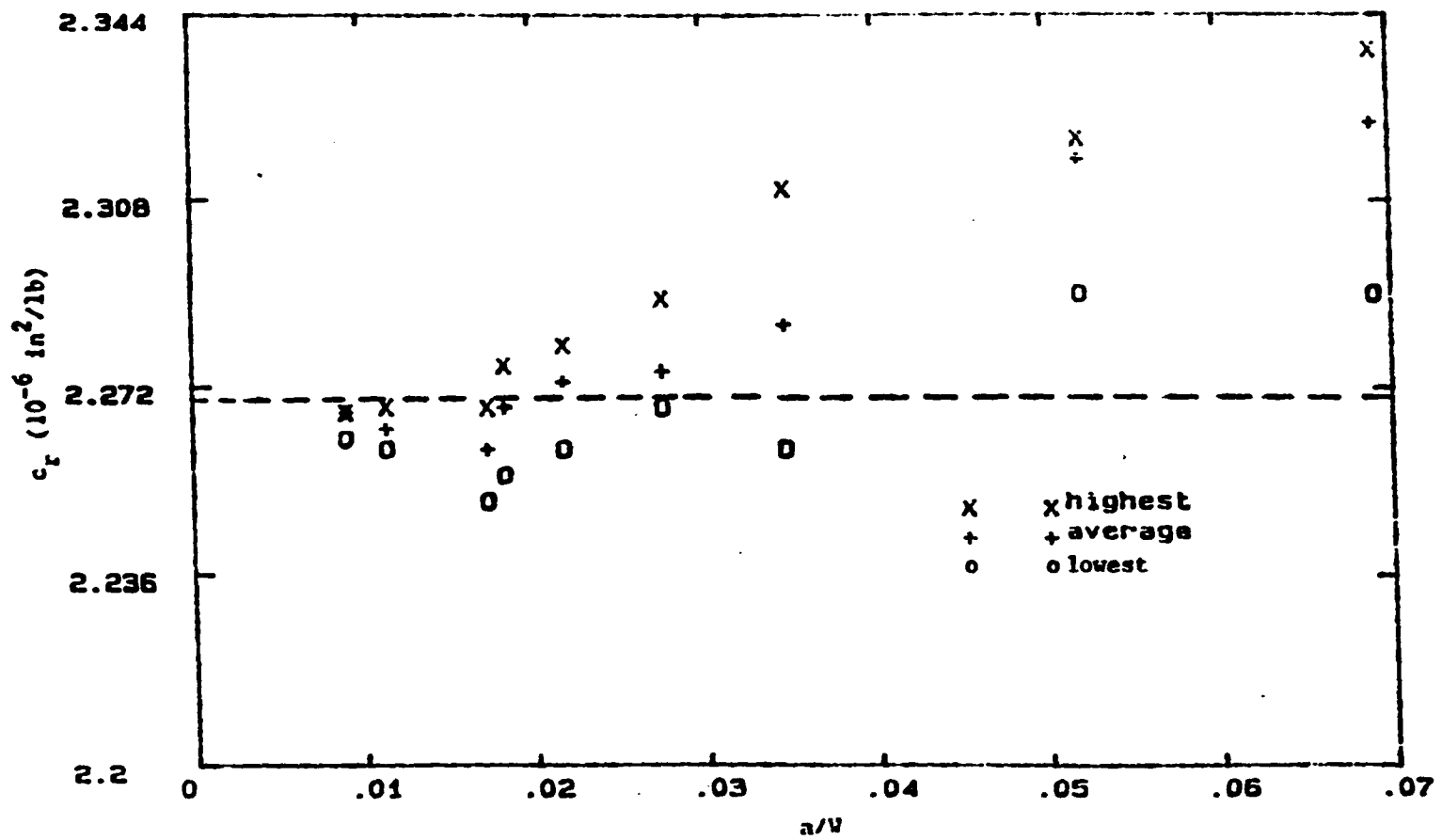


Fig. 5-8. Stress optical constant  $c_r$  versus  $a/W$

### C. Conclusions and Recommendations

A new experimental technique for the determination of the stress-optical constants for the transmitted caustic and the caustic reflected from the rear surface of the model was developed in this study using the experimental method of caustics. The stress-optical constants were determined by measuring the maximum longitudinal diameters of the caustic resulting from the monochromatic light transmitted or reflected from the area surrounding a circular hole in an infinite plate. The reflection from the front surface stress-optical constant was not considered in this study since its value is Poisson's ratio divided by Young's modulus.

The dashed line in the Fig. 5-6 represents  $c_t = 0.751 \times 10^{-6} \text{ in}^2/\text{lb}$  which compares to  $c_t = 0.744 \times 10^{-6} \text{ in}^2/\text{lb}$  as reported by Beinert and Kalthoff [24]. The dashed line in Fig. 5-7 is the average of the six smallest  $a/w$  ratios and represents  $c_r = 2.27 \times 10^{-6} \text{ in}^2/\text{lb}$ . The resulting  $c_r$  value is in a good agreement with the reported value of  $2.26 \times 10^{-6} \text{ in}^2/\text{lb}$  [64] and  $2.278 \times 10^{-6} \text{ in}^2/\text{lb}$  [65].

The proposed method is a direct and accurate technique for independently determining the transmitted and reflected stress-optical constants. It is seen from Figs. 5-6 and 5-7 that the size of the hole  $a$  should be very small compared to the width of the model. It is concluded that an  $a/w$  ratio less than 0.03 should be used for both reflected and transmitted studies and several load levels should be used for each hole size used.

An experiment was run with two extra holes at distance of  $w/2$  from the central hole in model B. The extra holes did not alter the readings of the original hole. Thus three hole sizes can be investigated using the same model.

## REFERENCES

1. A. A. Griffith. "The Phenomenon of Rupture and Flow in Solids." Philosophical Transactions, Royal Society of London Series, 221 (1920), 163-198.
2. G. R. Irwin. "Fracture Mechanics." Fracturing of Metals, American Society of Metals Publication, 29th Natl. Metal Congress and Symposium, Chicago, (1948), 147-166.
3. H. Neuber. Kerbspannungsleber. 2nd ed. New York: Julius Springer, 1958.
4. G. R. Irwin. "Linear Fracture Mechanics, Fracture Transition, and Fracture Control." Engineering Fracture Mechanics, 1 (1968) 241-257.
5. G. R. Irwin, J. A. Kies and H. L. Smith. "Fracture Strength Relative to Onset and Arrest of Crack Propagation." Proceedings of the American Society Testing Materials, 58 (1958), 640-651.
6. D. S. Dugdale. "Yielding of Steel Sheets Containing Slits." Journal of the Mechanics and Physics of Solids, 8 (1960), 100-104.
7. A. R. Rosenfield, P. K. Dai and G. T. Hahn. "Crack Extension and Propagation under Plane Stress." Proceedings of the First International Conference on Fracture, 1 (1966), 223-258.
8. R. G. Forman. "Experimental Program to Determine the Effect of Crack Buckling and Specimen Dimensions on Fracture Toughness of Thin Sheet Materials." Aerospace Research Laboratory Technical Report No. AFFDL-TR-65, 1966.
9. R. T. Ault and J. W. Spretnak. "Initial Yielding and Fracture in Notched Sheet Molybdenum." International Journal of Mechanical Sciences, 7 (1965), 87-102.
10. W. W. Gerberich. "Plastic Strains and Energy Density in Cracked Plates, Experimental Technique and Results." Experimental Mechanics, 4 (1964), 335-344.
11. P. S. Theocaris. "Local Yielding around a Crack Tip in Plexiglas." Journal of Applied Mechanics, Transactions of ASME, 37 (1970), 409-415.
12. P. S. Theocaris and E. G. Gdoutos. "An Optical Method for Determining Opening Mode and Edge-Sliding Mode Stress

- Intensity Factors." Journal of Applied Mechanics, 39 (1972), 91-97.
13. D. Broek. Elementary Engineering Fracture Mechanics. Third edition. Boston, MA: Martinus Nijhoff Publishers, 1982.
  14. G. R. Irwin, et al. "Photoelastic Studies of Damping, Crack Propagation and Crack Arrest in Polymers and 4340 Steel." Technical Report NO. NUREG/CR-1455. Division of Reactor Safety Research, Washington, D.C., 1980.
  15. G. R. Irwin. "Analysis of Stress and Strains Near the End of a Crack Traversing a plate." Journal of Applied Mechanics, 24 (1957), 361-364.
  16. J. N. Sneddon. "The Distribution of Stress in the Neighborhood of a Crack in an Elastic Solid." Proceedings of the Physical Society, 187 (1946), 229-260.
  17. P. Manogg. "Die Lichtablenkung Durch Eine Elastisch Beanspruchte Plate und die Schattenfiguren Von Kreis und Risskerbe." Clastechnische Berichte, 39 (1966), 229-239.
  18. P. S. Theocaris and N. Ioakimides. "Some Properties of Generalized Epicycloids Applied to Fracture Mechanics." Journal of Applied Mechanics, 22 (1971), 876-890.
  19. P. S. Theocaris. "Stress concentrations at Concentrated Loads." Experimental Mechanics, 13 (1973), 511-528.
  20. P. S. Theocaris. "Reflected Shadow Method for the Study of Constrained Zones in Cracked Plates." Applied Optics, 10 (1971), 2240-2247.
  21. A. J. Rosakis and L. B. Freund. "Optical Measurements of the Plastic Strain Concentration at a tip in a Ductile Steel Plate." Journal of Engineering Materials, 104 (1982), 115-125.
  22. A. J. Rosakis, C. C. Ma and L. B. Freund. "Analysis of the Optical Shadow Spot Method for a Tensile Crack in a Power-Law Hardening Material." Journal of Applied Mechanics, 50 (1983), 777-782.
  23. J. F. Kalthoff, J. Beinert and S. Winkler. "Analysis of Fast Running and Arresting Cracks by the Shadow Optical Method of Caustics." Proceedings of the I.U.T.A.M. Symposium on Optical Methods in Mechanics of Solids, (1980), 497-508.
  24. J. Beinert and J. F. Kalthoff. "Experimental determination of Dynamic Stress Intensity Factors by Shadow Patterns." Mechanics of Fracture, Vol. VII. G. C. Sih, ed., Noordhoff Int. Publishing, London, The Netherlands, 1981, 280-330.

25. P. S. Theocaris. "The Reflected Shadow Method for the Study of the Constrained Zones in Cracked Birefringent Media." Journal of Strain Analysis, 7 (1972), 75-83.
26. P. S. Theocaris. "Stress Concentration in Anisotropic Plates by the Method of Caustics." Journal of Strain Analysis, 11 (1976), 154-157.
27. P. S. Theocaris and G. A. Papadopoulos. "Stress Intensity Factors from Reflected Caustics in Birefringent Plates with Cracks." Journal of Strain Analysis, 16 (1981), 29-36.
28. P. S. Theocaris. "Caustics for the Determination of Singularities in Cracked Plates." Proceedings of the I.U.T.A.M. Symposium on Optical Methods in Mechanics of Solids, (1979), 395-422.
29. P. S. Theocaris and G. I. Razem. "Error Analysis in Evaluating Stress Intensity Factors by Reflected Caustics." International Journal of Mechanical Sciences, 23 (1981), 275-284.
30. E. E. Gdoutos and E. C. Aifantis. "The Method of Caustics in Environmental Cracking." Engineering Fracture Mechanics, 23 (1986), 423-430.
31. D. Papis. "Running Cracks Crossing Inclined Interfaces." Proceedings of First USA-Greece Symposium, (1980), 195-209.
32. J. Beinert and J. F. Kalthoff. "Experimental Determination of Dynamic Stress Intensity Factors by Shadow Patterns." Mechanics of Fracture, 7 (1981), 281-330.
33. P. S. Theocaris and G. A. Papadopoulos. "Interrelation between Static and Dynamic Stress Intensity Factors and Their Evaluation by Caustics." Journal of Strain Analysis, 19 (1984), 127-133.
34. P. S. Theocaris. "Interaction of Cracks with Other Cracks or Boundaries." International Journal of Fracture Mechanics, 8 (1972), 37-47.
35. P. S. Theocaris. "Interaction between Collinear Asymmetric Cracks." Journal of Strain Analysis, 7 (1971), 186-193.
36. P. S. Theocaris. "Complex Stress Intensity Factors at Bifurcated Cracks." Journal of the Mechanics and Physics of Solids, 20 (1972), 265-278.
37. P. S. Theocaris. "Determination of Crack Opening Displacement by the Method of caustic." Journal of Strain Analysis, 9 (1974), 197-205.

38. D. Zili, Z. Wenhua and S. Yanjun. "Study of Experimental Methods of Caustics for Determining COD of Metal Specimens." Proceedings of the 1986 SEM Spring Conference on Experimental Mechanics, (1986), 280-283.
39. A. A. Sukere. "Photometric Methods of Caustics." Engineering Fracture Mechanics, 26 (1987), 65-74.
40. T. Poston and I. Stewart. "Optics and Scattering Theory." In Catastrophe Theory and its Applications. Palo Alto, Calif.: Fearon, 1978.
41. S. M. Kamath and K. S. Kim. "Coherent-Light-Shadow Spot of a Crack under Mode I Loading: Theory and Experiment." Experimental Mechanics, 26 (1986), 386-393.
42. M. Born and E. Wolf. Principles of Optics. 4th edition. London: Pergamon Press, 1970.
43. R. J. Sanford. "Applications of the Least-Squares Method to Photoelastic Analysis." Experimental Mechanics, 20 (1980), 192-197.
44. M. L. James, G. M. Smith and J. C. Wolford. Applied Numerical Methods for Digital Computation with Fortran and CSMP. 2nd edition. New York, New York: Harper & Row Publishers, Inc., 1977.
45. N. R. Draper and H. Smith. Applied Regression Analysis. 2nd edition. New York, New York: John Wiley & Sons Publishers, Inc., 1981.
46. B. Koerner. FNROOT Program. Stress Analysis Laboratory, Department of Engineering Science and Mechanics, Iowa State University, Ames, Iowa, 1984.
47. N. T. Younis. CAUSTIC 1 Program. Stress Analysis Laboratory, Department of Engineering Science and Mechanics, Iowa State University, Ames, Iowa, 1985.
48. K. Shimizu, S. Takahashi and H. Shimada. "Some Propositions on Caustics and an Application to the Biaxial-Fracture Problem." Experimental Mechanics, 25 (1985), 154-160.
49. A. J. Rosakis and K. Ravi-Chandar. "On Crack tip Stress State: An Experimental Evaluation of Three Dimensional Effects." Technical report No. SM 84-2. California Institute of Technology, Pasadena, CA, 1984.
50. H. Nigam and A. Shukla. "Comparison of the Techniques of Caustic and Photoelasticity as Applied to Fracture." Proceedings of the 1986 SEM Spring Conference on Experimental Mechanics,

(1986), 760-766.

51. R. J. Sanford. "The Influence of Nonsingular Stresses on Experimental Measurements on the stress Intensity Factor." Proceedings of the Tenth Canadian Fracture Conference, (1983), 317-324.
52. J. W. Phillips, R. J. Sanford and J. Beinert. "Effect of the Constant Stress Term on Mode I Caustics." Technical Report No. 436. University of Illinois at Urbana-Champaign, Urbana, IL, 1979.
53. J. W. Phillips and R. J. Sanford. "Effect of Higher Order Stress Terms on Mode I Caustics in Birefringent Materials." In Fracture Mechanics. Ed. R. Roberts. American Society for Testing and Materials Special Technical Publication. Philadelphia, PA: ASTM, 1980.
54. P. S. Theocaris and J. G. Michopoulos. "The Exact Form of Mixed-Mode Fracture: A Comparison with Approximate Solutions." Acta Mechanica, 46 (1983), 77-97.
55. S. V. Kartalopoulos and D. D. Raftopoulos. "A Rapid Optical Method for the Determination of Optically Isotropic and Anisotropic Materials." J. Phys. D: Appl. Phys., 9 (1976), 2545-2553.
56. P. S. Theocaris and J. Prassianakis. "Interrelation of Mechanical and Optical Properties of Plasticized Epoxy Polymers." Journal of Applied Polymer Science, 22 (1978), 1725-1734.
57. P. S. Theocaris. "Dependence of Stress Optical Coefficients on the Mechanical and Optical Properties of Polymers." Journal of Strain Analysis, 8 (1973), 267-276.
58. D. D. Raftopoulos, D. Karapanos and P. S. Theocaris. "Static and Dynamic Mechanical and Optical Behaviour of High Polymers." J. Phys. D: Appl. Phys., 9 (1976), 869-877.
59. W. J. Dally and W. F. Riley. Experimental Stress Analysis. Second edition. New York, New York: McGraw Hill Publishers, 1978.
60. U. Seidelmann. "Anwendung Des Schattenoptischen Kaustikenverfahrens Zur Bestimmung Bruchmechanischer Kennwerte Bei Uberlagerter Normal und Scherbean-Spruchung." Technical Report No. 2/76. Institut Fur Festkorpermechanik, Freiburg, Germany, 1976.
61. L. W. Zachary and B. J. Skillings. "Displacement Discontinuity Method Applied to Nondestructive Testing Related Stress Problems." International Journal for Numerical Methods in Engineering, 18 (1982), 1231-1244.
62. A. S. Voloshin and C. P. Burger. "Half-Fringe Photoelasticity: A

New Approach to Whole-Field Stress Analysis." Experimental Mechanics, 23 (1983), 304-313.

63. N. T. Younis. CAUSTIC 2 Program. Stress Analysis Laboratory, Department of Engineering Science and Mechanics, Iowa State University, Ames, Iowa, 1987.
64. P. S. Theocaris. "Elastic Stress Intensity Factors Evaluated by Caustics." In Mechanics of Fracture, Vol. 7. Ed. G. C. Sih. The Netherlands: Noordhoff Int. Publishing, 1981.
65. J. N. Prassianakis and P. S. Theocaris. "Stress Intensity Factors at V-Notched Elastic, Symmetrically loaded, Plates by the Method of Caustics." J. Appl. Phys., 13 (1980), 1043-1053.

## VII. ACKNOWLEDGEMENTS

I would like to express by gratitude and thanks to Prof. Loren W. Zachary for his guidance and patience throughout this project. His encouragement was a constant on which I could depend. On a personal note, I would like to thank him for his support and understanding when the death of my daughter occurred. His help at that time can not be expressed by mere words.

I also would like to thank Professors F. M. Graham, J. C. Houston, W. F. Riley, B. S. Dahiya, and C. P. Cox for their interest in this project.

A special thanks to Mr. Thomas Elliot for the many hours help in laboratory preparations.

Without my wife, Lori Martin's support and my familys' patience, this would have been a very difficult journey.

**VIII. APPENDIX: PROGRAMS**

**A. CAUSTIC 1 PROGRAM**

F  
C  
C  
C  
C  
C  
C  
C

-----  
PROGRAM CAUSTIC 1  
-----

THIS PROGRAM IS FOR THE DETERMINATION OF MIXED MODE STRESS  
INTENSITY FACTORS AT A CRACK TIP USING THE EXPERIMENTAL METHOD  
OF CAUSTICS  
-----

COMMON /EYECOM/ VIDEO(4), PICTUR, GRAFIC, CURSOR, RED, BLUE, GREEN,  
+ ALUAF, ALUBG, SHIFT, STAT, RAM(8)

C

EXTERNAL PHI

COMMON/PARAM/ RO, XO, YO, TO

REAL\*4 L(100), LE(100), PH(100), ALPH(100), THETA(100), RO, C1, C2, XL

REAL\*4 DX, DY, SCALE, MU, MM, PICDIS, RDIST, XO, YO, TO, C

REAL\*4 DTR, K2, X(100), Y(100), DLE(100,4), M(4,4), B(4), ERR(4)

INTEGER IZ(600), IS(600)

C

CALL SETUP

CALL DISPLY (VIDEO)

PAUSE 'ARRANGE CAMERA TO SHOW THE CAUSTIC AND GRID.'

CALL DISPLY (PICTUR)

CALL ACCUM

CALL ERASE

CALL DISPLY(GRAFIC)

CALL DISPLY(CURSOR)

PI=4.\*ATAN(1.)

C

C

C

DETERMINING THE CRACK ORIENTATION

PAUSE 'PUT CURSOR ON THE FIRST DIRECTION POINT.HIT<RETURN>'

CALL COORDS(IATT, IYTT)

PAUSE 'PUT THE CURSOR ON THE SECOND DIRECTION POINT.HIT<RETURN>'

CALL COORDS(IAB, IYB)

XTT=FLOAT(IATT)

YTT=FLOAT(IYTT)

```
XD=FLOAT(IXD)
YD=FLOAT(IYD)
XL=SQRT((XD-XTT)**2.+(YD-YTT)**2.)
COSE=(YTT-YD)/XL
TYPE*, 'COSE=', COSE
SINB=(XTT-XD)/XL
```

C  
C  
C

#### DETERMINING THE SCALE

```
PAUSE 'PUT THE CURSOR ON THE FIRST GRID POINT.HIT<RETURN>'
CALL COORDS(IXQ1,IYQ1)
PAUSE 'PUT THE CURSOR ON THE SECOND GRID POINT.HIT<RETURN>'
CALL COORDS(IXQ2,IYQ2)
DX=FLOAT(IXQ2-IXQ1)
DY=FLOAT(IYQ2-IYQ1)
PICDIS=SQRT(DX**2.+DY**2.)
TYPE*, 'WHAT IS THE ACTUAL DISTANCE BETWEEN THESE TWO POINTS'
ACCEPT*, RDIST
SCALE=RDIST/PICDIS
TYPE*, 'SCALE=', SCALE
CALL DISPLY (VIDEO)
PAUSE 'ARRANGE CAMERA TO SHOW CAUSTIC.'
CALL DISPLY (PICTUR)
```

L  
C  
C

#### LOCATING THE CRACK TIP, THE MAXIMUM TRANSVERSE DIAMETER(D max)

```
CALL ACCUM
PAUSE 'PUT THE CURSOR ON LEFT CUSP.HIT <RETURN>'
CALL COORDS(IXP1,IYP1)
PAUSE 'PUT THE CURSOR ON RIGHT CUSP.HIT <RETURN>'
CALL COORDS(IXP2,IYP2)
PAUSE 'PUT THE CURSOR ON CUSP POINT.HIT <RETURN>'
CALL COORDS(IXP3,IYP3)
CALL SKIP(IXP1,IYP1)
CALL DRAW(IXP2,IYP2)
IDDX1=IYP2-IYP1
```

```

IDDY1=IXP1-IXP2
CALL SKIP(IXP3+6*IDDX1, IYP3+6*IDDY1)
CALL DRAW(IXP3-4*IDDX1, IYP3-4*IDDY1)
PAUSE 'PUT THE CURSOR ON LOWER D max POINT.HIT <RETURN>'
CALL COORDS(IXP5, IYP5)
PAUSE 'PUT THE CURSOR ON UPPER D max POINT.HIT <RETURN>'
CALL COORDS(IXP6, IYP6)
DCX=FLOAT(IXP6-IXP5)
DCY=FLOAT(IYP6-IYP5)
DTR=SQRT(DCX**2.+DCY**2.)
TYPE*, 'DTR=' ,DTR
ROO=(DTR*SCALE)/3.
TYPE*, 'ROO=' ,ROO
XP5=FLOAT(IXP5)
YP5=FLOAT(IYP5)
XP3=FLOAT(IXP3)
YP3=FLOAT(IYP3)
MM=SQRT((XP5-XP3)**2.+(YP5-YP3)**2.)
TYPE*, 'MM=' ,MM
COST=(XP5-XP3)/MM
SINT=(YP5-YP3)/MM
IXTE=IXP5-(1.666*ROO*COST)/SCALE
IYTE=IYP5-(1.666*ROO*SINT)/SCALE
CALL COLOR (*140)
CALL SKIP (IXP5, IYP5)
CALL DRAW (IXTE, IYTE)
PAUSE 'PUT THE CURSOR ON THE CRACK TIP.HIT <RETURN>'
CALL COORDS(IXT, IYT)

```

C  
C  
C

START COLLECTING DATA POINTS

```

TYPE*, 'NUMBER OF POINTS DESIRED'
ACCEPT*, NUM

```

```

C
C   PROGRAM PROFIL
C
COMMON /ALU  / ADD,ABDC,SUB,SUBC,AINC,ADEC,A,B,AINVT,BINVT,
+           AND,OR,ORINVT,XOR,XNOR,CLEAR,SET,DFLOW,FLAG

CALL DISPLY (CURSOR)
PAUSE 'Place cursor on black.'
CALL COORDS (IX,IY)
IMIN = 256
DO 10 I = -3,3
  DO 10 J = -3,3
    IZ(1) = INTENS (IX+I,IY+J)
    IF (IZ(1).LT.IMIN) IMIN = IZ(1)
10  PAUSE 'Place cursor on white.'
    CALL DISPLY (,CURSOR)
    CALL COORDS (IX,IY)
    IMAX = 0
    DO 20 I = -3,3
      DO 20 J = -3,3
        IZ(1) = INTENS (IX+I,IY+J)
        IF (IZ(1).GT.IMAX) IMAX = IZ(1)
20  CALL CONTR (IMIN,IMAX)
    DO 110 K1=1,NUM

C
C   Generate profiles of image.
C
CALL DISPLY (CURSOR)
PAUSE 'Select Origin Point.'
CALL COORDS (IX,IY)
PAUSE 'Select End Point.'
CALL COORDS (IX1,IY1)
CALL ERASE
CALL DISPLY (GRAEIC)
CALL COLOR (*140)
CALL SKIP (IX,IY)

```

```

CALL DRAW (IX1,IY1)
IBOT = IY - 20
IF (IY1.LT.IY) IBOT = IY1 - 20
IF (IBOT.LT.168) IBOT = IBOT + 168
ILEN = IABS(IX1-IX)
SLOPE = FLOAT(IY1 - IY)/FLOAT(IX1 - IX)
IF (IX1.LT.IX) IX = IX1
CALL BACK (IX,IX+ILEN,IBOT-128,IBOT)
CALL SKIP (IX,IBOT-INTENS(IX,IY)/2)
IXK=IX
IYK=IY
IS(1)=INTENS(IX,IY)/3
IMAX=IS(1)
GO 240 I = 1, ILEN
    IX = IX + 1
IS(I)=INTENS(IX,IY+INT(I*SLOPE))/2
IF (IS(I).LT.IMAX)GOTO 220
IMAX=IS(I)
IXK=IX
IYK=IY+INT(I*SLOPE)
220 CALL DRAW(IX,IBOT-IS(I))
240 CONTINUE
K=K1
XP=SCALE*FLOAT(IXK-IX1)
YP=SCALE*FLOAT(IYK-IY1)
X(K)=XP*SINE+YP*COSE
Y(K)=XP*COSE-YP*SINE
TYPE*, 'X(',K,')=',X(K)
TYPE*, 'Y(',K,')=',Y(K)
110 CONTINUE
CALL ERASE

```



```

A3=SQRT(13.+(12.)*A2)
A4=(COS(PH(I))*2.*RO*A1*(Y0-Y(I)))/((X0-X(I))*2.)
A5=(6.*(A1/A3)*2.+A2)/COS(PH(I)-THETA(I)-TO)+A3
A6=(COS(PH(I))*2.*RO*A1*(X(I)-X0))/((X0-X(I))*2.)
  DLE(I,1)=A3/3.          !RO
  DLE(I,2)=(X(I)-X0)/L(I)+(A4/A5)      !X0
  DLE(I,3)=(Y(I)-Y0)/L(I)-(A6/A5)      !Y0
  DLE(I,4)=RO*A1/A5        !TO
100  CONTINUE
C
C  CALCULATION OF M(N,N) AND Y(N) MATRICES.
C
  DO 200 J=1,4
    B(J)=0.0
    DO 200 I=1,NUM
      B(J)=B(J)+(L(I)-LE(I))*DLE(I,J)
200  CONTINUE
  DO 300 J=1,4
    DO 300 K=1,4
      M(J,K)=0.0
      DO 300 I=1,NUM
        M(J,K)=M(J,K)+DLE(I,K)*DLE(I,J)
300  CONTINUE
  CALL GAUSE(M,B,4,ERR)
  TYPE*, 'DRO  ', B(1)
  TYPE*, 'DXO  ', B(2)
  TYPE*, 'DYO  ', B(3)
  TYPE*, 'DTO  ', B(4)
  ERR2=(ABS(B(1))+ABS(B(2))+ABS(B(3))+ABS(B(4)))/4.
  IF(ERR2.LE..1E-2.OR.ICONT.GT.30)GOTO 400
  RO=RO+B(1)
  XO=XO+B(2)
  YO=YO+B(3)
  TO=TO+B(4)
  TYPE*, '

```

```

TYPE*, 'ICONT=', ICONT
TYPE*, 'RO ', RO
TYPE*, 'XO ', XO
TYPE*, 'YO ', YO
TYPE*, 'TO ', TO
MU=SIN(-TO/2.)/COS(-TO/2.)
TYPE*, 'MU ', MU
ICONT=ICONT+1
GOTO 5
400 TYPE*, '30 ITER.'
TYPE*, 'RO ', RO
TYPE*, 'XO ', XO
TYPE*, 'YO ', YO
TYPE*, 'TO ', TO
STOP
END

```

C  
C  
C  
C  
C  
C

-----  
ENROOT SUBROUTINE

-----  
THIS SUBROUTINE IS FOR THE DETERMINATION OF THE ANGLE THETA  
-----

```

REAL FUNCTION PHI (THETA)
COMMON/PARAM/ RO,XO,YO,TO
A1=SIN(THETA/2.)
A2=SQRT(3.25+3.*COS(THETA/2.))
ASIN=-ACOS(A1/A2)+3.1415927/2.
PHI=THETA+ASIN+TO
RETURN
END

```

```

C -----
C           SUBROUTINE GAUSE (M,Y,N,ERR)
C
C THIS SUBROUTINE CALCULATES THE INITIAL CURVE VALUE, THE
C CAUSTIC ANGLE OF SYMMETRY, THE CRACK TIP POSITION
C -----
C
C SUBROUTINE GAUSE (M,Y,N,ERR)
C REAL*4 M(N,N),Y(N),ERR(N)
C
C NORMALIZE COLUMNS.
C
C DO 110 I=1,N
C ERR(I)=0.0
C DO 100 J=1,N
100   ERR(I)=ERR(I)+ABS(M(J,I))
C ERR(I)=ERR(I)/N
C IF(ERR(I).LT.1E-36) GOTO 1
C DO 110 J=1,N
110   M(J,I)=M(J,I)/ERR(I)
C
C GAUSSIAN ELIMINATION.
C
C DO 230 I=1,N-1           'ELIMINATION ROW
C AMAX=0.0
C   DO 210 J=1,N           'LOCATE PIVOT ROW
C     AVG=0.0
C     DO 200 K=1,N
200   AVG=AVG+ABS(M(J,K))
C     AVG=AVG/(N-1+1)
C     IF (ABS(M(J,I)).LE.(AMAX*AVG)) GOTO 210
C     AMAX=ABS(M(J,I))/AVG
C     IMAX=J
210   CONTINUE
C   IF(AMAX.LT.1E-36) GOTO 1
C   M(J,I)=M(J,I)           'ELIMINATE PIVOT ROW

```

```

M(I,MAX,I)=N(I,I)
M(I,I)=AMAX
AMAX=TEMP
DO 220 J=I+1,N
    TEMP=M(I,MAX,J)/AMAX
    M(I,MAX,J)=M(I,J)
220 M(I,J)=TEMP
    TEMP=Y(INAX)/AMAX
    Y(INAX)=Y(I)
    Y(I)=TEMP
DO 230 J=I+1,N
    AMAX=M(J,I)
    Y(J)=Y(J)-Y(I)*AMAX
DO 230 K=I+1,N
230 M(J,K)=M(J,K)-M(I,K)*AMAX
    IF(ABS(M(N,N)).LT.ABS(Y(N)*1E-36)) GOTO 1
    Y(N)=Y(N)/M(N,N)
M(N,N)=1.0
C
C    BACK SUBSTITUTION.
C
DO 300 I=N,2,-1
    DO 300 J=I-1,1,-1
300 Y(J)=Y(J)-Y(I)*M(J,I)
DO 310 I=1,N
    Y(I)=Y(I)/ERR(I)
310 ERR(I)=M(I,I)
RETURN
C
C    IN CASE OF NO SOLUTION
C
ERR(N)=0.0
RETURN
END

```

...ING RELATED SIGNIFICANCE

PERFORM ELIMINATION

C  
C  
C  
F

-----  
COSINE INVERSE SUBROUTINE  
-----

```
REAL FUNCTION ACOS(Z)
REAL Z
PI=4.*ATAN(1.)
A=SQRT(1.-Z**2)
IF(Z.EQ.0)GOTO 10
B=A/Z
Z1=ATAN(B)
IF(Z.LT.0)Z1=PI+Z1
GOTO 20
10 Z1=PI/2.
20 ACOS=Z1
RETURN
END
```

**B. CAUSTIC 2 PROGRAM**

C  
C  
C  
C  
C

-----  
PROGRAM CAUSTIC 5  
-----

THIS PROGRAM LOCATES THE CAUSTIC MAXIMUM DIAMETER ACCURATELY

COMMON /EYECOM/ VIDEO(4), PICTUR, GRAFIC, CURSOR, RED, BLUE, GREEN.  
+ ALUAF, ALUBG, SHIFT, STAT, RAM(16)  
REAL\*4 SCALE, RDIST, PICDIS, X(100), Y(100), ALPHA1, ALPHA2  
REAL\*4 BETA1, BETA2, DD, D  
INTEGER IZ(600), IS(600)

C

CALL SETUP  
CALL DISPLY (VIDEO)  
PAUSE 'ARRANGE CAMERA.'  
CALL DISPLY (PICTUR)  
CALL ACCUM  
CALL ERASE  
CALL DISPLY(GRAFIC)  
CALL DISPLY(CURSOR)  
PI=3.1415926

C  
C  
C

DETERMINING THE SCALE

PAUSE 'PUT THE CURSOR ON THE FIRST GRID POINT.HIT<RETURN>'  
CALL COORDE (IXQ1, IYQ1)  
PAUSE 'PUT THE CURSOR ON THE SECOND GRID POINT.HIT<RETURN>'  
CALL COORDE (IXQ2, IYQ2)  
DX1=FLOAT(IXQ2-IXQ1)  
DY1=FLOAT(IYQ2-IYQ1)  
PICDIS=SQRT(DX1\*\*2+DY1\*\*2)  
TYPEA, 'WHAT IS THE ACTUAL DISTANCE BETWEEN THESE TWO POINTS'  
ACCEPTA, RDIST  
SCALE=RDIST/PICDIS  
TYPEA, 'SCALE= ', SCALE  
PAUSE 'PUT THE CURSOR ON THE CAUSTIC MAXIMUM POINT.HIT<RETURN>'



```

IXG1=IALHA1
IXG2=IALHA2
IYG1=IBETA1
IYG2=IBETA2
CALL DISPLY(GRAEFC)
CALL COLOR (*120)
CALL SKIP (IXG1,IYG1)
CALL DRAW (IXG2,IYG2)
121 continue
CALL DISPLY (PICTUR)
CALL ACCUM
CALL DISPLY (CURSOR)
PAUSE 'PLACE CURSOR ON BLACK.'
CALL COORDS (IX,IY)
IMIN= 256
DO 10 I=-3,3
DO 10 J=-3,3
IZ(1)=INTENS (IX+I,IY+J)
10 IF (IZ(1).LT.IMIN) IMIN=IZ(1)
PAUSE 'PLACE CURSOR ON WHITE.'
CALL DISPLY (,CURSOR)
CALL COORDS (IX,IY)
IMAX=0
DO 20 I=-3,3
DO 20 J=-3,3
IZ(1)=INTENS(IX+I,IY+J)
20 IF(IZ(1).GT.IMAX) IMAX=IZ(1)
CALL CONTR (IMIN,IMAX)
DO 110 KI=1,10
CALL DISPLY (CURSOR)
PAUSE 'SELECT ORIGIN POINT.'
CALL COORDS (IX,IY)
PAUSE 'SELECT END POINT.'
CALL COORDS (IX2,IY2)
CALL DISPLY (GRAEFC)
CALL COLOR (*120)

```

```

CALL SKIP (IX, IY)
CALL DRAW (IX1, IY1)
IBOT = IY - 20
IF (IY1.LT.IY) IBOT = IY1 - 30
IF (IBOT.LT.168) IBOT = IBOT + 168
ILEN = IABS (IX1 - IX)
SLOPE = FLOAT (IY1 - IY) / FLOAT (IX1 - IX)
IF (IX1.LT.IX) IX = IX1
CALL BACK (IX, IX + ILEN, IBOT - 128, IBOT)
CALL SKIP (IX, IBOT - INTENS (IX, IY) / 2)
IXK = IX
IYK = IY
IS (1) = INTENS (IX, IY) / 2
IMAX = IS (1)
DO 240 I = 1, ILEN
IX = IX + 1
IS (I) = INTENS (IX, IY + INT (I * SLOPE)) / 2
IF (IS (I).LT.IMAX) GOTO 220
IMAX = IS (I)
IXK = IX
IYK = IY + INT (I * SLOPE)
220 CALL DRAW (IX, IBOT - IS (I))
240 CONTINUE
K = KI
X (K) = SCALE * FLOAT (IXK)
Y (K) = SCALE * FLOAT (IYK)
TYPE *, 'X (', K, ') = ', X (K)
TYPE *, 'Y (', K, ') = ', Y (K)
110 CONTINUE
STOP
END

```